

# **Surgical probe and implant development for nucleus pulposus replacements**

THÈSE N° 6839 (2016)

PRÉSENTÉE LE 22 JANVIER 2016

À LA FACULTÉ DES SCIENCES ET TECHNIQUES DE L'INGÉNIEUR  
LABORATOIRE DE DISPOSITIFS PHOTONIQUES APPLIQUÉS  
PROGRAMME DOCTORAL EN PHOTONIQUE

ÉCOLE POLYTECHNIQUE FÉDÉRALE DE LAUSANNE

POUR L'OBTENTION DU GRADE DE DOCTEUR ÈS SCIENCES

PAR

**Andreas SCHMOCKER**

acceptée sur proposition du jury:

Prof. S. Roke, présidente du jury  
Prof. C. Moser, Prof. D. Pioletti, directeurs de thèse  
Prof. S. Ferguson, rapporteur  
Prof. K. Ito, rapporteur  
Prof. A. Radenovic, rapporteuse



ÉCOLE POLYTECHNIQUE  
FÉDÉRALE DE LAUSANNE

Suisse  
2016



At the end of my life,  
I want to be able to tell a nice story!  
— from a friend





This work is dedicated to  
Karolina and Norio.



# Acknowledgements

I express my deep gratitude to my thesis director Prof. Christophe Moser and my co-supervisor Prof. Dominique Pioletti for the opportunity to conduct this research in their laboratories. I thank you for your patience, your enthusiasm and the time you took at any moment to support me.

I thank my thesis committee, Prof. Sylvie Roke, Prof. Keita Ito, Prof. Stephen Ferguson and Prof. Aleksandra Radenovic for their interest in the topic, their availability and the effort to evaluate this thesis.

I highly acknowledge Azadeh Khoushabi, Dr. Pierre-Etienne Bourban, Dr. med Constantin Schizas, Daniela Frauchiger, Dr. Benjamin Gantenbein and Dr. med Pascal Mosimann for their contributions and their help, in particular for carrying out tests together, writing papers and discussing our ideas. Special thanks also go to Sandra Jaccoud for the tremendous help with cell culture assays. I acknowledge Marc Jeanneret for his advice and help with mechanical designs, Dr. Georges Wagnières for his advice on Monte Carlo models, Jessica Dessimoz for her help with histology and Eva Roth for her assistance with biochemical assays.

I kindly thank Prof. Ung-il Chung, Prof. Takamasa Sakai and Dr. Katashima Takuya for hosting me in their laboratory and supervising me during two months in Tokyo.

I warmly thank my co-workers for the support and fun they provided: In particular, Sarah Monemhagdoust, Volker Zagolla, Salma Farahi, Sabrina Martone, Mickaël Guillaumée, Eric Tremblay, Edgar Emilio Morales Delgado, David Ziegler, Damien Loterie, Manon Rostykus, Dino Carpentras, Miguel Modestino, Montfort Frédéric, Sebastien Walpen, Paul Delrot, Enrico Chinello, Gaël Nardin, Timothé Laforest, Laurent Descloux, Claudia Rodriguez, Arnaud Mader, Philippe Abdel-Sayed, Ulrike Kettenberger, Tanja Hausherr, Adeliya Latypova, Valérie Malfroy, Virginie Kokocinski, Naser Nasrollahzadeh, Jens Antons, Reza Nassajian, Ioannis Papadopoulos, Carlos Macias, Rüdiger Scheu, Michael Reinke, Cornelis Lütgebaucks, Yuri Kuzminykh, Guillaume Petit-Pierre, Evangelia Zdrali and Vitalijs Zubkovs. I also thank my semester students Stefania Rissone, Noémie Saint Raymond, Cédric Elmaleh, Blaise Robert, Martin Gunn-Sechehayé, David Maycotte and Alexis Schizas.

I thank my parents Ruth and Andreas and my brothers Daniel and Michael for their continuous and unconditional support.

Finally, but most important, I thank Karolina Hegyaljai for being an excellent mother and girlfriend, and for having spent four years together with me in Switzerland. Norio, there is nothing more beautiful on earth than your laughter.

*Lausanne, 9<sup>th</sup> of November 2015*

Andreas Schmocker



# Abstract

Intervertebral disc degeneration is a major reason why we experience low back pain. Intervertebral discs are located in-between the vertebrae of the spine. They act, among other, as shock absorbers by distributing the mechanical load applied to the spine while giving it its range of motion. An intervertebral disc is composed of a center – a soft core, called nucleus pulposus which is surrounded by a strong ring called the annulus fibrosus. By disc degeneration, we mean a physical deterioration of either the nucleus and/or the annulus. It has been posited that low back pain could be alleviated by replacing the degenerated nucleus pulposus by a synthetic implant. However, such nucleus pulposus replacements have been subjected to highly controversial discussions over the last 50 years and their use has not yet resulted in a positive outcome to treat degenerated disc disease.

In this thesis, we report on the development of an implant material consisting of poly(ethylene glycol)dimetacrylate – a hydrogel – loaded with nano-fibrillated cellulose. Photopolymerization was selected as a polymerization method to “harden” the implant *in situ*. Thus, the implant can be injected in a liquid state through the annulus fibrosus with a small diameter cannula. Furthermore, an *in situ* photopolymerization method was developed along with an implanting device which was used to insert the composite hydrogel into an intervertebral disc *ex vivo*.

The volume of a human nucleus pulposus is several 100's of mm<sup>3</sup>, which is a substantial volume to photopolymerize. In order to ensure a homogeneous photopolymerization of this volume, a Monte Carlo model was developed. The model is able to predict accurately the volume of the photopolymerized implant in tissue cavities. This simulation tool was used to tailor the light scattering properties of the hydrogel by loading it with lipid particles. Thus, spherical implant shapes could be photopolymerized.

An implanting device was developed to inject and photopolymerize the liquid implant while monitoring the cross-linking reaction of the implant during photopolymerization using fluorescence spectroscopy *in situ* and in real-time. Using this device, synthetic nucleus pulposus implants were successfully inserted through a 1 mm incision in the annulus fibrosus of an *ex vivo* bovine intervertebral disc model and the long-term performance of the proposed nucleus pulposus replacement was evaluated.

The changes of the fluorescence signal throughout the photopolymerization reaction could be shown to correlate with the photopolymerization volume. It was thus possible to insert the synthetic implant in a controlled manner into the bovine disc model. The implant was able to significantly re-establish intervertebral disc height after surgery ( $p < 0.0025$ ) and maintain it

## Abstract

---

over 0.5 million loading cycles ( $p < 0.025$ ). Disc height is one of the essential parameters to restore and maintain in an intervertebral disc.

The excellent results achieved in these *ex vivo* experiments validated the implantation method and the device. More importantly, they showed that the novel implant material might resist mechanical loads similar to the loads that would be experienced in everyday life. However, longer tests ( $\sim 10$  million cycles) are required to determine whether this material would truly resist during a clinical study.

Key words: medical device, minimally invasive surgery, orthopedic implant, photopolymerization, Monte Carlo simulations, poly(ethylene glycol)dimethacrylate, fluorescence monitoring

## Résumé

La dégénération du disque intervertébral est une des raisons principales pour laquelle nous avons mal au dos. Les disques intervertébraux se situent entre deux vertèbres de la colonne vertébrale et lui donnent ses degrés de liberté de mouvement. Entre autres, ils absorbent les chocs et distribuent les charges appliquées à la colonne. Le disque intervertébral est composé en son centre du nucleus pulposus qui est confiné périphériquement par un tissu fibreux, l'annulus fibrosus. La dégénération du disque consiste en une détérioration physique du nucleus et/ou de l'annulus. Dans ce contexte de dégénération du tissu, il a été proposé que le mal de dos peut être soulagé en remplaçant le nucleus pulposus avec un implant synthétique. Cependant de tel remplacement du nucleus pulposus ont été le sujet de discussions contradictoires durant les 50 dernières années et cette procédure n'a pas encore mené à des résultats favorables pour traiter les disques dégénérés.

Dans cette thèse, un hydrogel qui se compose de poly(éthylène glycol) diméthacrylate chargé avec de la fibres de cellulose a été utilisé. La photopolymérisation a été choisie comme méthode pour durcir l'implant *in situ*, ce qui permet de l'injecter en état liquide à travers l'annulus fibrosus en utilisant une canule de faible diamètre. Pour parvenir à ce résultat, une méthode de photopolymérisation *in situ* a été développée incluant un appareil d'injection.

Le volume d'un NP humain est de plusieurs centaines de  $\text{mm}^3$ , ce qui représente un défi important pour obtenir une photopolymérisation homogène. Pour optimiser la photopolymérisation, un modèle Monte Carlo a été développé. Ce modèle est capable de prédire le volume photopolymérisé à l'intérieur d'une cavité de tissu. Cet outil de simulation a été utilisé pour adapter les propriétés diffusantes de l'hydrogel en le chargeant avec des lipides. Cette approche a permis de photopolymériser des implants sphériques.

Un appareil d'implantation a été développé pour injecter et photopolymériser l'implant liquide en mesurant simultanément la réaction chimique de l'implant basé sur la spectroscopie de fluorescence *in situ* et en temps réel. En utilisant cet appareil, des implants ont pu être injectés à travers une incision d'un millimètre et leur performance a été évaluée à long terme *ex vivo* dans un modèle de disque bovin.

Les changements du signal de fluorescence pendant la réaction de photopolymérisation ont pu être corrélés avec le volume photopolymérisé. Il était possible d'insérer l'implant synthétique d'une manière contrôlée dans le modèle du disque bovin. L'implant pouvait rétablir significativement la hauteur de disque après la chirurgie ( $p < 0.0025$ ) et la maintenir pendant 0.5 million de chargement cyclique ( $p < 0.025$ ). La hauteur de disque est un paramètre essentiel pour la restauration du disque intervertébral.

## Résumé

---

Ces résultats excellents obtenus pendant l'expérience *ex vivo* valident la méthode et l'appareil d'implantation. Plus important encore, ils démontrent que le nouvel implant peut résister à des charges similaires à celles appliquées à la colonne durant la vie quotidienne. Cependant, plus de tests sont requis (~ 10 million cycles), pour pouvoir envisager la possibilité d'une étude clinique.

Mots clefs : appareil médical, chirurgie minimale invasive, implant orthopédique, photopolymérisation, simulation Monte Carlo, poly(éthylène glycol)diméthacrylate, spectroscopie de fluorescence



# Zusammenfassung

Die Degeneration der Bandscheibe ist eine der Hauptursachen von Rückenschmerzen. Die Bandscheiben befinden sich zwischen je zwei Rückenwirbeln und sind verantwortlich für deren Biegsamkeit. Neben anderen Aufgaben fungieren sie als Stossdämpfer und verteilen mechanische Belastung. Eine Bandscheibe besteht aus einem weichen Kern – dem sogenannten Nucleus Pulposus – umgeben von einem starken Ring – dem Annulus Fibrosus. Unter Diskusdegeneration verstehen wir eine physikalisch Degeneration des Nucleus oder des Annulus. Es wurde postuliert, dass Rückenschmerzen gelindert werden können, indem der degenerierte Nucleus mit einem künstlichen Material ersetzt wird. Allerdings sind solche Implantate seit mehr als 50 Jahren kontrovers und ihr Gebrauch führte bisher nicht zu positiven klinischen Ergebnissen.

In dieser Doktorarbeit wird ein kürzlich entwickeltes Hydrogel aus Poly(Ethylen Glycol) Dimethacrylat, welches zusätzlich mit Zellulosefasern verstärkt wurde, benützt. Als *in situ* Aushärtungsmethode wurde die Fotopolymerisation gewählt. Somit kann das Implantat in flüssigem Zustand durch den Annulus Fibrosus eingespritzt werden. Eine *in situ* Fotopolymerisationsmethode sowie ein Instrument für die Implantation wurden entwickelt um das Komposithydrogel in eine Bandscheibe *ex vivo* ein zu setzen.

Das Volumen eines menschlichen Nucleus Pulposus besteht aus mehreren Hundert Kubikmillimetern Material und ist somit eine beträchtliche Herausforderung um mit Licht ausgehärtet zu werden. Um es homogen fotopolymerisieren zu können wurde ein Monte Carlo Modell entwickelt. Dieses Modell kann Fotopolymerisation in Hohlräumen des Gewebes simulieren und das fotopolymerisierte Volumen genau vorhersagen. Mit Hilfe dieses Simulationsinstrumentes konnten die Lichtstreuungseigenschaften anhand von Lipidpartikeln ideal angepasst werden, was zu kugelförmigen Implantaten führt.

Weiter wurde ein Gerät für die Implantation entwickelt um das flüssige Implantat einzuspritzen und zu photopolymerisieren. Gleichzeitig erlaubt das Gerät die Photopolymerisationsreaktion zu überwachen in dem die Fluoreszenz *in situ* und in Echtzeit gemessen wird. Anhand dieses Geräts konnten synthetische Nucleus Pulposus Implantate durch einen 1 mm breiten Einschnitt im Annulus Fibrosus erfolgreich in ein *ex vivo* Bandscheibenmodell eingesetzt werden, und dessen langfristige Leistungsfähigkeit evaluiert werden.

Es konnte gezeigt werden, dass die Änderungen des Fluoreszenzsignals während der Photopolymerisation mit dem ausgehärteten Volumen korreliert. Dies ermöglichte das kontrollierte Einfügen des künstlichen Implantates in das bovine Diskusmodell. Ein essentieller Parameter einer funktionellen Bandscheibe, ist deren Höhe. Das Implantat konnte die Höhe der Band-

## Zusammenfassung

---

scheibe nach der Operation in signifikanter Weise ( $p < 0.0025$ ) wiederherstellen und diese Höhe während 0.5 Million Ladungszyklen beibehalten ( $p < 0.025$ ).

Die exzellenten Ergebnisse dieses *ex vivo* Experiments validieren die Methode und das Gerät, welches zum Implantieren benutzt wurde. Es zeigt auch, dass das neue synthetisch Hydrogel typischen Belastungen in einer Wirbelsäule standhalten könnte. Es ist jedoch nötig Tests während eines längern Zeitraums ( $\sim 10$  Millionen Zyklen) durch zu führen um heraus zu finden, ob die Lebensdauer des Hydrogels genügend hoch ist.

Stichwörter: Medizinaltgerät, minimal invasive Chirurgie, orthopädisches Implantat, Photopolymerisation, Monte Carlo Simulation, Poly(Ethylen Glycol) Dimethacrylat, Fluoreszenz Spektroskopie

# Contents

<b>Acknowledgements</b>	<b>i</b>
<b>Abstract (English/Français/Deutsch)</b>	<b>iii</b>
<b>Table of contents</b>	<b>xi</b>
<b>List of figures</b>	<b>xiii</b>
<b>List of tables</b>	<b>xix</b>
<b>1 Introduction</b>	<b>1</b>
1.1 Epidemiology of low back pain . . . . .	1
1.2 Anatomy of the intervertebral disc . . . . .	2
1.3 Current treatment options of low back pain . . . . .	3
1.3.1 Conservative treatments . . . . .	3
1.3.2 Surgical treatments . . . . .	4
1.3.3 Limitations of current treatments . . . . .	4
1.4 Nucleus pulposus replacements . . . . .	5
1.4.1 Clinical aspects . . . . .	5
1.4.2 General requirements for the nucleus pulposus replacement . . . . .	5
1.4.3 State of the art in the current NP replacement development . . . . .	6
1.4.4 Biomechanical aspects . . . . .	7
1.5 Photopolymerization . . . . .	11
1.5.1 Photopolymerization of hydrogels . . . . .	11
1.5.2 Initiation of photopolymerization . . . . .	11
1.5.3 Photopolymerization modelling . . . . .	12
1.5.4 Photopolymerization control . . . . .	14
1.6 Objectives of the thesis . . . . .	15
<b>2 Photopolymerizable hydrogels for implants: Monte-Carlo modeling and experimental in vitro validation</b>	<b>17</b>
2.1 Abstract . . . . .	17
2.2 Introduction . . . . .	17
2.3 Hydrogel material and illumination . . . . .	19
2.4 Determination of absorption and scattering coefficient . . . . .	20

## Contents

---

2.5	Monte Carlo model for photopolymerization . . . . .	21
2.6	Experimental validation of the Monte Carlo model . . . . .	25
2.7	Modeling and experimental application of photopolymerization in tissue cavities . . . . .	27
2.8	Conclusion . . . . .	29
<b>3</b>	<b>Miniature probe for the delivery and monitoring of a photopolymerizable material</b>	<b>31</b>
3.1	Abstract . . . . .	31
3.2	Introduction . . . . .	31
3.3	<i>in situ</i> Photopolymerization Monitoring . . . . .	32
3.4	Surgical Device for Injection, Illumination and Monitoring . . . . .	33
3.5	<i>In situ</i> Photopolymerization Monitoring Results . . . . .	35
3.6	<i>in vitro</i> photopolymerization monitoring . . . . .	40
3.7	Conclusion . . . . .	42
<b>4</b>	<b>A photopolymerized composite hydrogel and surgical implanting tool for a nucleus pulposus replacement</b>	<b>43</b>
4.1	Abstract . . . . .	43
4.2	Introduction . . . . .	43
4.3	Materials and Methodes . . . . .	45
4.3.1	Sample preparation . . . . .	45
4.3.2	Material characterization tests . . . . .	47
4.3.3	Cytotoxicity . . . . .	48
4.3.4	Implantation of the hydrogel into an organ model . . . . .	49
4.3.5	Statistics . . . . .	51
4.4	Results . . . . .	51
4.4.1	Hydrogel design and selection . . . . .	51
4.4.2	Functional testing . . . . .	52
4.4.3	Cytotoxicity . . . . .	54
4.4.4	Implantation . . . . .	54
4.4.5	Histology . . . . .	55
4.5	Discussion . . . . .	56
4.5.1	Material design . . . . .	57
4.5.2	Surgical device design . . . . .	58
4.5.3	Evaluation of minimally invasive implantation procedure . . . . .	59
4.6	Conclusion . . . . .	60
<b>5</b>	<b>General discussion and conclusions</b>	<b>61</b>
5.1	Monte Carlo model of photopolymerization . . . . .	61
5.2	Monitoring device . . . . .	62
5.3	<i>Ex vivo</i> evaluation . . . . .	62
5.4	Impact and potential of photopolymerized implants . . . . .	63
5.5	Requirement for a NP replacement . . . . .	63
5.6	Outlook . . . . .	64

<b>A</b>	<b>Appendix - Monte Carlo</b>	<b>65</b>
A.1	Probability distribution of a point source . . . . .	65
A.2	Refraction and reflection at interfaces . . . . .	66
A.3	Absorption . . . . .	66
A.4	Scattering . . . . .	66
A.5	Propagation . . . . .	66
<b>B</b>	<b>Appendix - Loading up to 3 MPa</b>	<b>69</b>
	<b>Bibliography</b>	<b>92</b>
	<b>Curriculum Vitae</b>	<b>93</b>



# List of Figures

1.1	Bovine intervertebral disc after loading with jelly nucleus pulposus (NP), collagen-fiber annulus fibrosus (AF) and endplates. The fibers of the inner annulus were deformed radially, partially due to disc bulging. . . . .	2
1.2	Invasiveness of treatments in function of intervertebral disc (IVD) degeneration. The least invasive treatments are conservative treatments, then decompression surgery and nucleotomy. Later arthroplasty or fusions are required. A promising alternative is tissue replacement. . . . .	4
1.3	Maximal allowed exposure limits for living human tissues between 200 and 400 nm (UVC, UVB and UVA ranges). The allowed exposure decreases to a minimum between 260 and 300 nm – a dangerous range for DNA strands. It is slightly higher below this range (due to the shallow light penetration and lower wavelength). the allowed exposure is significantly higher at wavelength close to visible light (400 nm) which is due to the lower energy per photon in this range. The red peak is the illumination wavelength used in this work (the units are arbitrary). . . . .	12
1.4	Double-integrating-spheres setup: Photons can be detected in the first sphere (det 1), the second sphere (det 2), on the detector at the back end (det 3) or on the reference-detector (det 4). Five different events are possible: 1) backscattering/reflection 2) forward-scattering 3) ballistic transmission 4) absorption and 5) loss of the photon. . . . .	14
2.1	Poly(ethylene-glycol) dimethacrylate hydrogels. Left: with scattering particles (intralipids). Right: No scattering particles. The hydrogel without scattering particles has a Methylene blue dye to visualize the photopolymerized volume. a) samples during illumination. Illumination is performed with the output of a 600 $\mu\text{m}$ core diameter optical fiber placed 5 mm from the cuvette; b) after extraction of the un-polymerized liquid. The red lines indicate the polymerized volumes. Light dose and illumination area are the same for both samples. . . . .	18
2.2	Absorption curves of the used photoinitiator (Irgacure-2959, 1% w/v). The photo-sensitizer reacts best around 300 nm, but can also be used at longer, more bio-acceptable wavelengths. . . . .	20

## List of Figures

---

- 2.3 Transmission set-up at 365 nm to measure the extinction coefficient of either a scattering or an absorbing compound. The collimated beam is split into two arms, one is used as reference the second passes through the sample. The chamber is fixed. Its content can be injected or extracted. . . . . 21
- 2.4 Monte Carlo simulation of photopolymerized volume. The light source is the output of an optical fiber. a) Distribution of absorbed energy calculated by the Monte Carlo model. b) Fitted iso-levels at a given time-step: solid hydrogel in the center and liquid hydrogel precursor outside c) polymer-volume-growth over time. . . . . 24
- 2.5 a) Photorheology measurement of the PEGDMA hydrogel: The gel point (change from liquid to solid) is reached after approximately 250 seconds corresponding to 40% of absorbed energy. b) Interactions of photons with a tissue-cavity: The red lines indicate the paths of the tracked photon package. . . . . 25
- 2.6 Fig. Four different photopolymerized hydrogel samples (Table 1). a) Cuvette-setup with a fiber immersed into the liquid hydrogel precursor. b) Volumes of experimentally polymerized samples (stars and triangles) and computed results (colored lines) are compared. c) Pictures of the shapes of experimentally polymerized and simulated samples (colored contours) after 3, 5 and 10 minutes of light illumination: The black arrow shows an area where the liquid hydrogel precursor did not solidify due to the size of the cuvette. The white arrow shows an area where polymerization took place due to polymer-diffusion, swelling and back-reflections. . . . . 26
- 2.7 a) Schematic: the purple arrows show possible reflections and refractions of back-scattered photons. b) autofluorescence of a bovine intervertebral disc tissue cavity [1] filled with a PEGDMA-hydrogel and illuminated with a light-probe consisting out of an 18 gauge needle and a 600  $\mu\text{m}$  fiber. . . . . 27
- 2.8 Fig. 8 Photopolymerization of a hydrogel within a tissue cavity: a) the hydrogel precursor ( $\mu_a = 0.43 \text{ cm}^{-1}$ , variable  $\mu_s$ ) is injected into the cavity. The surrounding tissue is modeled with an absorption coefficient of  $\mu_a = 0.33 \text{ cm}^{-1}$  and scattering coefficient  $\mu_s = 210 \text{ cm}^{-1}$ . An optical fiber (violet arrow) is introduced into/next to the cavity (NA=0.22, diameter 600  $\mu\text{m}$ ), the color-scale indicates the amount of absorbed energy per voxel. The hydrogel precursor requires a minimal irradiance of 0.52  $\mu\text{J}$  per voxel corresponding to a fluence of 520  $\text{mJ}/\text{cm}^2$  for photopolymerization. In a) the probe is placed several millimeters away from the cavity b) the probe is located next to the cavity wall c) the probe is in the cavity, no scattering additives are present in the gel ( $\mu_s = 0.000 \text{ cm}^{-1}$ ) d) low amount of scattering particles (SP) ( $\mu_s = 0.1 \text{ cm}^{-1}$ ) e) medium amount of SP ( $\mu_s = 1 \text{ cm}^{-1}$ ) f) high amount of SP ( $\mu_s = 10 \text{ cm}^{-1}$ ) . . . . . 28



3.1	Schematic illustration of a probe for a) <i>in situ</i> photopolymerization and b) <i>in situ</i> photopolymerization monitoring. In a) polymer precursor (orange) is injected into a tissue cavity and illuminated with a UV light for photopolymerization. Scattering particles enhance amount of photopolymerized polymer (violet) by homogenizing the light in the volume. In b) a second beam of light is used to monitor the polymerization reaction. This monitoring light can be reflected or backscattered by the polymer directly (1), the surrounding tissue (2) or via the scattering particles (3). . . . .	33
3.2	Schematic illustration of the illumination and detection system. The sample is illuminated with a LED light source (365 nm) to photopolymerize the injected photoreactive precursor and with a green light source (532 nm) to monitor photopolymerization. The spectrometer records the back-scattered fluorescence and Raman spectra. The distal tip of the device consists of a cannula containing the optical fiber and a circular chamber to inject the liquid photopolymer. . . .	34
3.3	Liquid samples were illuminated with a 600 $\mu\text{m}$ fiber. a) back-ground signal recorded when immersing the probe into water. b) spectra over time during photopolymerization of a PGDMA sample. c) the change in intensity over time for different samples measured at 580 nm without NFC fibers and d) with NFC fibers. e) resulting volumes after photopolymerization without NFC fibers and f) with NFC fibers . . . . .	36
3.4	The photopolymerized volume is imaged from outside the cuvette (a), a threshold is applied within a relevant area (b and c) and by a pixel count the size and the signal intensity plotted over time (d). The <i>ex situ</i> signal does not show any peak between 2 and 4 minutes, while during <i>in situ</i> monitoring of the same sample such a peak appears (e). In detail evolution of the sample size and geometry over time (f). . . . .	38
3.5	Saturation of the monitored fluorescence signal. The fiber tip was placed at 500 $\mu\text{m}$ from the bottom of an optical cuvette containing the liquid PEGDMA-NFC hydrogel (a). The UVA light (b) and visible light (c) are distributed within the entire volume. d) the monitoring signal, measured at three different wavelengths starts to saturate after approximately 120 minutes. e) photorheology of a 500 $\mu\text{m}$ layer of hydrogel to measure the elastic modulus during solidification. . . . .	39
3.6	PEGDMA hydrogel is injected into a bovine intervertebral disc. a) the probe is used in a monitoring-only-mode at 532 nm, number (1)-(4) denote different probing positions. b) and c) the UVA light (365 nm) is switched on to photopolymerized the injected sample. The different positions (1)-(4) were evaluated: d) at the front of the intervertebral disc, e) at the side, f) at the back without hydrogel and g) in the middle with hydrogel. h) <i>in vitro</i> photopolymerization monitoring: a spectra over time from 0 to 45 min (black arrow). i) fluorescence intensity is tracked in function of wavelength over time. . . . .	41

## List of Figures

---

- 4.1 Customized compression setups: a) unconfined compression setup in which the sample's area and applied load can be measured simultaneously using a transparent casing and an optical tracking system, b) confined compression setup for swelling pressure assays, c) extrusion setup for tissue extrusion d) bioreactor for long-term incubation and testing f) live IVD organ culture within the bioreactor chamber. . . . . 47
- 4.2 To measure the disc height, the disc is compressed using the sterilized caliper, (manually a short and high compressive force is applied: the disc should deform elastically) the caliper is released and the disc height is measured in the relaxed state (a). Four measurements are taken and averaged (b). The diameter of the disc is measured once after isolation in two directions using the same method. A special cutter is used to cut discs in the middle for histology (c). . . . . 49
- 4.3 Testing protocol and predicted evolution of IVD disc height during degeneration, surgery and loading. Discs were isolated at day 1, Papain was injected at day 2 to induce the degeneration of the IVD over an incubation period of 6 days (day 2-8), the composite hydrogel was implanted at day 8 followed by a 6 day cyclic loading period (day 9 - 15) and then evaluated using histology at day 16. All states (four red boxes) were compared between each other: healthy state (after disc isolation; disc height: h1), pre-operative state (impaired and degenerated organ; disc height: h2), post-operative state (repaired; disc height: h3) and state during follow-up (after cyclic loading; disc height: h4). Before evaluating the height of an IVD in one state the specimen was conditioned by a 12h free swelling (FS) and a 2h cyclic compression (CC). . . . . 50
- 4.4 Hydrogel properties tuning in function of a) modulus, b,c) maximal rupture strain and d) water content. Development step 1 (in red): PEGDMA 6 kDa hydrogel has a similar modulus (a) and water content (d) as the NP, but fails at a strain of 63% (b). Step 2 (in red): The PEGDMA molecular weight was increased to 20 kDa in order to improve the hydrogel deformability (c), however this hydrogel shows a lower modulus (a). Step 3 (in red): This hydrogel was then reinforced with 0.5 vol% NFC fibers to reach the desired modulus (a) while keeping the same deformability and high water content of the NP (d). . . . . 52
- 4.5 The three functional tests done in order to evaluate the PEGDMA-NFC composite (PEGDMA A20 kDa with 0.5 vol% NFC) in comparison to native nucleus pulposus tissue (a) confined compression stress-strain curves that evaluate the samples confined behavior similar as within the real intervertebral disc tissue, (b) swelling pressure which directly affects the disc height after implantation and (c) the maximum tolerated stress before extrusion which assesses the sample's resistance to extrusion and expulsion. . . . . 53
- 4.6 Live/Dead assay using human nucleus pulposus cells. Red box (a - g) liquid un-polymerized precursor on cells. h) and i) solid polymerized hydrogel on cells. 53

4.7	a) Customized minimally invasive surgical probe used for the hydrogel implantation. Liquid hydrogel precursor injection and illumination are combined within one single needle (cannula). Different joints ensure high pressurization during the injection. An optical fiber permits the light delivery for photopolymerization. b) At the distal tip of the instrument, the hydrogel precursor flows between cannula wall and optical fiber into the intervertebral disc. c) By recording the reflected illumination spectra a signal intensity is calculated. The intensity of the signal correlates with the amount of photopolymerized material and therefore provides valuable information about the reaction state of the implant in real time. d) Intervertebral disc during photopolymerization. . . . .	55
4.8	a) Disc height of bovine tail IVD (n = 3) before surgery (degenerated state), after surgery (repaired state) and after 0.5 million cycles of <i>ex vivo</i> compressive loading (loaded state) are compared to the initial disc height (healthy disc). The disc height significantly increased after implantation of the PEGDMA-NFC composite hydrogel. The increase in disc height remained significant after loading. b) Bovine tail IVD before surgery and c) after surgery. d) IVD cut in half showing the hydrogel, annulus fibrosus (AF) and the endplate (EP). Histological sections of the bovine IVD samples (H&E-staining): annulus fibrosus tissue (purple) and nucleus pulposus tissue (violet). e) Native nucleus pulposus, f) nucleus pulposus replaced with implanted hydrogel and g) interface between native tissue and implanted tissue. . . . .	56
4.9	a) Micro CT and b-c) MRI scans of an IVD. Red arrows: control with an empty cavity (grey) and cavity filled with composite hydrogel (whitish). The injected volume can be monitored by CT scans by replacing the water in the hydrogel with a water-based, biocompatible Iodine marker (Iopamiro® 370, Bracco Suisse SA, Manno, Switzerland). A similar effect can be achieved by exploiting the T2 signal of MRI without using a marker [64] . . . . .	59
B.1	High compressive loading of IVDs up to 3 MPa. a) Protocol: First, a cyclic load of $0.3 \pm 0.015$ MPa was applied over 300 cycles. Then the load was increased step-wise by 0.3 MPa with a loading amplitude of 10 % of the nominative load (each time 300 cycles) until reaching a load of $3 \text{ MPa} \pm 0.15 \text{ MPa}$ . b) The disc height was measured after each 300 loading cycles. The disc height decreased faster for healthy IVDs, than for IVDs with hydrogel and no NFC fibers or hydrogel with NFC fibers. However, the final disc height was not significantly different $p = 0.68$ (healthy vs. no NFC) $p = 0.26$ (healthy vs. NFC). . . . .	70



# List of Tables

1.1	Existing NP replacements: *assumed due to lacking literature information, **ac- cording to the Thompson & Pfirrmann grading system . . . . .	6
1.2	Nucleus pulposus (NP) and annulus fibrosus (AF) properties of humans (if not stated otherwise). 1: maximal stress which can be maintained by the tissue itself, without deswelling; 2: angle measured between the fiber and the superior- inferior axis; d: degenerated sample; h: healthy sample; B: bovine sample; r: radial direction; $\theta$ : circumferential direction; a: anterior; p: posterior. . . . .	8
1.3	Test profiles and associated parameters for lumbar IVD prostheses evaluation (source: ASTM [2]). . . . .	10
2.1	Preparation of PEGDMA – 6 kDA hydrogel samples . . . . .	19
2.2	Measured scattering and absorbing coefficients at 365 nm (mean and maximal measurement error). These values are used for the simulations (*assumed values for simulations) . . . . .	21
3.1	Preparation of PEGDMA hydrogel samples . . . . .	35



# 1 Introduction

This introduction includes five sections covering the epidemiology of low back pain (section 1.1), the anatomy of the intervertebral disc (IVD) (section 1.2), the current treatment options of low back pain (section 1.3), a state of the art on nucleus pulposus (NP) replacements (section 1.4) and photopolymerization (section 1.5). Section 1.6 covers the objectives of the thesis.

## 1.1 Epidemiology of low back pain

The impact of low back pain on society is tremendous [3]. Lower back pain is experienced by 70 to 85 % of the world's population once in their life. It has an annual average prevalence of 10-20 % in the adult population which rises to a maximum of 15-30 % at the age of 65 and then starts to drop again [4, 5]. In the United States of America at any given time 1 % of the population is disabled chronically and another percent temporarily due to low back pain [6]. Moreover, 50 % of the working population has symptoms of low back pain every year [7]. The direct costs were estimated to be up to 355 \$ per capita and annum and 507 \$ for indirect costs [8] which results in a total of 100 to 200 billion for a country such as the United States of America [9]. Low back pain is more prevalent in female than in male subjects (35.3 % vs. 29.4 %) and for people having a higher income than a medium or small income (32.9% vs. 25.4 % and 16.7 %), while there is no significant difference between patients living in urban or in rural areas (30.7 % vs. 31.9 %) [10].

Low back pain can be categorized in four groups [11, 12]: 1) mechanical low back pain (80-90 %), 2) low back pain with neurological involvements (10-15 %), 3) specific spinal pathologies (1-2 %) and 4) low back pain with non-spinal origins (1-3 %). Mechanical low back pain consists mainly of non-specific pain (65-70 %) with unknown origins and which is usually attributed to muscular strains or ligamentous injuries. Other reasons for mechanical low back pain are degenerative disc disease (DDD; also called discogenic pain), degenerative joint disease (pain induced at the facet or sacroiliac joint), vertebral fractures, congenital deformities (e.g. scoliosis, kyphosis or transitional vertebrae), spondylolysis, instability and failed back surgery syndrome. Neurological involvements include herniated disc (mechanical

and chemical irritation of the nerve root), annular fissures (chemical irritation of the nerve root), spinal stenosis, intervertebral foraminal stenosis (stenosis on the side arms of the main nerve root), failed back surgery syndrome (e.g. recurrent herniation or inflammation of the nerve root) and certain infections such as herpes zoster. Specific spinal pathologies include malignant tumors, infections such as osteomyelitis (infection of the bone or bone marrow), inflammatory arthritis and certain diseases such as Paget or Scheuermann disease. Finally, low back pain with non-spinal origins can be due to gastrointestinal diseases, renal diseases, abdominal aortic aneurysms, chronic widespread pain, somatoform disorders or malingering. Risk factors associated to low back pain are obesity [13], smoking, heavy lifting [14], history in spinal trauma, family history of low back pain, trunk asymmetry, increased height, female gender, competitive sports, high level of physical activity, depression and stress [15].

→ *Low back pain is major healthcare issue. There is a wide range of factors inducing low back pain. In 50 to 65 % of all low back pain cases the pain is of unknown origin.*

### 1.2 Anatomy of the intervertebral disc

The intervertebral disc (IVD), situated between two vertebrae, consists of the nucleus pulposus (NP) and the annulus fibrosus (AF) (fig. 1.1). As their names suggest, the annulus fibrosus is a fibrous ring surrounding the jelly “nucleus pulposus” core. Intervertebral discs and vertebrae are delimited by a cartilage tissue, the endplates. When the IVD is loaded, the poro-elastic NP is compressed and redistributes the vertically-applied body weight into radial directions, resulting in so called disc bulging [16]. The collagen fibers of the AF are stretched and the vertical load transformed into elastic strain energy [16]. The poro-elasticity of the NP and the fluid flow through the endplates [17] result in a viscoelastic response of the IVD segment including long relaxation times and strong creep behaviors [18]. Disc mechanics are significantly influenced by the non-linear disc permeability, the pressure at the endplates and the fluid content of the NP [19, 20]. The integrity of the AF is also key as the presence of tears in this structure was shown to affect the disc mechanical behavior [21, 22].

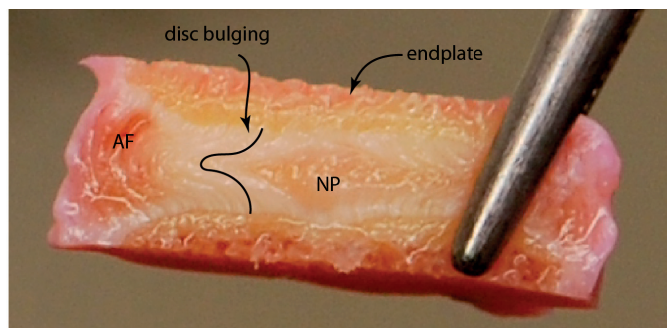


Figure 1.1: Bovine intervertebral disc after loading with jelly nucleus pulposus (NP), collagen-fiber annulus fibrosus (AF) and endplates. The fibers of the inner annulus were deformed radially, partially due to disc bulging.



### 1.3. Current treatment options of low back pain

---

Indeed, disc degeneration substantially changes the mechanical behavior of the disc [23] and may or may not lead to pain – an essential aspect which remains unclear in a considerable amount of cases [24]. Early degeneration is often associated with a lower capability to bind water to the proteoglycans in the NP. The NP fails then to distribute uniformly the pressure to the AF. Later degeneration is characterized by excessive motion of the spinal segment and pain (due to the motion itself, nerve impingement or inflammation). The final stage of degeneration is characterized by bony ingrowth and limited or no motion. Disc degeneration is commonly characterized using the Pfirrmann [25] and Thompson grading [26] ranging from 1 (healthy) to 5 (final degenerative stage).

→ *The poro-elastic properties of the NP play a crucial role in mechano-transduction and also during disc degeneration. Beside other factors, IVD degeneration is characterized by a loss of water in the NP which results in a natural fusion of the two adjacent vertebrae during the final stage of degeneration.*

### 1.3 Current treatment options of low back pain

Two basic approaches exist to treat low back pain: conservative and surgical treatments. Pain is treated with conservative measures first to postpone surgery as long as possible.

#### 1.3.1 Conservative treatments

Conservative treatments of low back pain include medication, rehabilitation, transcutaneous electrical nerve stimulation, epidural steroid injection, radiofrequency treatments, epidural neuromodulation, intrathecal drug administration, chiropractic manipulation, osteopathic manipulation, yoga, acupuncture, spa therapy, physical therapy and herbals [6, 27]. Ninety percent of people respond rapidly to such treatment and are able to recover and return to work in less than three month [5]. However, for instance, physical therapy was shown to be effective for acute low back pain, but wasn't able to improve outcomes in case of chronic low back pain [28]. Based on different reviews it was concluded that only 54% of the studies could show a better long-term outcome (in terms of costs) of physical therapy over surgery [29]. A similar, contradictory situation was found for opioid-based pain killers. On one hand patients who received opioids have a higher satisfaction than those who didn't [30]. On the other hand it was also shown that between 36% and 56% of chronic low back pain patients abuse of opiates when taking them [31]. Recently, it became generally accepted that additional factors related to psychological issues need to be accounted for. For instance sleep disturbance, fear avoidance, catastrophizing, obesity, depression, anxiety were proposed to be taken into account [32]. Therefore certain authors suggest to focus more on programs that encourage physical activation despite pain, address underlying mental health issues, and foster lifestyle behavior modification [32]. Finally, it was proposed that a major challenge is lower back pain prevention and an optimum management of disability as opposed to treating lower-back pain

as a serious health disorder [6, 33]. However, attempts to decrease the amount of incidents by primary prevention have failed and it was then suggested that prevention using negative consequences of low back pain might be more fruitful [5].

### 1.3.2 Surgical treatments

If a patient does not respond to conservative measures over a certain duration (e.g. six month), surgical treatments may be proposed. They consist mainly of decompression, nucleotomy, arthroplasty and fusion (fig. 1.2). During an early stage of degeneration decompression surgery is performed to reduce the pressure on the spinal canal. In case of a more severe degeneration including herniation, a nucleotomy (also discectomy) is performed. Later, arthroplasty options such as a total disc replacement may be used to reestablish joint motion. Finally, the joint is immobilized by a fusion. A fusion is the most invasive and, on the long term, also most expensive treatment. If conservative measures fail, currently in many cases the gold standard remains spinal fusion [34].

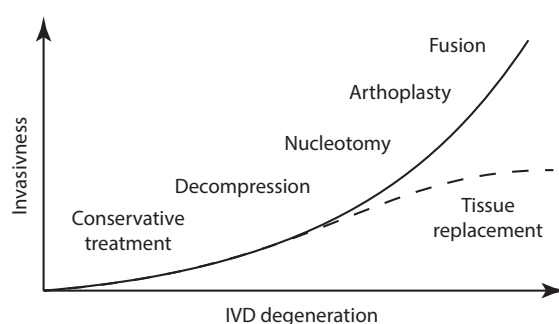


Figure 1.2: Invasiveness of treatments in function of intervertebral disc (IVD) degeneration. The least invasive treatments are conservative treatments, then decompression surgery and nucleotomy. Later arthroplasty or fusions are required. A promising alternative is tissue replacement.

### 1.3.3 Limitations of current treatments

The quantity of interventional treatment options increases steadily. The amount of spinal fusions increased by a factor 7 to 15 within an investigated period of 6 years [35, 36]. The efficacy of fusion still remains partially controversial [32]. A considerable amount of studies were not able to show that fusion is more efficient than conservative treatment [37]. While other studies showed that commonly used fusion techniques have better outcomes than conservative treatments, especially if patients are well selected [38, 39]. Another issue for fusion is that the pain may be alleviated temporally, but problems are shifted to an adjacent disc [40]. Finally, if fusion fails, the only option is another fusion [41]. Unfortunately surgical arthroplasty-options related to the IVD are not sufficiently effective [42] and it was not possible to show their superiority over fusion [43]. Yet, it is desirable to use less invasive treatments.

This may include any possible treatment stopping or slowing down spinal degeneration [44] such as tissue replacements (fig. 1.2). Anderson concluded in one of his studies that more extensive surgery on a patient's IVD does not prevent further surgery [45]. This essentially means that treatments should be kept simple (minimally invasive, cutting as few native tissue as possible, etc.). Finally, a cost analysis was able to demonstrate that percutaneous, minimally invasive techniques are less expensive in the long run and suggests that their appropriate use may further prevent the use of more invasive surgery [27]. Therefore, developing a minimally invasive technique to replace the NP or a part of the IVD could have a positive impact as it might be able to postpone the course of degeneration.

*→ DDD is treated by conservative and surgical measures. However, if conservative treatment fails, in many cases spinal fusion remains the gold standard. Less invasive techniques might have the potential to postpone the process of IVD degeneration.*

## 1.4 Nucleus pulposus replacements

### 1.4.1 Clinical aspects

In the development process of an NP replacement, it is essential not only to address a biomechanical function, but also a clinical need. The goal of re-establishing disc mechanics is pain relief. NP replacements might be able to address the following pathologies: DDD, degenerative joint disease, spondylolisthesis and instability. As mentioned in section 1.3.3 it is essential to carefully select patient groups for a specific treatment. As presented in section 1.1, 15-40 % of low back pain can be associated with intervertebral disc mechanics and intervertebral disc failures. Thus, if patients are thoroughly selected, surgical interventions to reestablish disc mechanics have the potential to postpone or even replace more invasive treatments. For DDD, degenerative joint disease, spondylolisthesis and spinal instability reestablishing disc mechanics can relieve pain. For herniated discs and certain cases of spinal stenosis, reestablishing disc mechanics might prevent pain. The less invasive the surgery is, the better the outcome will be.

*→ It is crucial to select patient groups and clinical targets carefully. It is essential to focus on the goal of an NP replacement which is pain relief.*

### 1.4.2 General requirements for the nucleus pulposus replacement

Any medical device has to comply with regulations in terms of security and biocompatibility. In this respect, the most advanced implant for nucleus pulposus replacement is probably GelStix, although it has not yet obtained approval from the US Food and Drug Administration (FDA). The major failure aspects in the development of NP replacements are implant expulsion, implant subsidence, endplate remodeling or poor disc kinematics [46, 47]. Factors

## Chapter 1. Introduction

Table 1.1: Existing NP replacements: \*assumed due to lacking literature information, \*\*according to the Thompson & Pfirrmann grading system.

Replacement	Type	Low in- vasive- ness	Failure / issue
Prosthetic Disc Nu- cleus & HydraFlex	Inserted cushions [51]	no	Extreme stiffness [52], implant migration [53]
Dascor	Injected in balloon, <i>in situ</i> cured [54]	+/-	Expulsion [55]
NeuDisc	Inserted at 25% hydration level, swollen <i>in situ</i>	+/-	Implant migration*
NuCore	<i>in situ</i> cured [56]	yes	Only for degradation lev- els 1 and 2**
BioDisc	Injected adhesive with covalent bonding [41]	yes	Inability to restore disc height [57]
Aquarelle	Strongly swelling hydrogel [51]	no	Extrusion [57]
Newcleus	Gradually introduced spiral	+/-	Elevated stiffness [58]
GelStix	Worm-like hydrophilic material [59]	yes	Only for degradation lev- els 1 and 2**
DiscCell	Injected water-in-oil-emulsion	yes	NA
InterCushion	<i>in situ</i> assembly	no	Implant migration

such as degradation, wear and aging play an important role as well [48, 2]. However, it is remarkable that no clear consensus for material properties exists for IVD tissue replacements [49]. For instance it is unclear whether mimicking the time-dependent or viscoelastic behavior is necessary or whether reestablishing nutrient transport and fluid equilibration, required for healthy tissue, is also required for an implant [50]. Moreover, it was found that other factors such as for instance adhesion between implant and native tissues were not sufficiently addressed in the past [46]. It is important to take into account such issues when designing a surgery technique or an implant.

→ *It is necessary to specifically address the risks of expulsion/extrusion, subsidence, remodeling of the endplate and poor disc kinematics when designing an NP replacement.*

### 1.4.3 State of the art in the current NP replacement development

Dozens of different tissue replacements and implants have been proposed to replace NP, AF or the entire IVD. Many of them consist of materials to replace or regenerate parts of the intervertebral disc tissue. In Table 1.1 recent mechanical option of NP replacements are listed.

Silk fibroin-polyurethane composite hydrogel [60], PNIPAAm-PEG branched copolymers [61, 62], photo-cross-linked carboxymethyl-cellulose hydrogels [63], poly (vinyl alcohol) [64],

collagen-hyaluronan hydrogel [65], oxidized-hyaluronic-acid/adipic-acid-dihydrazide hydrogel [66], gelatin-agar systems [67], tween 20 trimethacrylates composite hydrogel [68], amino acid sequences derived from proteins [69], alginate/chitosan, polyglycol/poyl acid, poly- $\epsilon$ -caprolactone [70], Poly(1,8 octanediol malate), PDLLA/bioglass and bone matrix gelatin/poly(polycapro-lactone triol malate) [71] have been reported as potential NP implants or scaffolds. Moreover, to seal the AF, tissue fibrin sealants [72, 73], synthetic agents, collagen-based compounds [74] and tissue adhesive glues including hydrogels have been proposed [46].

Many regenerative options are under investigation, but have not resulted in any significant clinical outcomes up to date [75]. It is commonly accepted that materials for biological IVD repair have to overcome significant obstacles until they can be used on patients [76]. This would indicate that mechanical solutions might be a reasonable intermediate step to address. As presented in Table 1.1 all recent tissue replacement or implant approaches failed or could not be used to treat DDD above a Pfirrmann grade of 2. Therefore, in view of this history of failure, we posit that the wrong choice of implant requirements have led to inappropriate treatments in the past. This implies that it is essential to attack the problem of low back pain in a structured manner taking into account clinical, pathological, design and engineering issues.

*→ Dozens of replacement approaches have been tested. None was able to treat DDD above a Pfirrmann grade of 2. It is necessary to develop devices which allow to treat discs with higher grades of degeneration.*

### 1.4.4 Biomechanical aspects

Many models are not able to reflect the tri-phasic (solid, fluid and ionic species) composite complexity of the NP or AF tissue. Several approaches were proposed, first at equilibrium for instance by Flory and Huggins [77] and under dynamic conditions by Mow [78]. Based on the energy balance and inequality of entropy the derivative of the material's energy function ( $F_{tot}$ ) and sum of partial pressures ( $\Pi_i$ ) is zero at equilibrium. The mechanical behavior of any biological tissue (or material) can be illustrated by the following formula :

$$\Pi_{tot} = \left. \frac{\partial F_{tot}}{\partial n} \right|_{equ} = \Pi_{el} + \Pi_{mix} + \Pi_{ion} + \Pi_{ext} = 0 \quad (1.1)$$

The elastic term ( $\Pi_{el}$ ) is a function of the invariants of the Cauchy-Green deformation tensor and eventually the tissue's fiber orientations [79], the mixture term  $\Pi_{mix}$  depends on the changes in enthalpy due to mixing between liquid and solid phase [80] (sometimes also referred to as liquid pressure term), the external forces term  $\Pi_{ext}$  is due to mechanical loads form outside and the ionic term  $\Pi_{ion} = RT(I^l - I^s)$  is a function of the ionic strength of the liquid ( $I^l$ ) and the solid phase ( $I^s$ ) which further depend on the degree of ionization and the pH; R being the Boltzmann constant and T the temperature.

## Chapter 1. Introduction

Table 1.2: Nucleus pulposus (NP) and annulus fibrosus (AF) properties of humans (if not stated otherwise). 1: maximal stress which can be maintained by the tissue itself, without deswelling; 2: angle measured between the fiber and the superior-inferior axis; d: degenerated sample; h: healthy sample; B: bovine sample; r: radial direction;  $\theta$ : circumferential direction; a: anterior; p: posterior.

Primary NP and AF properties	Min	Max
<b>NP</b>		
Hydrostatic pressure [81]	0.1 MPa	2.3 MPa
Equilibrium stress <sup>1</sup> [82]	0.1 MPa	0.23 MPa
Equilibrium stress <sup>1</sup> semi-confined [83]	0.15 MPa	0.4 MPa
Swelling pressure [23]	<sup>d</sup> 0.037 MPa	<sup>h</sup> 0.138 MPa
<sup>B</sup> Equilibrium stress <sup>1</sup> under compression [84]	0.005 MPa	0.062 MPa
<sup>B</sup> Swelling pressure [84]	0.017 MPa	0.039 MPa
Swelling ratio ( = water content) [48]	4.0 ( = 80%)	9.3 ( $\approx$ 90%)
Diurnal, overnight volume increase [20]	0.1 cm <sup>3</sup>	2.7 cm <sup>3</sup>
Strain [85]	$\pm 10\%$	$\pm 20\%$
Relevant relaxation-time	5 min [49]	9h [23]
Hydraulic permeability	<sup>B</sup> $0.7 \times 10^{-15} \text{ m}^4/\text{Ns}$ [84] <sup>h</sup> $0.9 \times 10^{-15} \text{ m}^4/\text{Ns}$ [23]	<sup>B</sup> $18 \times 10^{-15} \text{ m}^4/\text{Ns}$ <sup>d</sup> $1.4 \times 10^{-15} \text{ m}^4/\text{Ns}$
Poisson ratio [49]	0.35	0.62
Aggregate (confined compression) modulus	<sup>B</sup> 0.31 MPa [84]	1.01 MPa [23]
<sup>B</sup> Aggregate modulus with $\sigma_0$ [86]	26.7 kPa	69.4 kPa
Elastic toe modulus [49]	3.3 kPa	44 kPa
pH [87]	6.9	7.2
Dynamic shear modulus [88]	7 kPa	21 kPa
Viscous loss angle [88]	23°	30°
<b>AF</b>		
Elastic toe modulus [89]	<sup>r</sup> 0.19 MPa	$\theta$ 2.5 MPa
Linear elastic modulus [89]	<sup>r</sup> 0.45 MPa	$\theta$ 45 MPa
Ultimate tensile stress [90]	2.1 MPa	12.9 MPa
Dynamic shear modulus [91]	100 kPa	400 kPa
Fiber orientation <sup>2</sup> [92, 93, 94]	<sup>a</sup> 23.5°	<sup>p</sup> 67.3°
# of tissue layers [95]	15	25
Maximal tensile strains [16]	2.7 %	24.6 %

Before discussing the essential biomechanical aspects for a NP (or AF) replacement, it is important to understand the function of native NP or AF tissues. The NP is characterized by two essential properties its poro-elasticity [50] and its swelling behavior [89]. The poro-elasticity allows it to move almost freely within the IVD and to distribute the stress during loading to the surrounding AF [96]. The swelling properties induce an osmotic pressure which is essential for diffusion of nutrients [41, 50] such as oxygen or glucose and waste products such as lactic acid or carbon dioxide [97]. On average  $1.3 \text{ cm}^3$  of fluid are transported through the endplate or the AF every night by diffusion [20]. This is crucial because the NP is the biggest avascularized organ of the human body. The strength of the NP is dictated by type II collagen and the swelling by proteoglycans in the extra cellular matrix, where the charge density which is due to sulfated glycosaminoglycans imbibes water and induces the osmotic pressure [98]. NP cells express collagen type II, aggrecan and certain proteins such as HIF-1 $\alpha$  and MMP-2 [99]. Notochordal cells in the NP are implicated in the production of this extracellular matrix [100], but their role is not entirely clear yet [101].

The multilayered, criss-crossed patterned AF distributes loads along collagen bundles. It is characterized by different primary fiber orientations [95, 102], exceptional strength and the capability to reorient depending on the applied load [103]. The fibers consist up to 60% of stiffer type I collagen and softer type II collagen with varying ratios depending on the position in the AF [104]. The AF plays a crucial role in disc budging and holding in place the NP. Thus, its integrity, local stiffness and the anchorage within the neighboring endplate have a fundamental impact on the IVD joint mechanics and the mechano-transduction in the IVD [105]. In Table 1.2 different properties of the NP and AF are presented.

### 1.4.4.1 Review on biomechanical characterization of nucleus pulposus replacements

To evaluate a NP replacement, standardizing bodies recommend to perform static or dynamic axial-compression-, axial-torsion- and shear-tests including functional range of motion, and subsidence-, aging- and swelling-pressure-tests[106]. Also other tests and evaluation of properties were proposed, examples are resistance to radial bulging [107], self-exerted pressure, ability to return to a complete level of hydration, extrusion resistance, mechanical overloading until failure [108] and indentation [109]. Moreover, it was proposed to measure wear by measuring dry weight before and after a test [110]. If applicable, polymer degradation has to be considered [111]. Brittle materials lead also to more material degradation. Therefore the Poisson ratio [112] or its fracture energy [113], often correlated with ductility and low brittleness, could be measured. A range of compression and tensile tests exist [114, 115]. To evaluate adhesion of biomaterials, peel tests [116], adhesion to tape [117], scratching tests [118], shear strength of adhesives using pin-and-collar specimen [119] and lap shear tests [120] pull out and shear test [121] were proposed.

For biocompatibility the following tests are required: cytotoxicity, sensitization, irritation or intracuraneous reactivity, systemic toxicity (acute), subchronic toxicity (subacute toxicity), genotoxicity, implantation and haemocompatibility [122].

For implantation and mechanical evaluations three main options exist:



## Chapter 1. Introduction

1. Plastic IVD models resist the minimal two-month-period required for 10 Mio. fatigue cycles, but it should be questioned how close they can imitate *in vivo* conditions [114]. For such tests the use of AF-mimicking silicone molds and the following loads (Table 1.3) were suggested [2]. It was also proposed that the NP replacement's reliability could be assessed by a lower amount of fatigue cycles, if it is determined that a surrogate annulus will not survive a total of 10. Mio cycles [106].
2. *ex vivo* models (either animal or human) can provide information about subsidence and extrusion of an implant, but they degenerate due to apoptosis [123] and fail before reaching 10 Mio. fatigue cycles [124]. The most widely used animal models are bovine caudal discs. The pressure within bovine disc is similar to human discs (0.1 – 0.3 MPa). On the other hand however, they are also different and might not be compared to human lumbar discs because they are not weight bearing (which is also the case for most other animals) [124]. A review on disc models summarized that hydrostatic pressures between 0.2 and 0.8 MPa at 0.1-1Hz during 8h/d are physiological conditions and that pressures in the range of 0.1 to 2.5 MPa below 5Hz during 30min-4h/d are beneficial for samples or cells. Yet, these conditions may vary depending on the type of animal model used [123].
3. *in vivo* animal models are mouse, rat, pig, dog, chicken, baboon, sheep [125], rabbit [126] and goat [127].

Table 1.3: Test profiles and associated parameters for lumbar IVD prostheses evaluation (source: ASTM [2]).

Test Profile	Axial load N	Cyclic Load [N] min-max	Axial min-	Preferred placement Control: [degree]	Dis-ROM	Alternate Control: Applied Moments [Nm]	Load Ap-
Flexion / extension	1200	900-1850		+/- 7.5		+/- 10	
Rotation	1200	900-1850		+/- 3		+/- 10	
Lateral bending	1200	900-1850		+/- 6		+/- 12	

→ The properties of the NP have been investigated extensively. For tissue replacement design it seems to be essential to replicate swelling properties, such as the maximal equilibrium stress which can be maintained by the material without deswelling.



## 1.5 Photopolymerization

### 1.5.1 Photopolymerization of hydrogels

Hydrogels are a promising option for IVD tissue replacements because their mechanical properties depend on cross-linking density, polymer composition, degree of swelling [128] and polymerization conditions [129, 130]. Thus, material properties can be chosen adequately by adapting composition and cross-linking density when mixing the components. The polymerization of a gel is a chemical reaction which can be induced by mixing two different compounds or by light irradiation or by changing the pH, temperature or pressure. A controllable mean to activate and control the degree of polymerization is via light irradiation, or so called photopolymerization. The controllability of photopolymerization via exposure dose is an important advantage over other techniques. Other advantages are the degree of acceptance of NP cells which is higher in cell-seeded photopolymerized hydrogels than in ionically cross-linked hydrogels consisting of two different compounds [131]. Finally, photopolymerization is the only polymerization type which allows dispensing a material in a completely liquid state. Thus, the liquid material can be first dispensed within tissue and surface interstices in a minimally invasive manner for example via a small gauge needle. We hypothesize that this property increases the adhesion of the polymer biomaterial to tissue [132, 133].

→ *Hydrogels can be tailored to reach specific, desired properties and dispensed in a minimally invasive manner through a small gauge needle. Any material with chemically active groups can be photopolymerized or photocrosslinked in combination with a photoinitiator and light illumination. Dispensing the material first in liquid state may show promising adhesion properties.*

### 1.5.2 Initiation of photopolymerization

In photopolymerization, a photoinitiator forms radicals either by cleavage or hydrogen abstraction [134] which are induced by the absorption of a photon. The radical induces the chain formation of the polymer. Also other options such as cation or anion based photoinitiators exist. A photoinitiator has a certain absorption spectrum, often in the ultraviolet (UV) range, where the energy per photon is higher than for visible light. In the UV range, light exposure (in energy per surface area) is harmful to biological tissues (especially below 315 nm) [135]. The tabulated maximum light exposure that is wavelength dependent is shown in figure 1.3. Among photoinitiators, the following are high efficiency (meaning requires low light exposure to initiate polymerization) and low cytotoxicity for biomedical applications: Eosin Y + triethanolamine (wavelength range : 430 to 570 nm) [136], LAP ( 200 to 420 nm) and Irgacure 2959 ( 200 to 365 nm) [137]. In biotechnology, photopolymerized hydrogels are used for drug delivery [136], 3D tissue scaffolds [138] and cell-encapsulation [134]. When choosing a photoinitiator, a compromise needs to be found between light exposure, cytotoxicity of the photoinitiator and available light sources. Light emitting diodes are available at wavelengths

such as 365, 385 and 405 nm. Lasers are available for instance at 325, 337, 355, 380, 395 and 405 nm [139, 140]. In this study Irgacure 2959 was chosen because it is easily available and can be used as a one component initiator.

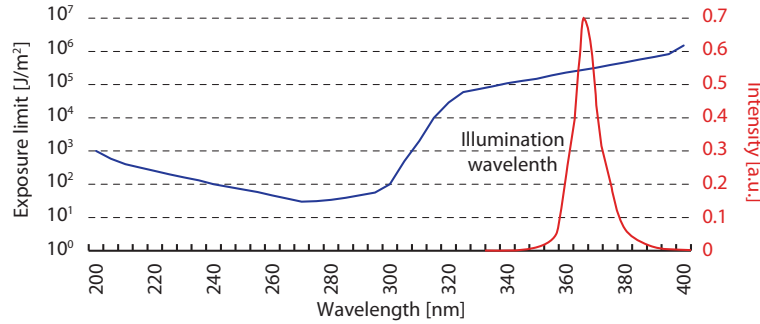


Figure 1.3: Maximal allowed exposure limits for living human tissues between 200 and 400 nm (UVC, UVB and UVA ranges). The allowed exposure decreases to a minimum between 260 and 300 nm – a dangerous range for DNA strands. It is slightly higher below this range (due to the shallow light penetration and lower wavelength). the allowed exposure is significantly higher at wavelength close to visible light (400 nm) which is due to the lower energy per photon in this range. The red peak is the illumination wavelength used in this work (the units are arbitrary).

→ Wavelength below 315 nm should be avoided for cytotoxicity reasons. There are existing photoinitiators and light sources in the range between 315 and 400 nm. Irgacure 2959 was selected because it is easily available, can be used as a one component initiator and has been shown to work with 365 nm light excitation.

### 1.5.3 Photopolymerization modelling

We propose to develop a simulation model for the photopolymerization of our implant in order to predict the shape of the implant after photopolymerization, the time to reach full photopolymerization. Photopolymerization has been modeled by others using molecular dynamics [141] and using the Beer-Lambert law to predict the speed of photopolymerization and the thickness of a photopolymerized layer [142, 143]. When the illumination is performed through tissues to reach a subcutaneous volume, light scattering and absorption within the tissue decreases the available light dose for photopolymerization [144]. Monte Carlo simulations are often used to model light scattering in tissues [145]. The scattering properties depend on the size and shape of the scatterers. Rayleigh scattering is a regime valid for particles much smaller than the wavelength. In the so-called Mie regime, the particle has a size comparable to the wavelength and has an index of refraction different than its surrounding. Biological tissues are made up of scatterers with a size range distribution and thus the overall scattering is quite complex. In linear scattering (the wavelength does not change), scattering is described by a scattering cross-section  $\sigma_s$  (different to its geometrical cross-section). The

scattering coefficient  $\mu_s$  is the product of the cross-section and the volume density of the medium  $\rho_s$ . Thus, the probability of transmission of a photon through a scattering medium of length  $L$  and maintaining its incident direction of propagation is given by:

$$p_{trans} = e^{-\mu_s L} = e^{-\sigma_s \rho_s L} \quad (1.2)$$

This formula relates the fraction of photons transmitted through a scattering medium which have maintained their original direction. These photons are called ballistic photons. They are those which have not encountered a scattering particle. For the other fraction of photons which interacted with the particle, we need to find an expression which indicates the direction they took after the interaction. This is described by a so-called scattering probability function  $p(\theta)$ . A commonly used scattering function was developed by Henyey and Greenstein (1941) [146]:

$$p(\theta) = \frac{1}{4\pi} \frac{1 - g^2}{(1 + g^2 - 2g \cos \theta)^{3/2}} \quad (1.3)$$

where  $\theta$  is the angle between the incident and the scattered photon and  $g$  is an anisotropy coefficient.  $p(\theta)$  and  $g$  are related in the following manner:

$$\int_0^\pi 2\pi p(\theta) \cos \theta \sin \theta d\theta = g \quad (1.4)$$

And where:

$$\int_0^\pi 2\pi p(\theta) \sin \theta d\theta = 1 \quad (1.5)$$

If  $g$  is equal to zero, it results in isotropic scattering (uniform in all directions). If it is equal to one, then all photons are forward scattered (same direction as the incident vector). Common values of  $g$  for biological tissues are between 0.5 and 0.95 [147].

Photopolymerization was modeled in 2D using Monte Carlo taking into account absorption, but neglecting light scattering [148]. A prerequisite for a Monte Carlo simulation that include absorption and scattering is the measurement of the material's optical absorption and scattering coefficients. A range of approaches exists for such measurements [149] including transmission-, reflectance- or pulsed measurements. One of the simplest methods is to use a double-integration-sphere system [150, 151, 152] calibrated by fat emulsions [153], dyes [154] or titanium oxide [155] phantoms. An example of such a setup is presented in figure 1.4. A similar setup was used in the experiment described in chapter 2.

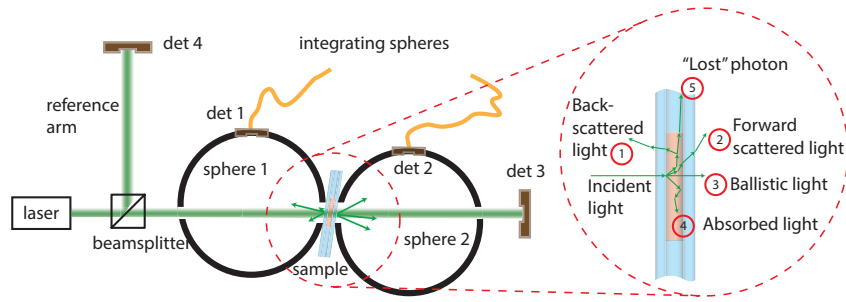


Figure 1.4: Double-integrating-spheres setup: Photons can be detected in the first sphere (det 1), the second sphere (det 2), on the detector at the back end (det 3) or on the reference-detector (det 4). Five different events are possible: 1) backscattering/reflection 2) forward-scattering 3) ballistic transmission 4) absorption and 5) loss of the photon.

→ *Material scattering properties determine the amount of photons available at a specific location in a volume. To control the photopolymerization geometry and volume, photons need to be guided to the right position. We will use a Monte Carlo model to simulate the light distribution in our photopolymer.*

### 1.5.4 Photopolymerization control

Examples of applications using photopolymerization are dental cements, coatings and photolithography where light is used to control the reaction spatially and temporally while providing at the same time other advantages such as minimal exothermic reaction or material dilatation during the reaction. For our application, the liquid photopolymer is injected to the implant location via a small conduit such as a needle. Thus the light also needs to be guided within the same conduit. This is achieved with an optical fiber. A vast range of optical fibers are commercially available. These fibers have small diameters (several hundred micrometers) and thus are, by virtue of their size, minimally invasive [156]. Light probes are used for illumination, tissue characterization [157], spectroscopy [158], measurement and monitoring [159, 160] and imaging. During polymerization, the liquid monomer or polymer compound is transformed into a solid polymer-network. Chemical, mechanical and optical properties change as a result of polymerization or cross-linking. These changes can be monitored to track the state of polymerization. A considerable amount of polymerization-monitoring-methods exists. In our application, there is no direct viewing of the illuminating zone. For implant monitoring only *in situ* soft-sensing techniques are of interest. For example, calorimetry or gas-chromatography are not applicable. Speckle interferometry [161], Raman spectroscopy [162], transmittance measurements [163], fluorescence monitoring [164, 165], UV-, Vis-, NIR-, MIR-spectroscopy, nuclear magnetic resonance spectroscopy and acoustic monitoring [166] were used for polymerization monitoring *in situ*. Furthermore, optical coherence tomography was used for monitoring PEG-hydrogels within tissues [163, 164] and for strain field analysis in polymers [167]. Photopolymerization of dimethacrylates was already monitored with a

fluorescence probe [168].

→ *Photopolymerization has been extensively used to pattern surfaces and volumes in a controlled manner. The light illumination can be delivered with a probe to locations, which are difficult to reach by other means. A large range of methods to monitor photopolymerization exists. An optical feedback method based on backscattering will be used and tailored for the photopolymer material.*

## 1.6 Objectives of the thesis

This thesis is part of a larger project to design a NP replacement. The general project consist of designing the implant material, developing an implantation device for photopolymerization and evaluating material and device together during implantation. The present thesis covers mainly the two last aspects. The development of the material is done by Azadeh Khoushabi from the Laboratory of Polymer and Composite Technology at EPFL in the framework of a parallel thesis. In the present thesis, photopolymerization of hydrogel implants shall be assessed to determine whether they are an alternative which can address the recently observed failures of intervertebral disc tissue replacements. Specifically, a method, device and test setups shall be developed to simulate and test different potential implant materials. Selected materials shall be implanted in a controllable, minimally invasive manner and be evaluated within *in vitro* or *ex vivo* animal models. In summary, the objectives of the thesis are:

- Model an implant during photopolymerization using Monte Carlo simulations. These simulations should predict the spatial and temporal evolution of a polymer-volume and take into account the interactions between tissue, light and polymer. The results should allow designing the light probe, tailoring the surgical procedure and find optimal bio-optical material properties.
- Develop different polymerization probes and monitoring options to inject, photo-activate and control a material *in situ*. Combine injection, photopolymerization and monitoring function in one single probe within a cannula which allows for photopolymerization and surgery within real tissue.
- Develop through cyclic iterations an implant and device with known reliability in terms of mechanical performance and biocompatibility. Starting by evaluating an existing Tween 20 hydrogel [169], materials and device generations are tested. Physical performance such as hydrogel's hydrostatic pressure, water content and moduli for example will be evaluated. At a second stage the materials are evaluated *in vitro* to test their biocompatibility. At the last stage, the material is implanted into an *ex vivo* bovine model and evaluated over 0.5 million loading cycles within a bioreactor (collaboration with ARTROG, University of Bern).



## 2 Photopolymerizable hydrogels for implants: Monte-Carlo modeling and experimental in vitro validation

This chapter mainly consists of an article published in the journal of biomedical optics [170]. The co-authors are A. Khoushabi, C. Schizas, P.E. Bourban, D.P. Pioletti and C. Moser

### 2.1 Abstract

Photopolymerization is commonly used in a broad range of bio-applications such as drug-delivery, tissue-engineering and surgical implants where liquid materials are injected and then hardened by means of illumination to create a solid polymer-network. However, photopolymerization using a probe, e.g. needle guiding both the liquid and the curing illumination, has not been thoroughly investigated. In this paper, we present a Monte Carlo model that takes into account the dynamic absorption- and scattering-parameters as well as solid-liquid boundaries of the photopolymer to yield the shape and volume of minimally-invasively injected, photopolymerized hydrogels. In the first part of the paper, our model is validated using a set of well-known Poly(ethylene glycol) dimethacrylate (PEGDMA) hydrogels showing an excellent agreement between simulated and experimental volume-growth-rates. In the second part, in situ experimental results and simulations for photopolymerization in tissue cavities are presented. It was found that a cavity with a volume of  $152 \text{ mm}^3$  can be photopolymerized from the output of a  $0.28 \text{ mm}^2$  fiber by adding scattering lipid particles while only a volume of  $38 \text{ mm}^3$  (25 %) was achieved without particles. The proposed model provides a simple and robust method to solve complex photopolymerization problems where the dimension of the light source is much smaller than the volume of the photopolymerizable hydrogel.

### 2.2 Introduction

Photopolymerization [171, 172] is a widely used method to harden polymers in controllable manner by illuminating a liquid monomer or an uncured polymer precursor. Originally used in the field of coatings, printing, paints, adhesives, optical fibers, etch resist or printed circuits



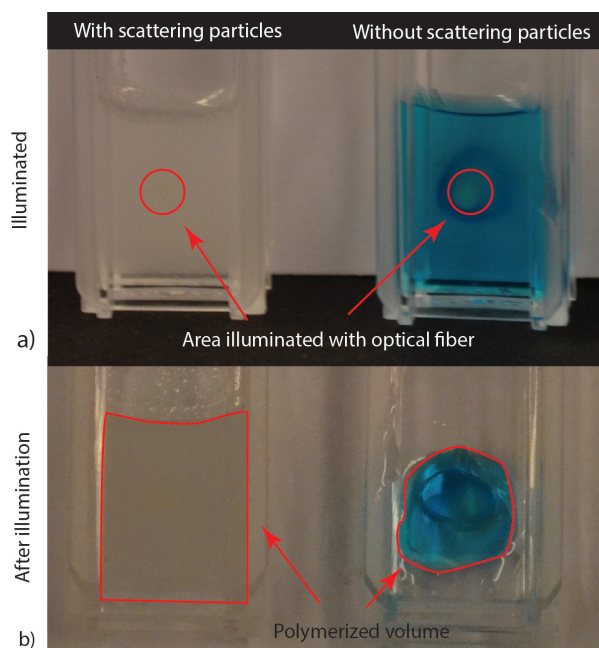


Figure 2.1: Poly(ethylene-glycol) dimethacrylate hydrogels. Left: with scattering particles (intralipids). Right: No scattering particles. The hydrogel without scattering particles has a Methylene blue dye to visualize the photopolymerized volume. a) samples during illumination. Illumination is performed with the output of a  $600\text{ }\mu\text{m}$  core diameter optical fiber placed 5 mm from the cuvette; b) after extraction of the un-polymerized liquid. The red lines indicate the polymerized volumes. Light dose and illumination area are the same for both samples.

[173, 174, 175, 176], it quickly found its way into the biomedical sector where photopolymerizable materials are used for dental implants [177], cell encapsulation [178], tissue-replacements [138, 121], drug delivery [136], implant coatings, bio-glues [62] and microfluidics [130]. However, when materials are introduced and cross-linked in the body by means of photopolymerization, illumination becomes challenging since surgical procedures tend to be minimally invasive [134]: large polymer volumes have to be illuminated with small light emitting surfaces, for example through the tip of an optical fiber.

Bulk or mass photopolymerization is used for thin and thick films [179]. For uniform illumination of non-scattering polymers, the process of photopolymerization is well understood and mostly modeled using Beer-Lambert law that describes the exponential decay of the incident light intensity. The extinction coefficient is equal to the absorption coefficient since scattering is neglected and the photopolymerized surface area is that of the illumination area. Figure 2.1 illustrates the effect of an additive in the form of scattering particles on photopolymerized volumes. Although the illumination time and incident illumination area are the same for the polymer with and without scattering particles, the polymerized volume varies significantly. Therefore, a model which takes into account scattering and absorption, light dose and illumination pattern is required to better predict the photopolymerized volume.

In this paper, we investigate photopolymerization of implantable tissue replacement which



are injected through a thin needle and then hardened by illumination with an optical light guide. Based on a statistical Monte Carlo[145, 180] approach, a model for photopolymerization is presented. Monte Carlo is a well-known method to model light transport through a scattering medium. It consists of tracking single photon packages and predicting their way throughout a predefined volume based on the media's absorption ( $\mu_a$ ), scattering ( $\mu_s$ ) and anisotropy coefficient (g). Monte Carlo studies have been conducted on a broad selection of tissues, for optical neural stimulation [181], glucose monitoring [182], cancer detection [183] and many others. Bulk-photopolymerization induced by an incident laser beam has been studied using Monte Carlo [179] or analytical models [148]. However, Monte Carlo modeling of photopolymerization with different absorption, scattering coefficients and its experimental validation has not been investigated to our knowledge.

This paper is organized as follows: the hydrogel precursor composition and fiber based illumination is introduced in section 2.3. The experimental method to measure the absorption and scattering coefficients is presented in section 2.4. Section 2.5 describes the Monte Carlo simulation model to predict a photopolymerization volume and section 2.6 describes its experimental validation. Section 2.7 models photopolymerization of hydrogels in tissue cavities. An application example of an intervertebral disc replacement is presented. The effect of scattering additives on final polymerization volume is shown. A simple method is proposed to integrate any type of tissue geometry into the simulations.

## 2.3 Hydrogel material and illumination

We selected a Poly(ethylene-glycol) hydrogel because of its commercial availability and interesting biomechanical properties. Due to their elastic strength [128][22], swelling ability [134] and bio-compatibility [137] Poly(ethylene-glycol) hydrogels systems are promising for cartilage [138], tissue replacements [169], arterial coating [136] and bio-sensors [184]. Four different Poly(ethylene-glycol)dimethacrylate (PEGDMA) systems were prepared with the following combination of absorption ( $\mu_a$ ) and scattering ( $\mu_s$ ) coefficients: 1. low  $\mu_a$  and low  $\mu_s$  2. high  $\mu_a$  and low  $\mu_s$  3. low  $\mu_a$  and high  $\mu_s$  4. high  $\mu_a$  and high  $\mu_s$ . PEGDMA 6 kDa was synthesized as previously described[185], the used photoinitiator was Irgacure-2959 (BASF) and the scattering additive were Intralipids (Fresenius Kabi).  $\mu_a$  is adjusted by varying the concentration of the photoinitiator and  $\mu_s$  is adjusted by adding Intralipids. Phosphate Buffer

Table 2.1: Preparation of PEGDMA – 6 kDa hydrogel samples.

Sample	PEGDMA 6000 [mg]	Irgacure 2959 (1 % w/v) [ml]	Intralipids (10% w/v) [ml]	PBS [ml]
1. low $\mu_a$ and low $\mu_s$	220	0.22	-	0.659
2. high $\mu_a$ and low $\mu_s$	220	0.66	-	0.217
3. low $\mu_a$ and high $\mu_s$	220	0.22	0.1	0.659
4. high $\mu_a$ and high $\mu_s$	220	0.66	0.1	0.217

## Chapter 2. Photopolymerizable hydrogels for implants: Monte-Carlo modeling and experimental in vitro validation

Solution (PBS) was used as the liquid in the hydrogel. Quantities and concentrations are presented in table 2.1.

The photoinitiator Irgacure - 2959 (1% w/v) absorbs most efficiently between 280 and 320 nm (Fig. 2.2). Unfortunately, DNA nucleotides have their main absorption peaks in this wavelength range [186] and therefore admissible light doses for in vivo applications in this range are extremely low [187]. Thus, we opted for a longer wavelength to increase significantly the admissible dose and selected 365 nm, a wavelength where Solid State Light Emitting Diodes have high brightness and are commercially available. An optical fiber with 600  $\mu\text{m}$  core diameter, 0.22 numerical aperture, (Polymicron Technologies, FVPE60060710/2M) was butt-coupled to a high-power LEDs chip with emission area of 0.72  $\text{mm}^2$  (Nichia, NCSU033B). The final fiber optical output power at the fiber tip was 6.5 mW.

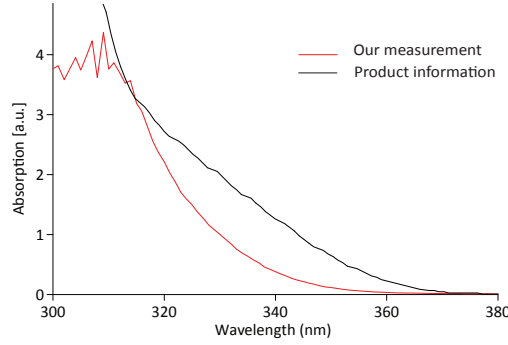


Figure 2.2: Absorption curves of the used photoinitiator (Irgacure-2959, 1% w/v). The photosensitizer reacts best around 300 nm, but can also be used at longer, more bio-acceptable wavelengths.

### 2.4 Determination of absorption and scattering coefficient

In an absorbing and scattering compound, the scattering and absorption coefficients can be measured separately if  $\mu_a \gg \mu_s$ ,  $\mu_{ext} = \mu_a + \mu_s \simeq \mu_a$  and vice versa for  $\mu_a \ll \mu_s$ . In Fig. 2.3, the setup is presented: the previously described output of the LED fiber-coupled light source is collimated and incident on a 1 mm-thick hydrogel sample sandwiched between two 1 mm-thick glass slides that forms a chamber to confine the liquid and uncrosslinked polymer. The extinction coefficient can be measured throughout the transition from liquid to solid hydrogel. To reduce the optical noise (glass interfaces, local tilts etc.), the chamber is fixed and can be filled or emptied without moving it. Water is used at a reference before each test. One detector measures the transmitted light and another serves as a reference.

During photopolymerization, the photoinitiator is consumed and a polymer-network forms. Thus it can be expected that optical properties change during photopolymerization. In the case of the PEGDMA hydrogel, we did not find a significant increase or decrease of the extinction coefficient throughout the photopolymerization reaction for any of the four tested hydrogels. Table 2.2 shows the measured results for the scattering and absorbing coefficients.

## 2.5. Monte Carlo model for photopolymerization

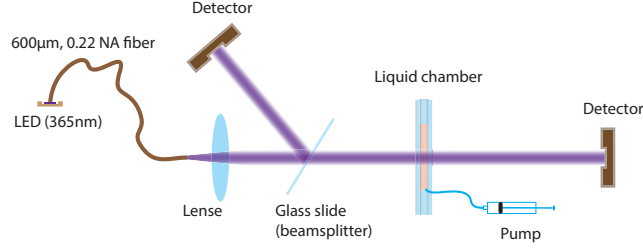


Figure 2.3: Transmission set-up at 365 nm to measure the extinction coefficient of either a scattering or an absorbing compound. The collimated beam is split into two arms, one is used as reference the second passes through the sample. The chamber is fixed. Its content can be injected or extracted.

Table 2.2: Measured scattering and absorbing coefficients at 365 nm (mean and maximal measurement error). These values are used for the simulations (\*assumed values for simulations)

	Absorption coefficient $\mu_a$ (cm <sup>-1</sup> )	Scattering coefficient $\mu_s$ (cm <sup>-1</sup> )
1. low $\mu_a$ and low $\mu_s$	$0.131 \pm 0.003$	0.00*
2. high $\mu_a$ and low $\mu_s$	$0.430 \pm 0.004$	0.00*
3. low $\mu_a$ and high $\mu_s$	0.131*	$6.76 \pm 0.48$
4. high $\mu_a$ and high $\mu_s$	0.430*	$6.85 \pm 0.62$

As extinction-, absorption- and scattering coefficients linearly depend on molar concentrations of a certain compound, they can be measured individually and then be summed up in a mixed solution.

## 2.5 Monte Carlo model for photopolymerization

Photopolymerization is a multi-physics problem which includes light transport, bi-phasic (liquid and solid) mass transport (swelling and diffusion), molecular dynamics and photo-chemical reactions. The Monte Carlo approach consists of tracking energy packages through space and thus can account for a maximum of effects. Events like absorption or scattering are characterized statistically. Wang's Monte Carlo model [145, 180] (C++ code) was rewritten in Matlab. This reduced computational speed considerably, but drastically simplified programming and code validation due to amount of available filter- and spline-functions in Matlab. The following assumptions were taken in the model: 1) The initially liquid hydrogel-precursor absorbs energy step-wise and at a given threshold, a sub-volume (voxel) changes into solid material. 2) The liquid hydrogel precursor and the solid hydrogel are separated by a discrete boundary (different refractive index). As the reaction goes on, this interface changes dynamically. 3) Photons (photon-packages) can be reflected or refracted at this interface and also at the polymer-tissue interface. 4) Scattering and absorption coefficients are dependent on the

## Chapter 2. Photopolymerizable hydrogels for implants: Monte-Carlo modeling and experimental in vitro validation

---

photon package's position (photon in liquid hydrogel precursor, in solid hydrogel or within tissue). 5) Scattering and absorption coefficients can vary over time (throughout the reaction). The method developed by Wang models light scattering and absorption in tissue layers by predicting the path of flight of photon packages (a detailed description is given in Appendix A). In summary, these packages are guided through space by a series of statistical events. A package is defined by a position (x,y,z), a directional vector (u,v,w) and an energy also called photon weight. All events i.e. photon-mater interactions are described by statistical distributions which are linked to randomly computed parameter  $\xi$  using the following equation:

$$\int_{-\infty}^{\chi} p(\chi) d\chi = \xi \quad \text{for } \epsilon[0,1] \quad (2.1)$$

Where  $\chi$  is the random variable (e.g. coordinates of the light source) and  $p(\chi)$  its probability density function.  $\xi$  is a second random variable between 0 and 1 generated by the computer. The result of the integral is a function of the type  $f(\chi) = \xi$ . Its inverse function is used to compute a final random distribution. An example of a uniform point source is given in Appendix A.1. Laser beams were simulated using Gaussian profiles. Solving 2.1 for a Gaussian profile leads to:

$$x = f_x^{-1}(\xi) = 2\sqrt{2}\omega_0 \cdot \text{erf}^{-1}(1 - 2\xi) \quad (2.2)$$

Where  $x$  is a position of the photon package orthogonal to direction of the beam,  $\text{erf}^{-1}$  is the inverse of the error function and  $\omega_0$  the half beam waist. Moreover,  $u = v = 0$  and  $w = 1$  will result in a collimated beam. The output of an optical fiber was modeled as following:

$$x = f_x^{-1}(\xi) = d \cdot \left( 0.5 - \frac{\cos^{-1}(1 - 2\xi)}{\pi} \right) \quad (2.3)$$

And:

$$u = \cos \left( \beta \cdot \left( 1 - \frac{2\cos^{-1}(1 - 2\xi)}{\pi} \right) \right) \quad (2.4)$$

$$w = \sin \left( \beta \cdot \left( 1 - \frac{2\cos^{-1}(1 - 2\xi)}{\pi} \right) \right) \quad (2.5)$$

## 2.5. Monte Carlo model for photopolymerization

Where  $d$  is the fiber's core diameter and  $\beta = \sin^{-1}(NA/n_{liquid})$ ,  $NA$  being the numerical apperture of the fiber and  $n_{liquid}$  the refractive index of the liquid polymer. In the Monte Carlo approach, at every interaction, a photon package loses some of its energy (photon-weight), depending on the material's absorption properties. Parts of the absorbed photons will induce a photopolymerization reaction. Thus, the degree of polymerization  $Poly_{\Delta V_{i,j,k}}$  of the volume element  $\Delta V_{i,j,k}$  ( $i, j$  and  $k$  being the elements position) is introduced. At every step  $Poly_{\Delta V_{i,j,k}}$  is updated:

$$Poly_{\Delta V_{i,j,k}} \leftarrow Poly_{\Delta V_{i,j,k}} + \alpha \cdot \Delta W \quad (2.6)$$

Where  $\Delta W$  is the absorbed energy of the volume element  $\Delta V_{i,j,k}$  and  $\alpha$  the fraction of energy consumed for photopolymerization.  $Poly_{\Delta V_{i,j,k}}$  is initially equal to zero indicating that no polymerization at  $\Delta V_{i,j,k}$  took place. It can also reach a predefined maximal value which defines the state where all reactive groups in the volume  $\Delta V_{i,j,k}$  are consumed. As the polymerization goes on, particle sizes and chemical properties change, and thus scattering and absorption coefficients, which directly influence the path of light and the polymerization structure, also change. Therefore scattering and absorption coefficients are directly linked to the degree of polymerization.

$$\mu_a = \mu_a(t, \vec{r}) = \mu_a(Poly_{\Delta V_{i,j,k}}) \equiv \mu_{a,\Delta V_{i,j,k}} \quad (2.7)$$

$$\mu_s = \mu_s(t, \vec{r}) = \mu_s(Poly_{\Delta V_{i,j,k}}) \equiv \mu_{s,\Delta V_{i,j,k}} \quad (2.8)$$

$\mu_n(Poly_{\Delta V_{i,j,k}})$  were chosen as linear combination between an initial  $\mu_{n,un-polymerized}$  and a final  $\mu_{n,polymerized}$ . This spatial variation in optical properties induces that a photon package is exposed to changes in scattering and absorption coefficient between two interaction sites. This effect was modeled by averaging  $\mu_a$  and  $\mu_s$  between the two sites:

$$\mu_{n,real} = \frac{\mu_{n,\Delta V_1} + \mu_{n,\Delta V_2}}{2} \quad (2.9)$$

Figure 2.4 shows the modeled intensity distribution of an optical fiber output in hydrogel precursor. One simulation consists of  $10^8$  photons. After every million photon-package, iso-intensity-levels are computed (Fig. 2.4b). One iso-level is chosen as boundary between solid and liquid hydrogel (e.g. 0.3 or 0.5). This selected iso-level is extracted, and thus the

## Chapter 2. Photopolymerizable hydrogels for implants: Monte-Carlo modeling and experimental in vitro validation

volume-growth can be plotted over time (Fig. 2.4c). The voxel size was chosen to be  $10 \times 10 \mu\text{m}$ .

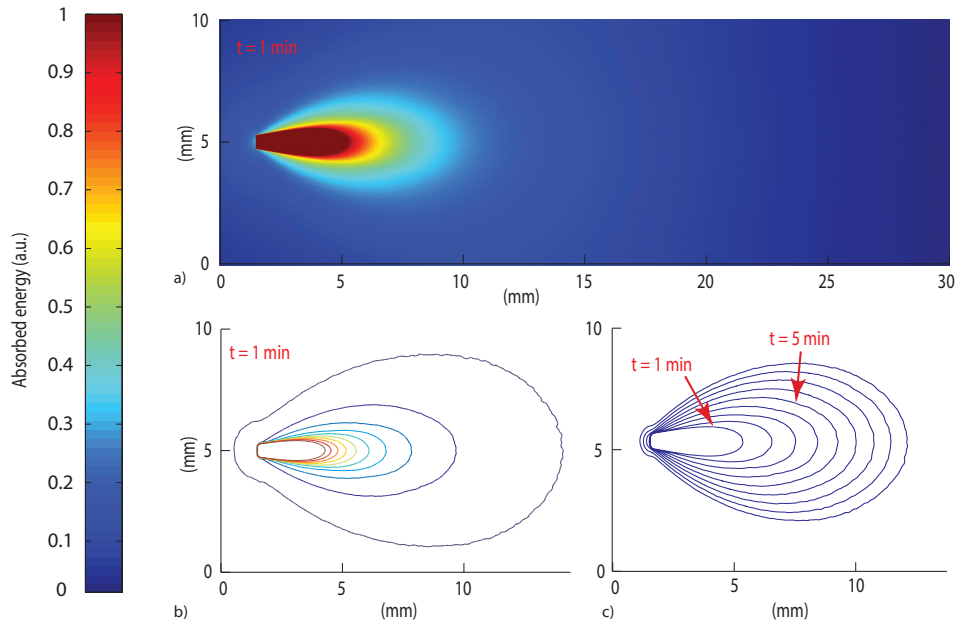


Figure 2.4: Monte Carlo simulation of photopolymerized volume. The light source is the output of an optical fiber. a) Distribution of absorbed energy calculated by the Monte Carlo model. b) Fitted iso-levels at a given time-step: solid hydrogel in the center and liquid hydrogel precursor outside c) polymer-volume-growth over time.

Due to the statistical nature of Monte Carlo-models, solutions have to be averaged over local areas to create proper surfaces between different domains. A median filter (Matlab) applied over a neighborhood of  $15 \times 15$  voxels gives good results as it showed the most similar surfaces compared to experimentally photopolymerized hydrogel samples. The plots in Fig. 2.4b) indicate the amount of absorbed energy and need to be correlated to a solid or liquid material state by setting a gel point, the boundary between liquid and solid hydrogel. Brulle et al. [148] proposed, via simulation, to set the gel point at 57% of totally absorbed light energy. Photo-rheology measurements were performed on the 6 kDa PEGDMA hydrogel and data is shown in Fig. 2.5a). Results show that the hydrogel changes from liquid to solid after about 40% of total irradiation energy. Using this information one iso-level (Fig. 2.4b) can be extracted at every time-step to form a growth-pattern over time (Fig. 2.4c).

During a simulation run, a photon knows its position, but not the material it is crossing, thus

## 2.6. Experimental validation of the Monte Carlo model

a level-set function  $\varphi$ , attributed to each voxel, is defined:

$$\varphi = \begin{cases} 0 & \text{outside of investigated area} \\ 1 & \text{liquid} \\ 2 & \text{solid} \\ 3 & \text{tissue} \end{cases} \quad (2.10)$$

If a photon-package crosses the solid-liquid boundary, the stepping algorithm calculates the change in  $\varphi$ , the position where the boundary is crossed and computes its orientation at the intersection with the photon path (Fig. 2.5b). Thus refractions or reflections are calculated dynamically while interfaces change their position. Circularly or linearly polarized light are averaged to compute reflection and refraction probabilities [180]. The algorithm also takes into account time-dependent changes in absorption and scattering coefficients which can be defined using a desired polynomial function (e.g.  $\mu_s(t) = \mu_{s0} + a_1 \cdot t$ ). Further information on the algorithm is detailed in [188].

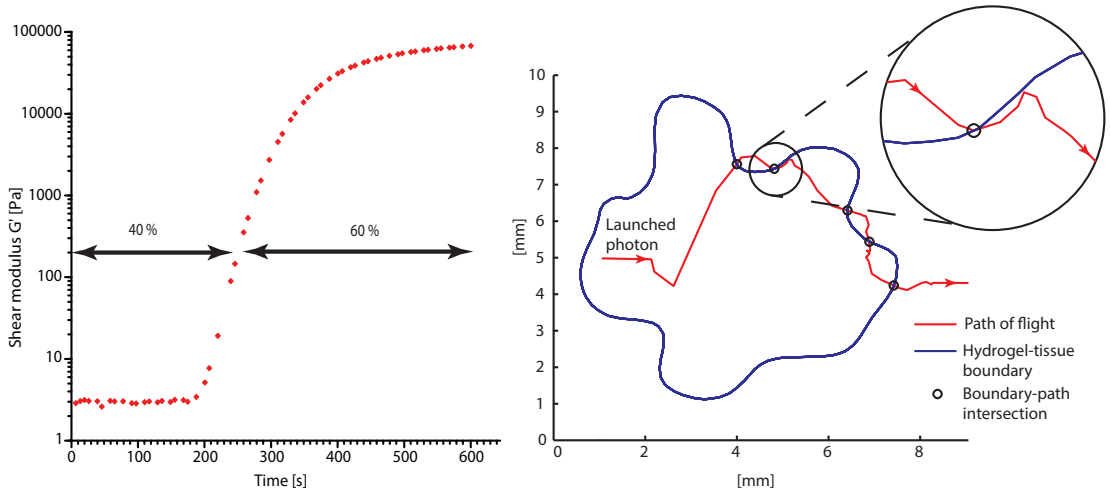


Figure 2.5: a) Photorheology measurement of the PEGDMA hydrogel: The gel point (change from liquid to solid) is reached after approximately 250 seconds corresponding to 40% of absorbed energy. b) Interactions of photons with a tissue-cavity: The red lines indicate the paths of the tracked photon package.

## 2.6 Experimental validation of the Monte Carlo model

To validate the Monte Carlo model introduced in section 4, four hydrogel samples (Table 2.1) were placed in a cuvette and illuminated by the previously described, 600  $\mu\text{m}$  core optical fiber (365 nm). The fiber is touching the liquid polymer (Fig. 2.6a). The output power at the fiber tip is 6.5 mW. A constant volume of 2 ml of uncross-linked polymer was injected into the



## Chapter 2. Photopolymerizable hydrogels for implants: Monte-Carlo modeling and experimental in vitro validation

test cuvettes. Samples were photopolymerized during 3, 5 and 10 minutes. After illumination the solid polymer was extracted, dried from un-bonded liquid and weighted. In Fig. 2.6b) and c), the volumes and shapes between simulation and experimental results are compared.

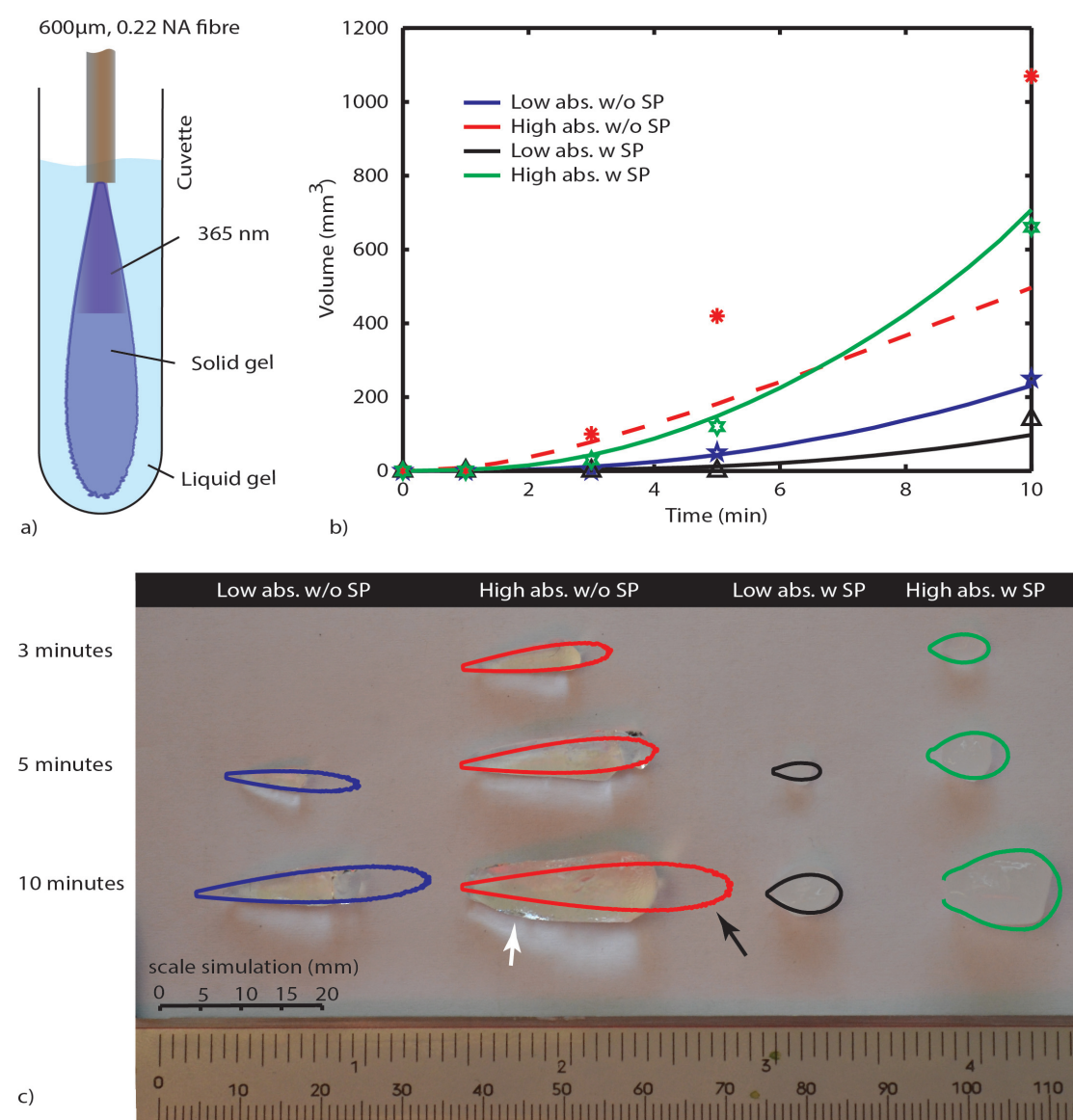


Figure 2.6: Fig. Four different photopolymerized hydrogel samples (Table 1). a) Cuvette-setup with a fiber immersed into the liquid hydrogel precursor. b) Volumes of experimentally polymerized samples (stars and triangles) and computed results (colored lines) are compared. c) Pictures of the shapes of experimentally polymerized and simulated samples (colored contours) after 3, 5 and 10 minutes of light illumination: The black arrow shows an area where the liquid hydrogel precursor did not solidify due to the size of the cuvette. The white arrow shows an area where polymerization took place due to polymer-diffusion, swelling and back-reflections.



## 2.7. Modeling and experimental application of photopolymerization in tissue cavities

The experimental volumes and shapes agree very well with the simulated results except for the samples with high absorption and low scattering. This discrepancy can be explained by the following factors: 1) The Fresnel reflections of the cuvette's side glass walls are taken into account, but not on the cuvette's bottom. 2) The length of the cuvette limits the size (length) of the hydrogel-shape. 3) The simulations do not take into account polymer diffusion which strongly influences the outcome of photopolymerization [189, 190]. As the material diffuses, nucleation is only possible next to already existing solid polymer, thus hydrogel-shapes tend to grow outward of the cone of light (given by the output of the fiber) whereas in the Monte Carlo simulations the volumes grow within the cone of light.

In the simulations, the energy per photon package is 65 nJ ( $10^8$  photon packages over 16.7 minutes at 6.5 mW). The amount of photons is  $1.2 \times 10^{11}$  per photon package at 365 nm. We found that refractions and reflections on the liquid/solid interfaces do not influence photopolymerization outcomes in a significant way. This is because the refractive index, between the liquid and solid is approximately  $\Delta n = 0.01$  [148]. We also report that by pre-illuminating the hydrogel it was possible to photopolymerize volumes up to  $3500 \text{ mm}^3$  within 10 min using the previously mentioned  $600 \mu\text{m}$  fiber. The pre-illumination time was chosen to be equal to the time for which the liquid polymer starts to change its shear modulus (inflexion point in fig. 2.5).

## 2.7 Modeling and experimental application of photopolymerization in tissue cavities

Figure 2.7a illustrates light scattering and photopolymerization in a tissue cavity. Figure 2.7b) shows the autofluorescence of an intervertebral bovine disc cavity injected with a liquid hydrogel monomer and illuminated with 365 nm light from a fiber housed in a rigid needle.

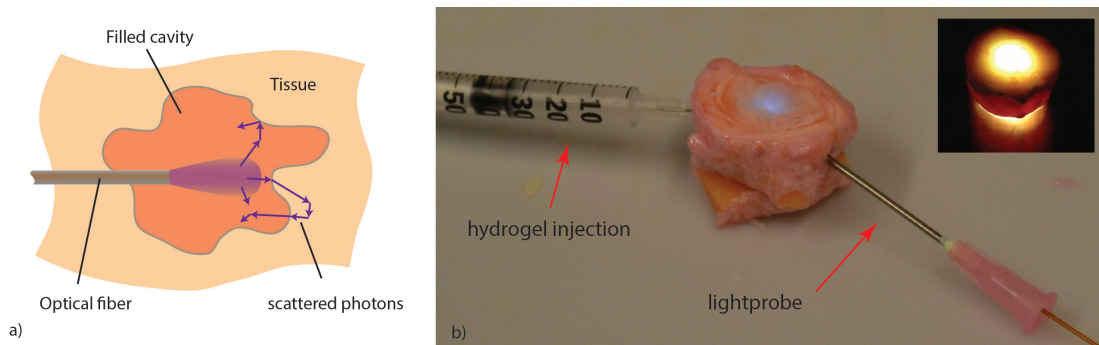


Figure 2.7: a) Schematic: the purple arrows show possible reflections and refractions of back-scattered photons. b) autofluorescence of a bovine intervertebral disc tissue cavity [1] filled with a PEGDMA-hydrogel and illuminated with a light-probe consisting out of an 18 gauge needle and a  $600 \mu\text{m}$  fiber.

## Chapter 2. Photopolymerizable hydrogels for implants: Monte-Carlo modeling and experimental in vitro validation

The surrounding tissue absorbs light, but it can also reflect and scatter it, which directly alters the local irradiance and thus photopolymerization (Fig. 2.7b). Photopolymerization, light source and interactions of tissue/polymer-interfaces with photons were modeled with the Monte Carlo model presented in section 4 and 5. The energy absorbed (light dose) by the hydrogel is shown in Fig. 2.8). The tissue cavity was designed arbitrarily using a drawing software (Illustrator).

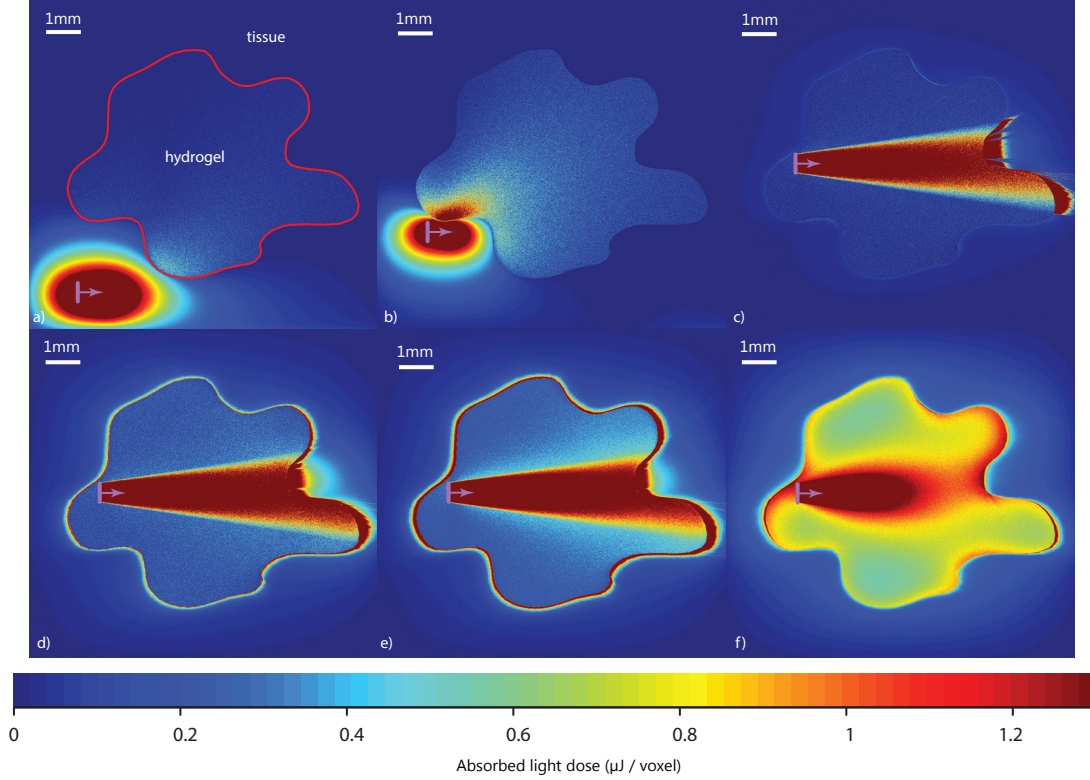


Figure 2.8: Fig. 8 Photopolymerization of a hydrogel within a tissue cavity: a) the hydrogel precursor ( $\mu_a = 0.43 \text{ cm}^{-1}$ , variable  $\mu_s$ ) is injected into the cavity. The surrounding tissue is modeled with an absorption coefficient of  $\mu_a = 0.33 \text{ cm}^{-1}$  and scattering coefficient  $\mu_s = 210 \text{ cm}^{-1}$ . An optical fiber (violet arrow) is introduced into/next to the cavity (NA=0.22, diameter  $600 \mu\text{m}$ ), the color-scale indicates the amount of absorbed energy per voxel. The hydrogel precursor requires a minimal irradiance of  $0.52 \mu\text{J}$  per voxel corresponding to a fluence of  $520 \text{ mJ/cm}^2$  for photopolymerization. In a) the probe is placed several millimeters away from the cavity b) the probe is located next to the cavity wall c) the probe is in the cavity, no scattering additives are present in the gel ( $\mu_s = 0.000 \text{ cm}^{-1}$ ) d) low amount of scattering particles (SP) ( $\mu_s = 0.1 \text{ cm}^{-1}$ ) e) medium amount of SP ( $\mu_s = 1 \text{ cm}^{-1}$ ) f) high amount of SP ( $\mu_s = 10 \text{ cm}^{-1}$ )

The position of the fiber-tip is important (Fig. 2.8a-c). Missing the cavity by a distance of less than  $500 \mu\text{m}$  (Fig. 2.8b) leads to no significant light dose in the cavity. In c) the polymerized volume is  $38.1 \text{ mm}^2$  whereas in b) it is only  $2.2 \text{ mm}^2$  and in a) it is  $0 \text{ mm}^2$ . We observe in Fig. 2.8c) that even if the probe is placed at the right position the low scattering coefficient and the

high absorption coefficient do not lead to a complete polymerization of the cavity volume. By adding scattering particles, the scattering coefficient rises (Fig. 2.8c-f) and the amount of photopolymerized hydrogel can be increased by a factor 4 to  $152.4 \text{ mm}^2$  (Fig. 2.8f) where the cavity is completely filled with solid polymer. There is an optimal amount of scattering particles which can be added to the gel. If this amount is too low (Fig. 2.8e) light is scattered weakly and most of it is absorbed at the cavity edge. We find that a scattering coefficient  $\mu_s = 10 \text{ cm}^{-1}$  leads to an adequate level of scattering that provides a uniformly absorbed light-dose in the cavity. If the concentration of scattering particles increases further, the light is not able anymore to reach the edges of the cavity.

## 2.8 Conclusion

A simple and robust photopolymerization Monte Carlo model is presented and applied to the case where the dimension of the light source is much smaller than the volume of the photopolymerizable hydrogel. The model was validated and compared to experimental results by using a PEGDMA hydrogel. Good agreement between predicted and actual polymer volumes and shapes was found. Reflection and refraction effects at solid-liquid-interfaces did not impact the shape or volume of photopolymerized material. Our in-vitro experiments show that uniform spherical volumes up to  $700 \text{ mm}^3$  can be photopolymerized in 10 min using Intralipids, and that by pre-illuminating a hydrogel precursor, a volume of up to  $3500 \text{ mm}^3$  can be reached. Simulations and photopolymerization experiments inside a cavity filled with a hydrogel provide insights into the polymer-light-tissue-interactions. We observed that the probe-position is crucial and that a certain amount of scattering particles increases the polymerized volume by a factor 4. Furthermore, it is conceivable that a gradient of scattering particles in the hydrogel is used to tailor the polymerization rates of certain areas and hence their mechanical properties. Thus, by means of simulations and in situ experiments, this article shows the potential for injecting and hardening photopolymerizable, optically scattering hydrogel-implants through a small diameter fiber thus paving the way for minimal invasively implanted tissue replacements or scaffolds.



## 3 Miniature probe for the delivery and monitoring of a photopolymerizable material

This chapter mainly consists of an article published in the journal of biomedical optics [191]. The co-authors are A. Khoushabi, C. Schizas, P.E. Bourban, D.P. Pioletti and C. Moser

### 3.1 Abstract

Photopolymerization is a common method to cure materials initially in a liquid state, such as dental implants or bone or tissue fillers. Recent advances in the development of biocompatible gel- and cement-systems open up a new avenue for *in situ* photopolymerization. For minimally invasive surgery, such procedures require miniaturized surgical endoscopic probes to activate and control photopolymerization *in situ*. In this work, we present a miniaturized light probe in which a photoactive material can be 1) mixed, pressurized and injected 2) photopolymerized/photoactivated and 3) monitored during the chemical reaction. The device is used to implant and cure Poly(Ethylene Glycol) Dimethacrylate-hydrogel-precursor *in situ* with UVA light (365 nm) while the polymerization reaction is monitored in real time by collecting the fluorescence and Raman signals generated by the 532 nm excitation light source. Hydrogels could be delivered, photopolymerized and monitored by the probe up to a curing depth of 4 cm. The size of the photopolymerized samples could be correlated to the fluorescent signal collected by the probe and the reproducibility of the procedure could be demonstrated. The position of the probe tip inside a bovine caudal intervertebral disc could be estimated *in vitro* based on the collected fluorescence and Raman signal.

### 3.2 Introduction

Photopolymerization [171, 172] is widely used to harden polymers in controllable manner by illuminating a liquid monomer or an uncured polymer precursor. Initially photopolymerization was used for coatings, printing, paints, adhesives, optical fibers, etch resist or printed circuits [174, 175, 176, 173]. It found its way into the biomedical sector where photopolymerizable

materials are used for dental implants [177], cell encapsulation [178, 132], tissue-replacements [138, 121], drug delivery [136], implant coatings, bio-glues [62] and microfluidics [130]. One of the advantages of photopolymerization is that by using light illumination, the initiation and speed of the polymerization reaction can be controlled actively [192]. To monitor photopolymerization reactions, methods such as speckle interferometry [161], Raman spectroscopy [162], transmittance measurements [163], fluorescence spectroscopy [164, 165, 168], UV-, Vis-, NIR-, MIR-spectroscopy, nuclear magnetic resonance spectroscopy and acoustic monitoring [166] have been proposed.

However, during minimally invasive, surgical implantation of a photopolymerizable material, the implant is hardly accessible which makes the methods above difficult to implement. To our knowledge, there is no report of a system to simultaneously photopolymerize and monitor a photopolymerization reaction in a minimally invasive manner [134]. In certain cases there is sufficient access to illuminate and monitor polymer injected into a tissue cavity. For instance in dentistry while placing a dental implant a hole is drilled and the tissue cavity can easily be filled and illuminated. The monitoring is done by visual and haptic inspection. In minimally invasive surgery, such as the case of an intervertebral disc replacement, this is more complicated because of the limited space. Having the means to monitor whether the implant is well polymerized is essential: the geometry of the tissue cavity is unknown, tissue pieces can cover the probe tip or the light can be absorbed by blood. All these issues make the effective polymerization time change at each intervention. Therefore it is necessary to have *in situ* photopolymerization monitoring.

We thus report on a method and device that enables photopolymerization in a minimally invasive way and provides *in situ* monitoring of the photopolymerization state during illumination. We show that the liquid-to-solid-transition during photopolymerization can be monitored, which potentially gives the surgeon a real time feedback during a surgery. We developed a custom surgical probe in which a photoactive material can be 1) mixed, pressurized and injected 2) photopolymerized/photoactivated and 3) monitored during the chemical curing reaction. To illustrate the device performance, we report experiments of hydrogel samples implanted into a bovine intervertebral disc model.

### 3.3 *in situ* Photopolymerization Monitoring

Figure 3.1a) illustrates the probe concept: A cannula or catheter containing an optical light guide is inserted into a living tissue. In the empty space around the optical fiber, a liquid polymer precursor is injected which flows out to the distal end of the cannula to fill a tissue cavity, such as the degenerated core of an intervertebral disc. The polymer precursor is photopolymerized by light brought by the optical fiber. The photopolymerized, solid volume will grow gradually over time. In order to homogenize the light distribution in the volume, scattering particles are added to the photopolymer. In figure 3.1b) the principle of *in situ* photopolymerization monitoring is illustrated: a second beam of light is sent through the optical light guide. This monitoring light can be reflected, backscattered by the liquid or solid



### 3.4. Surgical Device for Injection, Illumination and Monitoring

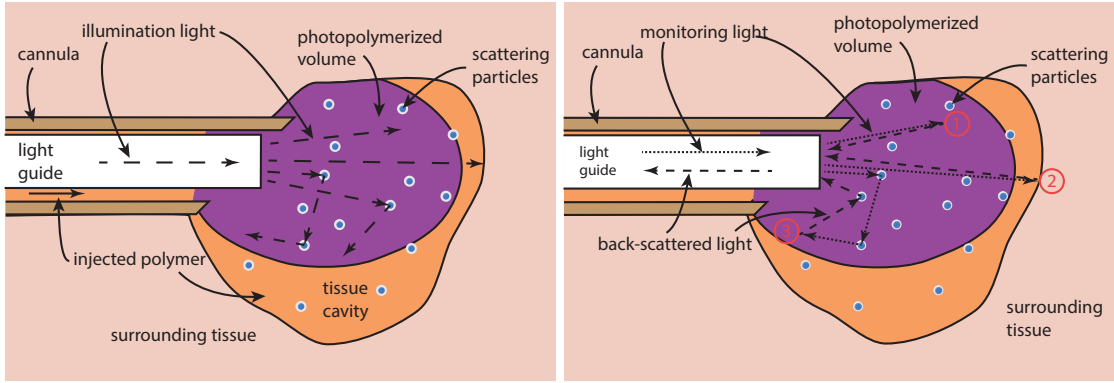


Figure 3.1: Schematic illustration of a probe for a) *in situ* photopolymerization and b) *in situ* photopolymerization monitoring. In a) polymer precursor (orange) is injected into a tissue cavity and illuminated with a UV light for photopolymerization. Scattering particles enhance amount of photopolymerized polymer (violet) by homogenizing the light in the volume. In b) a second beam of light is used to monitor the polymerization reaction. This monitoring light can be reflected or backscattered by the polymer directly (1), the surrounding tissue (2) or via the scattering particles (3).

polymer or the surrounding tissue. The scattering particles further allow collecting photons which originate from positions outside of the illumination cone of the light guide (e.g. figure 3.1b, number 3). This light is then collected by the same light guide and then detected on the proximal side to provide an electronic signal. We expect that the intensity and the spectrum of this signal provide information about the current photopolymerization state in real time and *in situ*.

### 3.4 Surgical Device for Injection, Illumination and Monitoring

In figure 3.2, the illumination and detection system as well as the custom surgical probe are presented. The illumination system consists of two arms that are combined by a dichroic, long pass filter at 400 nm and coupled in a multimode fiber (600  $\mu\text{m}$  core, Polymicron Technologies, FVPE60060710/2M) to provide an illumination source for photopolymerization (LED source at 365 nm, Nichia, NCSU033B) and a source for monitoring the photopolymerization reaction (laser source at 532 nm, CNI Technology, MSL-FN-532). The optical fiber is inserted into the surgical probe (lower right picture). Within the surgical injection probe, the fiber and the liquid polymer-flow are combined. At the distal tip of the probe, the liquid polymer surrounds the fiber flowing in the interspace between the fiber and the cannula wall. A pressurization joint and an integrated Luer-Loc connector ensure that the polymer can be injected at high pressures (up to 50 MPa) without any backflow. During illumination, back-scattered and reflected photons are collected at the distal end of the illumination fiber and back-propagated through the fiber (as illustrated in fig. 3.1b). The dichroic, long pass filter (550 nm) separates the illumination light from fluorescence and Raman signal generated by the illuminated sample. The band pass filter (532 nm) filters out the excitation laser light and the spectrometer

### Chapter 3. Miniature probe for the delivery and monitoring of a photopolymerizable material

(Princeton Instruments, Acton SP2300) records the fluorescence and Raman spectra of the sample.

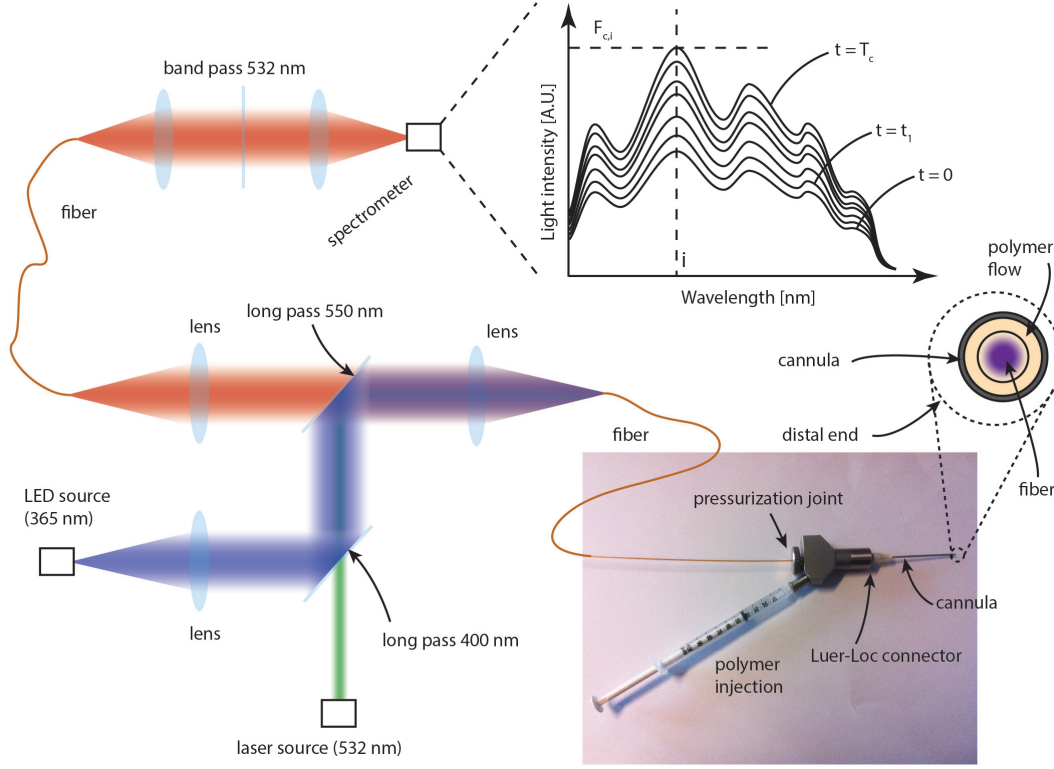


Figure 3.2: Schematic illustration of the illumination and detection system. The sample is illuminated with a LED light source (365 nm) to photopolymerize the injected photoreactive precursor and with a green light source (532 nm) to monitor photopolymerization. The spectrometer records the back-scattered fluorescence and Raman spectra. The distal tip of the device consists of a cannula containing the optical fiber and a circular chamber to inject the liquid photopolymer.

Throughout photopolymerization, the spectrum of the backscattered light changes. The evolution of the spectrum intensity is described using a function  $F$  that depends on time  $t$  and the wavelength  $\omega$ :

$$F(\omega, t) \quad (3.1)$$

Let's denote by index  $i$ , the frequency position of the  $i^{th}$  spectral peak in the spectrum (e.g. a peak at 600 nm).

$$F_i(t) = F(\omega_i, t) \quad (3.2)$$

Critical values  $F_{c,i}$  can be defined which indicate that the photopolymerization reached a



### 3.5. *In situ* Photopolymerization Monitoring Results

critical threshold after time  $T_c$ :

$$F_{c,i} = F(\omega_i, T_c) \quad (3.3)$$

A critical threshold could be for instance a 90% conversion from un-cured precursor to cured network. The polymerization is stopped once such a critical value is reached.

### 3.5 *In situ* Photopolymerization Monitoring Results

Two types of polymer materials were chosen for *in situ* tests: 6 kDa Poly(Ethylene Glycole) Dimethacrylate, so called PEGDMA was synthesized 25, and samples 1. with and 2. without Nano-fibrillated cellulose (NFC) fibers (EMPA, Switzerland) were prepared. The cellulose fibers act as scattering particles which leads to a more uniform distribution of the light in the hydrogel. On the other hand, they also strengthen the polymer-matrix, acting as a reinforcing fiber composite. Irgacure 2959 (BASF, Germany) was used as photoinitiator. The used concentrations are indicated in table 3.1.

Table 3.1: Preparation of PEGDMA hydrogel samples

Sample	PEGDMA 6 kDa [wt%]	NFC [wt%]	Irgacure 2959 [wt%]	PBS [wt%]
1. Neat hydrogel	10	0	0.1	89.9
2. Composite hydrogel	10	0.72	0.1	89.18

The tip of the probe was immersed into a large volume of polymer precursor (fig. 3.3a) and the samples were illuminated with UVA light (365 nm, 3.4 mW) and green light (532 nm, 13.3 mW). A spectrum was recorded every 15 seconds. To reduce noise, the exposure time was set to 10 seconds. The experiment was stopped at different time-intervals to evaluate the volume of photopolymerized PEGDMA hydrogel. As a hydrogel is a water-based polymer, the Raman/fluorescence signal of water is used as a reference signal. This signal does not change during photopolymerization.

As a baseline reference, the spectrum shown in fig. 3.3a) was recorded during immersion of the probe into a phosphate buffer solution (PBS, i.e. water). The first peak at 532 nm is due to the linear scattering and reflections of the excitation beam. Between 532 and 580 nm the silica Raman bands of the fiber are present with their double peak around 540 nm ( $\sim 450 \text{ cm}^{-1}$ ) and four smaller peaks between 550 and 580 nm ( $\sim 600 - 1200 \text{ cm}^{-1}$ ). Between 580 nm and 700 nm the signal is dominated by fluorescence. No Raman signal of the water can be seen between 625 nm and 658nm ( $2800 \text{ cm}^{-1}$  and  $3600 \text{ cm}^{-1}$ ). Between 700 and 780 nm the spectrum originates from the 365 nm LED itself.

### Chapter 3. Miniature probe for the delivery and monitoring of a photopolymerizable material

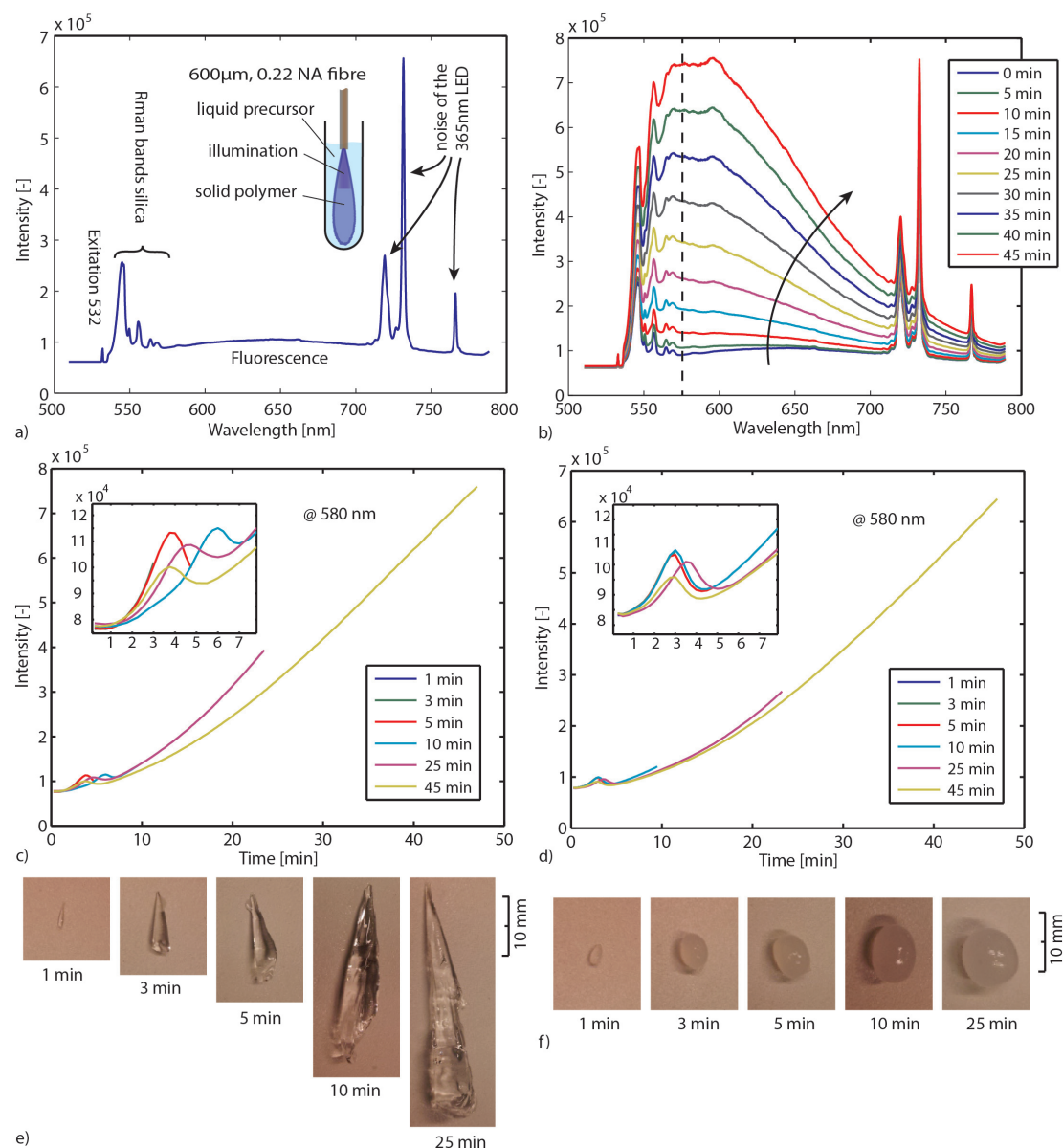


Figure 3.3: Liquid samples were illuminated with a 600  $\mu\text{m}$  fiber. a) back-ground signal recorded when immersing the probe into water. b) spectra over time during photopolymerization of a PGDMA sample. c) the change in intensity over time for different samples measured at 580 nm without NFC fibers and d) with NFC fibers. e) resulting volumes after photopolymerization without NFC fibers and f) with NFC fibers

In fig. 3.3b) the spectra of a PEGDMA hydrogel during photopolymerization and monitoring is shown (both the 365 nm LED and the 532 nm laser are turned on). At the beginning (0 min) the spectrum is not significantly different to water. The hydrogel is transparent. No fluorescence is induced. Over time the sample starts to solidify, the spectra gradually change and a strong fluorescence signal centered between 550 and 600 nm appears. A wavelength of 580 nm in the

### 3.5. *In situ* Photopolymerization Monitoring Results

spectrum ( $F_{i=580nm}=f_{580}(t)$ ) was chosen arbitrarily for monitoring the photopolymerization. In fig. 3.3c) and 3.3e) a PEGDMA samples without NFC fibers are presented. Hydrogels were illuminated while the fluorescence at 580 nm was monitored. The samples were retrieved and photographed. The samples grew steadily up to a final length of 40 mm after 25 minutes (after 25 minutes the polymer growth is limited by the glass container). For the hydrogels without NFC, we observe that the resulting shapes are irregular and the monitoring signal shows peaks appearing between 3 and 5 minutes. The peaks' position varies from sample to sample.

The results of the hydrogels with NFC are shown in fig. 3.3d) and 3.3f). The resulting shapes are more sphere-like due to the scattering properties of the hydrogel caused by the presence of the nano fibrils of cellulose. The fluorescence intensity curves are reproducible. We observe that the inter-sample variance of the signal is smaller for the hydrogel with NFC. During photopolymerization, the injected liquid material in front of the probe solidifies first. Thus, its refractive index, particle size and therefore scattering properties change. A change in refractive index and a higher amount of scattering events increases the backscattered signal collected by the fiber. This could partly explain the increase in signal around 3-5 min, however it remains unclear why these peaks decrease after this time before growing again.

The particle size can significantly influences the scattering properties of a material. The critical particle size is  $x = 2\pi r / \lambda$  where  $r$  is the particle diameter and  $\lambda$  the wavelength of the light. If  $x \ll 1$  is true, Rayleigh scattering will occur. If  $x \sim 1$  the scattering can be characterized by Mie's theory for spherical particles. Other Mie solutions for different shapes such as infinite cylinders also exist. The size of the NFC fibers has been studied previously using cryo scanning electron microscopy (cryo-SEM) [169]. However, the results are partially controversial: 1) the fiber size (diameters and length) were not uniform 2) the fibers also agglomerate. The filament diameter was estimated to be between a few and  $\sim 100$  nm. Therefore, most probably, the occurring scattering is a mixture between Rayleigh and Mie scattering. Moreover, the liquid or solid gel has a white color without any bluish shade, which would occur in the Rayleigh regime (the scattering intensity is proportional to  $1/\lambda^4$ ). This indicates that Mie scattering might be dominant. The hydrogel alone is almost transparent (before, during and after photopolymerization). After the photopolymerization of the hydrogel the NFC fiber network remains incorporated within the hydrogel and the fiber orientation remains unchanged. Therefore, it can be concluded that the scattering properties of the solid or liquid composite hydrogel should be the same.

To better understand how such a polymer develops in time, the *in situ* measured fluorescence signal (via the fiber) was compared to an *ex situ* fluorescence signal (collected from outside of the cuvette). The polymerized volumes induce scattering and fluorescence which can be recorded from outside the cuvette (fig. 3.4a). By applying an intensity threshold to each image (fig. 3.4b) and counting the pixel values within a relevant area (fig. 4c) the current shape and an *ex situ* intensity are generated. At the same time, the *in situ* fluorescence is measured using the probe (fig. 3.4e). No significant change of either the *ex situ* signal or polymerized sample volume could be observed between 2 and 4 minutes (position of the peak in fig. 3.4e). Thus, it can be concluded that the peaks occurring during the 3-5 min are not related to the photopolymerized volume.

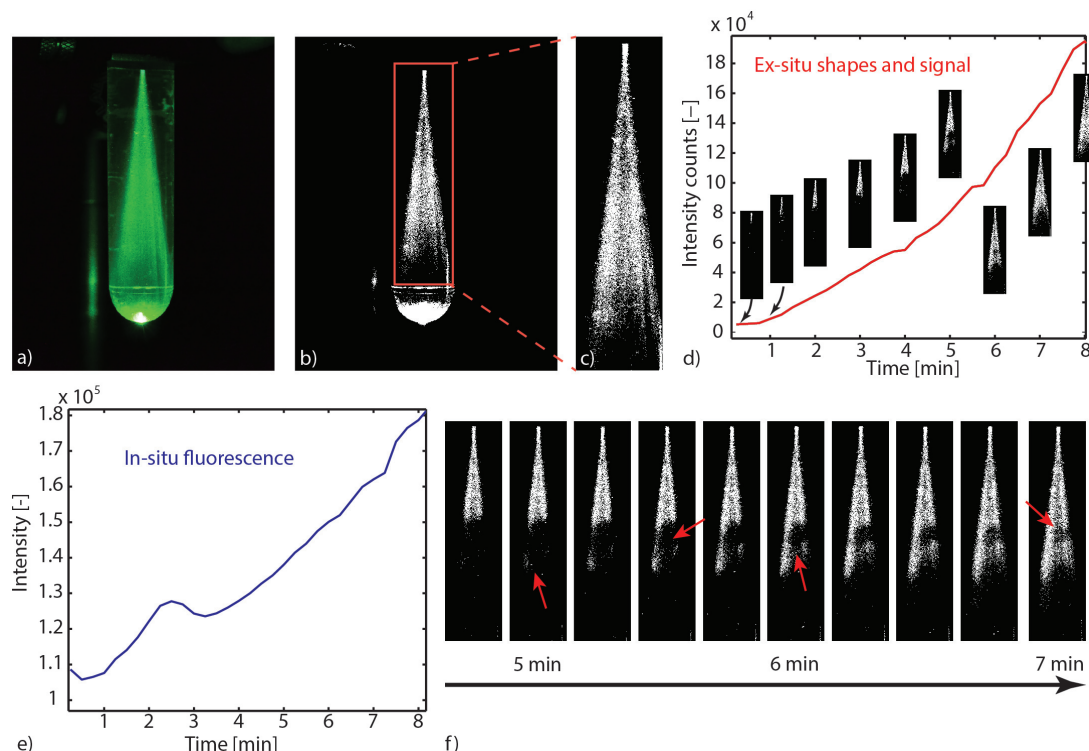


Figure 3.4: The photopolymerized volume is imaged from outside the cuvette (a), a threshold is applied within a relevant area (b and c) and by a pixel count the size and the signal intensity plotted over time (d). The *ex situ* signal does not show any peak between 2 and 4 minutes, while during *in situ* monitoring of the same sample such a peak appears (e). In detail evolution of the sample size and geometry over time (f).

Furthermore, using the *ex situ* data, the polymer growth is monitored and certain irregularities of the polymer volume are observed, such as shown in figure 3.3e). In figure 3.4f), a nucleation is happening locally away from the main volume (red arrow, 5 min). There is an empty or less dense space in between the main volume and the nucleation (red arrow, 5 min 30 s). Then, the polymer more distal to illumination fiber starts to form (red arrow, 6 min) and only later the empty space is closed (red arrow, 7 min).

In the monitoring experiments shown in figures 3-4, the fluorescence signal does not exhibit a saturation effect. We expect that when the hydrogel is fully photopolymerized, the fluorescence signal should saturate. In the experiments above, the volume of the hydrogel was large and the UVA exposure time (up to 50 min) was not enough to fully photopolymerize the whole volume. We thus perform the following experiment with a lower amount of hydrogel and compare the results with photorheology.

In figure 3.5a), the illuminating fiber was placed at a distance of 500  $\mu\text{m}$  away from the bottom of an optical cuvette (fig. 3.5a). To avoid that the precursor dries out or reacts with air during illumination, the cuvette was filled with polymer precursor. Some of the illumination light reaches the volume above the fiber (black arrow) by reflection off the cuvettes' wall and by

### 3.5. *In situ* Photopolymerization Monitoring Results

scattering from the NFC fibers. Finally, the entire volume in the cuvette is cured. Fluorescence photons generated above the fiber tip can still be collected by the same fiber via reflection and scattering (dotted arrow). Fig. 3.5b and c) show the cured sample with fiber tip at 365 nm (illumination light) and at 532 nm (monitoring light). Figure 3.6d) shows the time dependence the fluorescence spectrum at three monitoring wavelengths. We observe that the signal intensity starts to saturate after approximately 120 minutes. We then compare this time scale with a photorheology measurement (fig. 3.5e). The illumination in the photorheology apparatus is uniform across the area of the hydrogel (illumination intensity: 5 mW / cm<sup>2</sup>). The thickness of the hydrogel is 500  $\mu$ m. The chemical conversion can be associated to the elastic modulus [193] which is measured using the cyclically rotating plate. The curve saturates after 20 minutes. The difference in saturation time comes from the illumination geometry. In the case of the fiber, the illumination area is small (0.28 mm<sup>2</sup>) and light needs to be scattered to reach the volume whereas in the photorheology apparatus, the whole volume is illuminated with the same intensity at once.

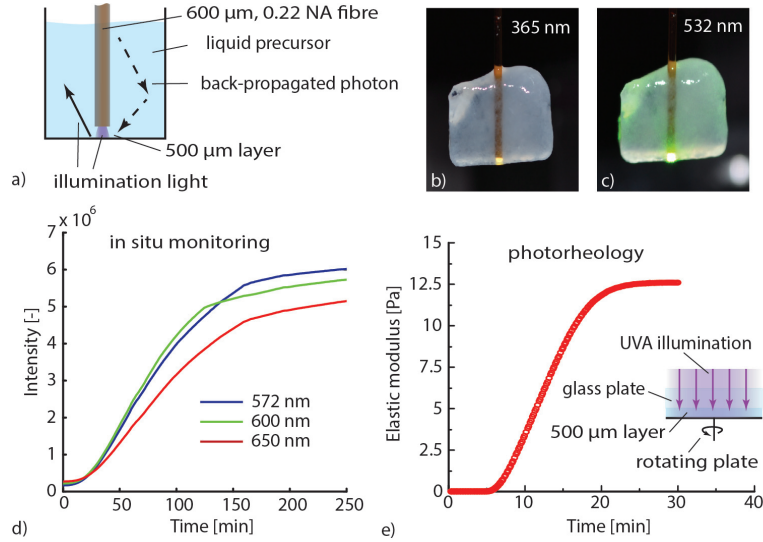


Figure 3.5: Saturation of the monitored fluorescence signal. The fiber tip was placed at 500  $\mu$ m from the bottom of an optical cuvette containing the liquid PEGDMA-NFC hydrogel (a). The UVA light (b) and visible light (c) are distributed within the entire volume. d) the monitoring signal, measured at three different wavelengths starts to saturate after approximately 120 minutes. e) photorheology of a 500  $\mu$ m layer of hydrogel to measure the elastic modulus during solidification.

This experiment shows that the fluorescence measurement exhibit a saturation effect that might be attributed to a solidification of the whole volume. However, we cannot exactly monitor a specific conversion state at a given position in the polymer. Figure 3.5 indicates that the device can still monitor changes of the material which occur up to 10 mm away from the probe tip only using back-scattered photons. Yet, there is no information about a specific position. The overall collected backscattered fluorescence gives an average over the sample

and we correlated the change in fluorescence with the actual polymerized volume. To retrieve more specific information it would be necessary to emit and collect light at different positions (e.g. using a multicore fiber). Based on the recorded signal and by using a model, for instance Monte Carlo, a conversion rate at a given position could be calculated.

In practice, the surgery time is strongly limited and it would not be possible to illuminate a sample during 120 minutes. Thus, to further improve the photopolymerization of an injectable implant, either the illumination power can be increased or a more efficient photoinitiator could be used. However, it is also not necessary to achieve a full conversion of the polymer precursor to have sufficient mechanical strength. Conversions of 30 or 50 % might already be sufficient to achieve a sufficiently cured material [194].

As PEG-base gels usually swell when immersed into water or PBS [195] the increase in volume could also be attributed to swelling and not photopolymerization. Yet, the impact of dissolved PEG molecules on the ionic strength of the solvent is much higher than the impact of dissolved ions in the PBS ( $\text{Na}^+$ ,  $\text{Cl}^-$ ,  $\text{K}^+$ ,  $\text{PO}_4^{3-}$ , etc.). Therefore, whether PEG is dissolved into water or PBS the resulting solution will be governed by the PEG-solute. As the hydrophilic PEG backbone is the driving swelling force, the hydrogel swelling will not change throughout the photopolymerization reaction because the PEG backbone itself does not change. Therefore the osmotic pressure within the solid and the liquid will be the same at any time of the reaction, even independent on whether the hydrogel was prepared with water or PBS. However, this is only true for an isolated system, if the PEG is photopolymerized within a tissue cavity for instance, there will be an osmotic pressure difference between tissue and hydrogel. The hydrogel may attract water from the tissue or vice-versa. In the first case the hydrogel will swell and exert a pressure onto the cavity wall. The second case results in contraction of the hydrogel and a negative pressure.

### 3.6 *in vitro* photopolymerization monitoring

To further evaluate the probe, the PEGDMA-NFC hydrogels were implanted into intervertebral discs. Bovine tails were obtained from a local slaughter house. Following dissection, papain, an enzyme which degenerates the core of the intervertebral disc, was injected in the IVD (100-200  $\mu\text{l}$ , 100 U/ml) and each disc was cultured in an incubator (medium: Dulbecco's Modified Eagle's Medium with 10 % Fetal Bovine Serum and 1 % L-Glutamine) during 7 days. The surgeries were performed through a 19 gauge needle (outer diameter: 1.07 mm, inner diameter: 0.69 mm) connected to the probe (fig. 3.6). The PEGDM-NFC hydrogel was injected and then illuminated. During surgery the position of the needle's tip needs to be located in the middle of the IVD (in the void). If the light emitting needle tip is covered by a tissue layer, most of the emitted light will be absorbed in the tissue and not in the hydrogel. In figure 3.6a) an intervertebral disc is illuminated at 532 nm only. This wavelength does not induce any photopolymerization and the space inside the IVD is probed at different positions. If the tip is placed in front of a tissue layer (position 1 & fig. 3.6d), the scattering is almost as important as the Raman peak of the silica fiber. The signal decreases if the probe is placed at the side of the



### 3.6. *in vitro* photopolymerization monitoring

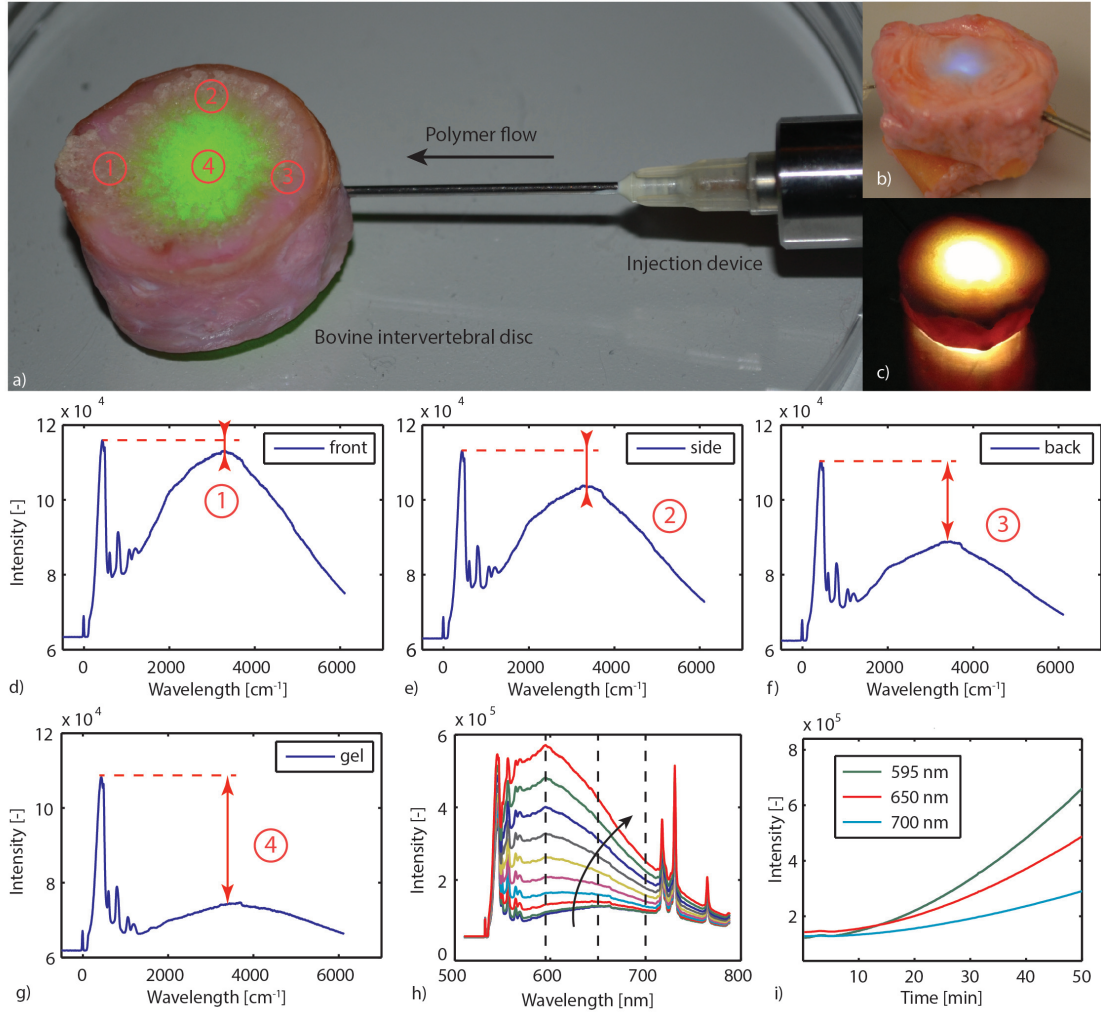


Figure 3.6: PEGDMA hydrogel is injected into a bovine intervertebral disc. a) the probe is used in a monitoring-only-mode at 532 nm, number (1)-(4) denote different probing positions. b) and c) the UVA light (365 nm) is switched on to photopolymerized the injected sample. The different positions (1)-(4) were evaluated: d) at the front of the intervertebral disc, e) at the side, f) at the back without hydrogel and g) in the middle with hydrogel. h) *in vitro* photopolymerization monitoring: a spectra over time from 0 to 45 min (black arrow). i) fluorescence intensity is tracked in function of wavelength over time.

intervertebral disc (position 2 & fig. 3.6e) or at the back of the intervertebral disc (position 3 & fig. 3.5f). When the PEGDMA hydrogel is injected, tissue scattering is further decreased because the space in front of the tip is filled with the hydrogel (position 4 & fig. 3.6g). The hydrogel is then activated by switching on the UVA light (fig. 3.5b and c). Although the tissue scattering background signal is present, the intensity of the backscattered signal develops (fig. 3.6h) in a similar way as predicted by *in situ* monitoring in a simple cuvette (fig. 3.3d). The intensity measured at different wavelengths ( $F_{i=595;600;650nm}$ ) increases steadily, indicating

that the injected hydrogel is photopolymerizing (fig. 3.5i). The critical value  $F_{c,i}$ , which indicates a given volume of solid hydrogel can be tabulated for a given volume of injected polymer. For instance for a cavity size of 5 mm (diameter)  $F_{c,i}$  would be set at  $1.5 \times 10^5$  (fig. 3.3 d,f) assuming that the illumination intensity is kept constant. Another option is to define  $F_{c,i}$  as a relative value such as  $F_{c,relative} = F_{i=595nm} / F_{j=540nm}$ . In this case  $F_{c,relative}$  would be set at  $\sim 0.53$  ( $\sim 2 \times 10^5 / 3.8 \times 10^5$ ) for the same 5-mm-cavity (fig. 3.3 d). Look up tables can be integrated into the device architecture and the values can be adapted depending on the size of the cavity or the injected volume, the illumination power, the injected polymer and the type of surrounding tissue.

## 3.7 Conclusion

We showed that photopolymerization of PEGDMA can be monitored by fluorescence spectroscopy. Although PEGDMA is transparent to the eye (without NFC) and the used hydrogel solution has a water content of around 90%, the fluorescence light contains enough spectral information that changes as a function of UV illumination time. We have experimentally correlated and quantified the photopolymerized volume growth with the fluorescence signal. It was found that the fluorescence signal increases during the crosslinking reaction. We have demonstrated that the custom probe and transportable photopolymerization monitoring device is functional in an *in vitro* bovine intervertebral disc. The underlining physics including scattering anisotropies and swelling behavior of the hydrogel during photopolymerization need to be further investigated. This monitoring probe and system could potentially be used as a mean to control the polymerization state for *in situ* and *in vivo* placed implants or drug delivery systems in field of orthopedic or cardiovascular surgery, oncology or dentistry. This work also shows the need for more effective and faster photoinitiators.



## **4 A photopolymerized composite hydrogel and surgical implanting tool for a nucleus pulposus replacement**

This chapter mainly consists of an article under review in Biomaterials. A. Khoushabi developed the implantation material and is also a first author of the article. The co-authors are D. Frauchiger, B. Gantenbein, C. Schizas, C. Moser, P.E. Bourban and D.P. Pioletti.

### **4.1 Abstract**

Nucleus pulposus replacements have been subjected to highly controversial discussions over the last 50 years. Their use has not yet resulted in a positive outcome to treat herniated disc or degenerated disc disease. The main reason is that not a single implant or tissue replacement was able to withstand the loads within an intervertebral disc. Here, we report on the development of a photo-polymerizable poly(ethylene glycol)dimetacrylate nano-fibrillated cellulose composite hydrogel which was tuned according to native tissue properties. Using a customized minimally-invasive medical device to inject and photopolymerize the hydrogel in-situ, samples were implanted through an incision of 1 mm into an intervertebral disc of a bovine organ model to evaluate their long-term performance. When implanted into the bovine disc model, the composite hydrogel implant was able to significantly re-establish disc height after surgery ( $p < 0.0025$ ). The height was maintained after 0.5 million loading cycles ( $p < 0.025$ ). The mechanical resistance of the novel composite hydrogel material combined with the minimally invasive implantation procedure into a bovine disc resulted in a promising functional orthopedic implant for the replacement of the nucleus pulposus.

### **4.2 Introduction**

The impact of low back pain on society is tremendous [3]. The economic burden was estimated to be up to 355 \$ per capita and annum for direct costs and 507 \$ for indirect costs [8] which results in a total of 200 billion per annum for a country such as the United States of America [9]. In its early stage, low back pain with or without sciatica is addressed with

## Chapter 4. A photopolymerized composite hydrogel and surgical implanting tool for a nucleus pulposus replacement

---

conservative treatments such as physical therapy or medication [196, 197]. In a later stage, decompression surgery might be warranted [198] and in the case of disc herniation a more invasive procedure such as discectomy is undertaken [131]. For persisting pain due to disc degeneration fusion of one or several spinal segments might become necessary [38]. The reasons for more severe surgery are mainly disc protrusion and herniation, degenerative disc disease [199] and spondylolisthesis [200]. For all these conditions, the range of motion of the spinal segment increases which leads to a segment instability and pain [201].

The ideal solution is a stabilization of the joint by reinforcing the degenerated or missing tissue of the nucleus pulposus (NP) [202] which is the core of the intervertebral disc (IVD). However, up to date, all implantation attempts with a NP replacement material have failed due to extrusion, expulsion or subsidence of the implanted material [46, 41]. The required material properties have been subject of controversial discussions over the last two decades. The current, general consensus is that more mechanically resistant materials need to be developed [203, 89, 204]. What is clear, is that a material needs to be implanted in a minimally invasive manner to avoid damaging existing tissue [203]. It also needs to re-establish disc height without destroying the endplate [202, 89] and should not extrude when the spinal segment is cyclically loaded [46, 205]. We propose an implant solution based on a photopolymerizable material. The low viscosity of the material is ideal for injecting it through a small capillary and for flowing into tissue interstices. The capillary also guides the curing light, thus providing an original solution for minimal intrusion and optimal control.

Photopolymerized implants first appeared more than 50 years ago in dentistry [206] where the initiation of the photopolymerization reaction by light was a significant advantage in terms of control and integration into enamel. Recent advances in water-based and biocompatible materials which allows photopolymerization of volumes of several cm<sup>3</sup>, open a new avenue for *in situ* photopolymerized implants for orthopedics [207], oncology [208] and ophthalmology [209]. Especially, photopolymerized hydrogels provide promising solutions for tissue replacements [134]. However, despite the large body of work in photopolymerized hydrogels, none of them to our knowledge, has the performance required for a NP replacement, and there are no devices available for controlled, minimally invasive placement of photopolymerized hydrogels.

Hydrogels lack structural strength, and thus are not adapted to cases of high mechanical stress, such as in the IVD [129]. Conventional methods to improve the hydrogel stiffness, such as increasing the cross-linker density, usually result in a loss of strength and water content [210, 211, 129]. Different hydrogel designs have been proposed to tackle this issue [210, 212] such as slip-link hydrogels [213] and double network hydrogels [214]. Although these methods result in significant improvement of stiffness and toughness, their long and/or sequential preparation makes *in situ* curing impractical. The use of a composite hydrogel is an alternative approach. Composite hydrogels combine the high stiffness and strength while preserving the one-step hydrogel preparation. The composite material retains the short curing time making the composite material suitable for *in situ* insertion. Minimally invasive photopolymerization has been achieved *in situ* by transdermal illumination [215] and irradiation through the walls of blood vessels [216]. To achieve the photocuring deeper within tissue, methods and devices

need to be developed.

Photopolymerized poly(ethylene glycol)dimethacrylate (PEGDMA) has been widely investigated for biomedical applications such as cell encapsulation [217], tissue engineering [218] and drug delivery [219]. PEGDMA is highly hydrophilic and the resulting hydrogel properties are tunable by changing the polymer's molecular weight and water content. Cellulose fibers showed to be a promising composite material for the reinforcement of the polymeric matrixes [220, 221]. The use of cellulose fibers to reinforce the hydrogel matrix is advantageous because cellulose is biocompatible and its addition only slightly influences the equilibrium water content [222]. Recently, in a separate study, we have shown that nano-fibrillated cellulose (NFC) fibers also have a positive impact onto the bio-optical scattering properties of a hydrogel which results in a more efficient and homogenous curing during light illumination [185].

In this study, we have prepared and tested a customized photopolymerizable composite hydrogel composed of PEGDMA and NFC. The relative concentration of reinforcement and molecular weight of polymer in the composite hydrogel can be tuned to match closely the properties of the NP native tissue. We further hypothesize that by injecting the liquid precursor and activating it through photopolymerization, the tissue integration of the implanted material is strongly enhanced.

## 4.3 Materials and Methodes

A hydrogel was first tailored to match the properties of native NP tissue in terms of elasticity and water content. A selected hydrogel was then evaluated against native bovine NP tissue during specifically designed functional tests: 1) confined compression was done to avoid subsidence into the IVD endplate, 2) the hydrogel's swelling pressure was tested to be able to re-establish disc height and 3) an extrusion test was performed to evaluate the hydrogel's resistance to extrusion or expulsion. Following material testing, a surgical injection, illumination and monitoring device was developed and applied to implant the composite hydrogel into an ex vivo bovine IVD organ culture model.

### 4.3.1 Sample preparation

#### 4.3.1.1 PEGDMA synthesis

PEGDMA was synthesized according to the description by Lin-Gibson et al. [185]. Poly(ethylene glycol) with molecular weights of 6 and 20 kDa and triethanolamine (99%) were purchased from Sigma Aldrich, Buchs, Switzerland. Poly(ethylene glycol) was dried by the aid of dean-stark distillation. Extra dry dichloromethane (99.8%) and diethyl ether (99.5%, extra dry over molecular sieve) were purchased from Acros, Basel, Switzerland. Dried poly(ethylene glycol) (20 g) was dissolved in 60 ml dichloromethane. Methacrylic anhydride (303 mg) and triethanolamine (462 mg) were added to the solution and the methacrylation was carried out under dry argon flow. After five days, the solution was precipitated in diethyl ether, filtered and dried overnight in vacuum at room temperature. The H-NMR spectrum revealed a 74%

## **Chapter 4. A photopolymerized composite hydrogel and surgical implanting tool for a nucleus pulposus replacement**

---

and 90% degree of methacrylation for the PEGDMA 6 and 20 kDa respectively.

### **4.3.1.2 NFC preparation**

Cellulose pulp (bleached softwood pulp, elemental chlorine free) with a residual chlorine content of 0.4 wt% was purchased from Zellstoff Stendal, Arneburg, Germany. Cellulose pulp was fibrillated with a high-shear homogenizer by pumping the suspension through two consecutive chambers with diameters of 400 and 200  $\mu\text{m}$  (i.e., H230Z 400  $\mu\text{m}$  and H30Z 200  $\mu\text{m}$ , respectively) for 12 passes. The resulting NFC suspension was concentrated with the aid of centrifugation (5'000 rpm, 25°C, three times during 15 min). According to cryo-SEM images the NFCs diameter was in the range of 2-100 nm and their length in the range of a few micrometers.

### **4.3.1.3 Composite hydrogel preparation**

Phosphate buffered saline (PBS, pH 7.4) was purchased from Gibco, Basel, Switzerland and 4-(2-hydroxyethoxy) phenyl-(2-hydroxy-2-propyl) ketone (Irgacure 2959) was purchased from BASF, Basel, Switzerland. PEGDMA powder (10 wt%) and NFC (0.5 vol%) were added to PBS. The PEGDMA was dissolved by keeping the solution in 37°C water bath for 15 min and the photoinitiator. Irgacure 2959 (0.1 wt%) was added to the suspension. The suspension was then homogenized by ultra turex (IKA T25 digital, SN 25 10G, Staufen, Germany) for 20 min in a dark chamber. The homogenized suspension was degassed at a pressure of 20 mbar. In order to characterize the hydrogel properties, the precursors were cast in plastic molds with a diameter of 8 mm and height of 4 mm, covered by microscope slides and illuminated by monochromatic 365 nm ultra violet lamp (AxonLab, Baden, Switzerland) with an intensity of 5  $\text{mWcm}^{-2}$  during 30 min.

### **4.3.1.4 Sample sterilization**

The photoinitiator solution and the PEGDMA dissolved in PBS were passed through the 0.22  $\mu\text{m}$  filter (Millex®GS, Millipore Corporation, Bedford, MA). NFC were autoclaved and the NFC solution was sterilized by UV light illumination during 30 min.

### **4.3.1.5 Nucleus pulposus preparation**

IVDs were isolated from bovine tails (age < 1 year old) obtained from a local abattoir. The endplates were removed surgically and the discs immediately frozen. An 8 mm surgical biopsy punch (Stiefel, Brentford, United Kingdom) was used to extract the frozen NPs from the IVDs. To unfreeze the samples, they were put in a closed plastic bag during 5 to 10 min to avoid any evaporation of water.

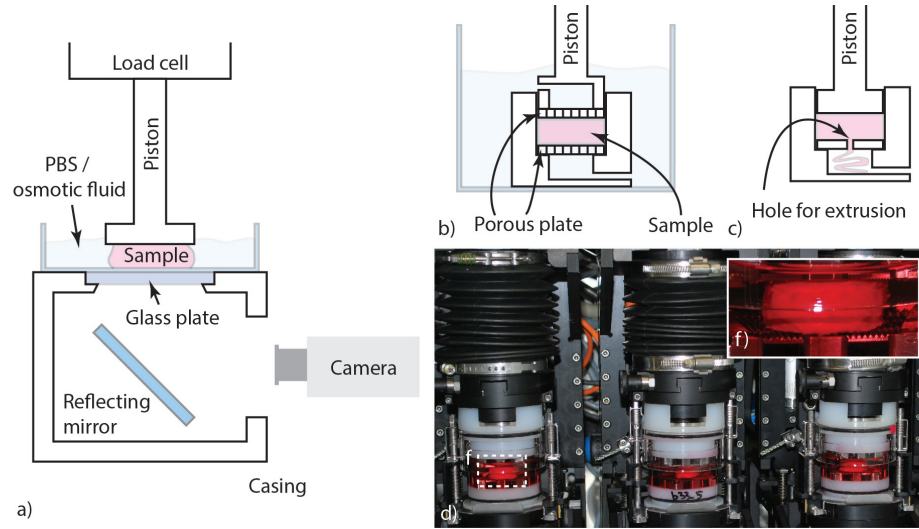


Figure 4.1: Customized compression setups: a) unconfined compression setup in which the sample's area and applied load can be measured simultaneously using a transparent casing and an optical tracking system, b) confined compression setup for swelling pressure assays, c) extrusion setup for tissue extrusion d) bioreactor for long-term incubation and testing f) live IVD organ culture within the bioreactor chamber.

### 4.3.2 Material characterization tests

#### 4.3.2.1 Water content evaluation

Hydrogels and NP weights were measured after swelling in PBS ( $W_s$ ) and after 2 days of drying ( $W_d$ ) in a vacuum oven (40 °C). The water content was then calculated from:  $100 \times (W_s - W_d) / W_s$ .

#### 4.3.2.2 Unconfined compression

Mechanical properties of the swollen hydrogels and NP were characterized under displacement-controlled monotonic loading (1 mm/min) until reaching 80% compressive engineering strain of the sample. Measurements were performed with an Instron E3000 linear mechanical testing machine (Norwood, MA, United States). As illustrated in fig. 4.1a, the samples were placed in a chamber filled with PBS during compression. A transparent substrate and a high-resolution camera were employed to measure the sample's area throughout the test. With the measurement of the deformation area, the stress-strain curves were calculated. The elastic moduli were calculated as linear extrapolations of the true stress-strain curves in the linear range of 0.15 - 0.25 strain.

## **Chapter 4. A photopolymerized composite hydrogel and surgical implanting tool for a nucleus pulposus replacement**

---

### **4.3.2.3 Confined compression**

A custom-made confinement setup with a porous upper and lower plate (fig. 4.1b) was used to compress the samples. The used rate was 10 mm/min. The porous upper and lower plates were covered additionally with filter paper (11  $\mu\text{m}$ , grade 1, Whatman, Kent, United Kingdom) in order to avoid any type of extrusion through the holes of the porous plate.

### **4.3.2.4 Swelling pressure**

To evaluate the swelling pressure, a pre-load of 0.15 N was applied and the corresponding displacement represented the zero position. The chamber (fig. 4.1b) was filled with PBS and the load was monitored while keeping the displacement constant. A preliminary 48 h test showed that all the samples reach the equilibrium pressure after 8 h, thus all the tests were done over a period of 8 h. The initial load of 0.15 N was subtracted and the swelling pressure calculated as the average pressure during the last hour of the test.

### **4.3.2.5 Extrusion**

Samples were compressed at a rate of 1 mm/min until they extruded through the hole in the lower plate (fig. 4.1c). Plates with different diameters of 0.5, 0.7, 1, 1.5 and 2 mm were used. The maximally applied pressure before the sample's extrusion was reported as the extrusion pressure.

## **4.3.3 Cytotoxicity**

For a clinical application it is crucial to make an injected hydrogel visible under X-ray. Thus, 155.2 mg/ml of Iodine (Iopamiro®300, Bracco Suisse SA, Manno, Switzerland) were added to the liquid hydrogel precursor. Liquid precursor before illumination and solid hydrogels after illumination were evaluated. For liquid samples, cells (50'000 cells/cm<sup>2</sup>) were placed in a 48 well plate and 250  $\mu\text{l}$  of precursor at different concentrations (1% to 50%) and 250  $\mu\text{l}$  of cell culture medium were added. For solid hydrogels, cylindrical samples ( $\phi$ : 8.4 mm, height:  $\sim$  8 mm) were photopolymerized during 30 min (LED light at 365 nm), placed in petri dishes ( $\phi$ : 35 mm) on top of cells (100'000 cells/cm<sup>2</sup>) and fixed with clamps to assure contact during incubation. After four days of incubation the hydrogels were retrieved to perform a Live/Dead® (Molecular Probes) assay. EthD-1 (4  $\mu\text{M}$ ) and Calcein (2  $\mu\text{M}$ ) were added (200  $\mu\text{l}$  for 48 well plates and 1 ml for 35 mm petri dishes) and the samples incubated during 40 min. For imaging samples were existed at 495 and 544 nm.



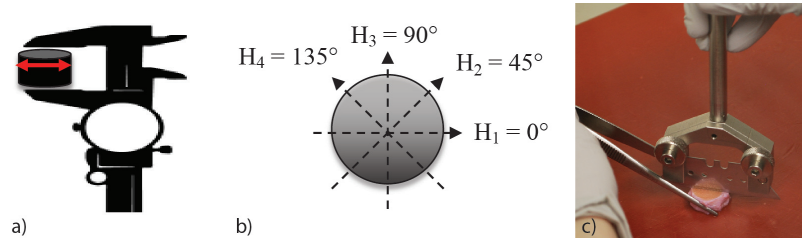


Figure 4.2: To measure the disc height, the disc is compressed using the sterilized caliper, (manually a short and high compressive force is applied: the disc should deform elastically) the caliper is released and the disc height is measured in the relaxed state (a). Four measurements are taken and averaged (b). The diameter of the disc is measured once after isolation in two directions using the same method. A special cutter is used to cut discs in the middle for histology (c).

#### 4.3.4 Implantation of the hydrogel into an organ model

##### 4.3.4.1 General protocol

To test the performance of the composite hydrogel as a potential NP replacement, we used bovine ex vivo IVD organ culture models, which have been proven to be a adequate option [1, 223]. Bovine caudal discs showed to be similar to human IVDs in terms of size, biomechanical behavior and biology [224, 225]. Figure 4.3 illustrates the protocol which was used to prepare the IVD organ model and to evaluate the implanted photopolymerized composite hydrogels. The success of a NP replacement can be evaluated by measuring the height of an IVD during cyclic loading [226, 227]. To evaluate the performance of the implant, the height of the implant was measured at four different “states”: 1) healthy state (after disc isolation), 2) pre-operative state (degenerated disc), 3) post-operative state (repaired disc after hydrogel injection and photopolymerization) and 4) state during follow up (disc after cyclic loading). For each state, the organ height was measured by a caliper according to the method presented in fig. 4.2. Before performing the measurement, a preconditioning was performed on each sample to assure inter-state comparability (red boxes in fig. 4.3). The results were all normalized to the healthy disc state.

##### 4.3.4.2 Organ model preparation

Fresh bovine tails (animal age < 1 year old) were obtained at a local abattoir. IVDs were isolated according to the previously described protocol [1, 228]. Briefly, to create the degenerated IVD model, papain (Sigma Aldrich, Buchs, Switzerland) was injected into the discs at a concentration of 100 U/ml. A buffer was prepared with 55 mM Na-Citrate, 150 mM NaCl and 5 mM EDTA in 400 ml H<sub>2</sub>O. The pH was set to 6.0 and the volume was adjusted to 500 ml with H<sub>2</sub>O. Before injection, the papain solution was prepared by adding 5 mM of Cysteine-HCl and papain (100 U/ml) to the buffer. Between 100 to 200  $\mu$ l of Papain solution were injected via a 25 Gauge needle (outer diameter 0.51 mm) into each disc and the injection position was

## Chapter 4. A photopolymerized composite hydrogel and surgical implanting tool for a nucleus pulposus replacement

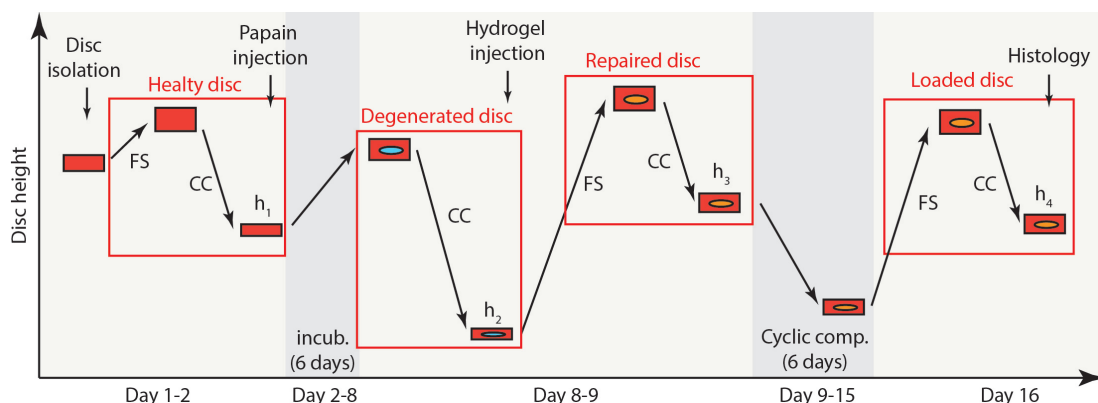


Figure 4.3: Testing protocol and predicted evolution of IVD disc height during degeneration, surgery and loading. Discs were isolated at day 1, Papain was injected at day 2 to induce the degeneration of the IVD over an incubation period of 6 days (day 2-8), the composite hydrogel was implanted at day 8 followed by a 6 day cyclic loading period (day 9 - 15) and then evaluated using histology at day 16. All states (four red boxes) were compared between each other: healthy state (after disc isolation; disc height:  $h_1$ ), pre-operative state (impaired and degenerated organ; disc height:  $h_2$ ), post-operative state (repaired; disc height:  $h_3$ ) and state during follow-up (after cyclic loading; disc height:  $h_4$ ). Before evaluating the height of an IVD in one state the specimen was conditioned by a 12h free swelling (FS) and a 2h cyclic compression (CC).

marked by a surgical thread. The injected discs were incubated (37 °C, 0.5 % CO<sub>2</sub>) during 6 days to digest the NP and form the cavity.

### 4.3.4.3 Surgery device for injection, photoactivation and reaction monitoring

To perform surgeries in a minimally invasive manner, a surgical device with the following functionalities was developed: 1) pressurization and injection of the liquid hydrogel, 2) illumination and photoactivation of the hydrogel and 3) reaction monitoring of the photopolymerization reaction. This was achieved by building a customized probe which combines an injection and an illumination channel at the same time. The sample is illuminated with UVA light at 365 nm (photopolymerization) and visible light at 532 nm (monitoring). A combination of fluorescence and Raman spectroscopy is used to track the photopolymerization reaction *in situ*. A more extensive description of the probe and the device is presented here [229].

### 4.3.4.4 Surgical procedure

A 19 Gauge needle (outer diameter 1.06 mm) containing the optical fiber (600  $\mu$ m core, NA of 0.22, Polymicron Technologies, Phoenix, AZ, United States) was connected to the customized probe. The area between the optical fiber and the needle was used for injection. The composite hydrogel was injected at the same location as the Papain previously. The precursor was then illuminated during 45 minutes using the LED light (365 nm, Nichia, Tokyo, Japan) butt-coupled



to the proximal end of the optical fiber.

#### 4.3.4.5 Bioreactor loading parameters

Each preconditioning (red boxes in fig. 2) consisted of a 12 h free swelling (FS) phase and 2 h cyclic compression (CC) phase (1 Hz, 0.1-0.2 MPa). During the incubation phase (day 2 to 8) the IVDs were left under free swelling condition. During the cyclic compression phase (day 9 to 15) the samples were cyclically loaded (0.2 Hz, 16 h per day at 0.1-0.2 MPa and 8 h per day at 0.075-0.05 MPa).

#### 4.3.4.6 Histology

Histology was done on day 16 i.e at the end of the cyclic loading. Each IVD was cut on the transverse plain using a specifically designed cutter (fig. 4.2c). After removal of the endplates by a scalpel, samples were frozen and sliced along the sagittal plain by a microtome (Leica CM3050 S, Leica Microsystems, Heerbrugg, Switzerland). Due to the high water content of the hydrogel (< 90 wt%), the slice thickness was increased to 100  $\mu$ m. Tissue sections were placed on a cover slip and fixed in 10 % formalin solution (Sigma Aldrich, Buchs, Switzerland) during 15 min. Sections were then stained with Hematoxyline & Eosin (H&E) solution and mounted with xylene-based glas<sup>TM</sup> medium (Sakura, Horgen, Switzerland). A light-transmitting microscope (Axiovert 100, Zeiss, Feldbach, Switzerland) was used for imaging. The magnification of the objective was 20x.

#### 4.3.5 Statistics

All values are presented as mean ( $\pm$  standard deviation). The statistical data analysis was done using Matlab (Mathworks, Natick MA, United States). Un-paired t-tests were used to compare different populations. For populations which changed over time (e.g. the organ model), paired *t*-tests were used for comparison. The population size (*n*) was always between 3 and 5 samples.  $P < 0.05$  was considered as a significant result (denoted as \*).  $P > 0.05$  was considered as a non-significant result (ns).  $P < 0.01$  was denoted as \*\* and  $p < 0.001$  as \*\*\*.

## 4.4 Results

### 4.4.1 Hydrogel design and selection

The material selection was done iteratively by comparing equilibrium water content, ultimate rupture strain and elastic modulus of native NP tissue and candidate hydrogels (fig. 4.4). The hydrogel properties were tuned by changing the cross-linker density and concentration of NFC reinforcement in order to achieve high deformability and strength.

## Chapter 4. A photopolymerized composite hydrogel and surgical implanting tool for a nucleus pulposus replacement

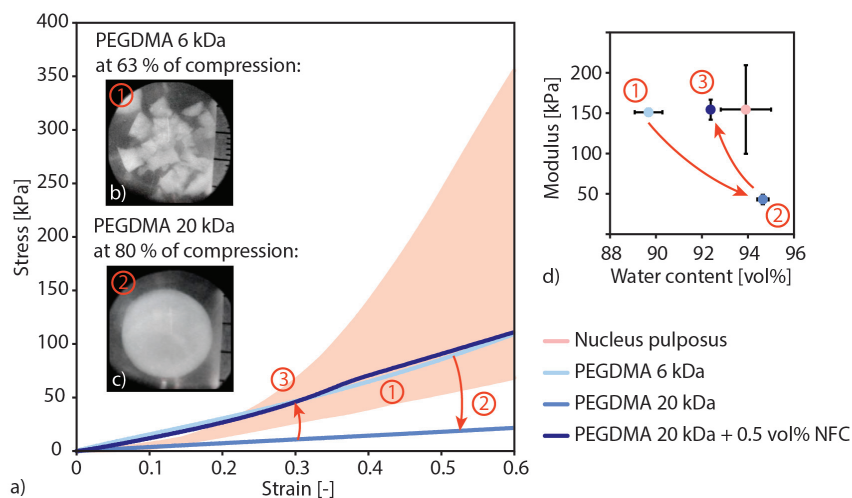


Figure 4.4: Hydrogel properties tuning in function of a) modulus, b,c) maximal rupture strain and d) water content. Development step 1 (in red): PEGDMA 6 kDa hydrogel has a similar modulus (a) and water content (d) as the NP, but fails at a strain of 63% (b). Step 2 (in red): The PEGDMA molecular weight was increased to 20 kDa in order to improve the hydrogel deformability (c), however this hydrogel shows a lower modulus (a). Step 3 (in red): This hydrogel was then reinforced with 0.5 vol% NFC fibers to reach the desired modulus (a) while keeping the same deformability and high water content of the NP (d).

The photopolymerizable PEGDMA hydrogel with the molecular weight of 6 kDa had a modulus and water content similar to the NP. However, this hydrogel failed under compression at a strain of 63 % and a stress of 220 kPa (fig. 4.4b – development step 1). The hydrogel cross-linker density was then reduced by increasing the PEGDMA molecular weight from 6 kDa to 20 kDa which improved the hydrogel's ultimate rupture strain (fig. 4.4c – step 2). The resulting hydrogel was able to withstand the maximally applied strain level of 80 % and had 5 wt% higher water content. Yet, this improvement in deformability was associated with a loss in elastic modulus (fig. 4.4a,d – step 2). To compensate for this loss, the material was strengthened using the NFC as reinforcement which increased the material's stiffness and toughness while keeping the high equilibrium water content (fig. 4.4a,d – step 3). Figure 4.4a, illustrates the stress-strain curve of the PEGDMA 20 kDa reinforced with 0.5 vol% of NFC. The composite hydrogel achieved a targeted modulus range of the tissue (150 kPa), reached high water content (> 90 wt%) and withstood the maximum applied strain of 80 % without failure. This composite hydrogel was chosen for further tests directly associated to the function of the implant.

### 4.4.2 Functional testing

The confined compressive behavior, swelling pressure and extrusion properties are specific to the organ or implant function of the IVD or the NP tissue replacement. Both native tissue and composite hydrogel resisted pressures up to 3.5 MPa in confined compression (fig. 4.5a).

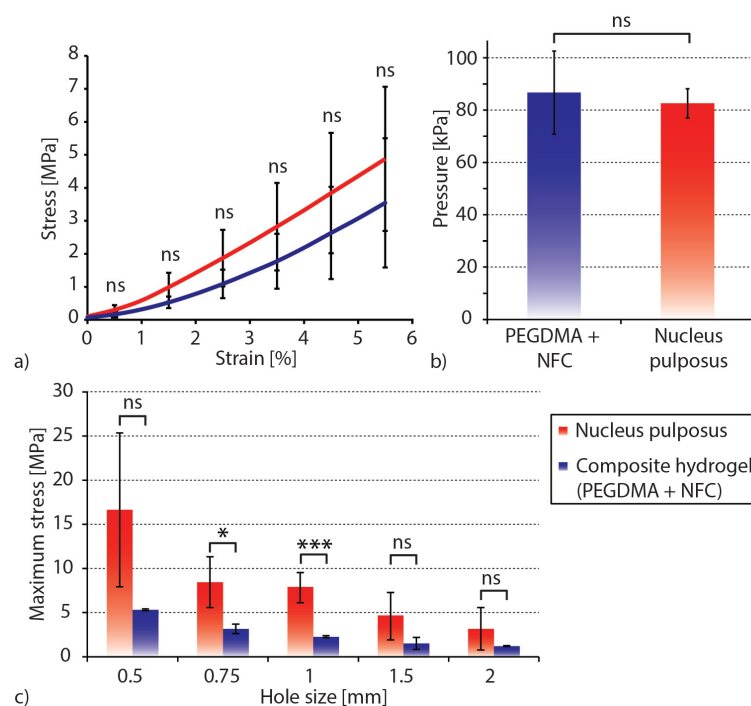


Figure 4.5: The three functional tests done in order to evaluate the PEGDMA-NFC composite (PEGDMA A20 kDa with 0.5 vol% NFC) in comparison to native nucleus pulposus tissue (a) confined compression stress-strain curves that evaluate the samples confined behavior similar as within the real intervertebral disc tissue, (b) swelling pressure which directly affects the disc height after implantation and (c) the maximum tolerated stress before extrusion which assesses the sample's resistance to extrusion and expulsion.

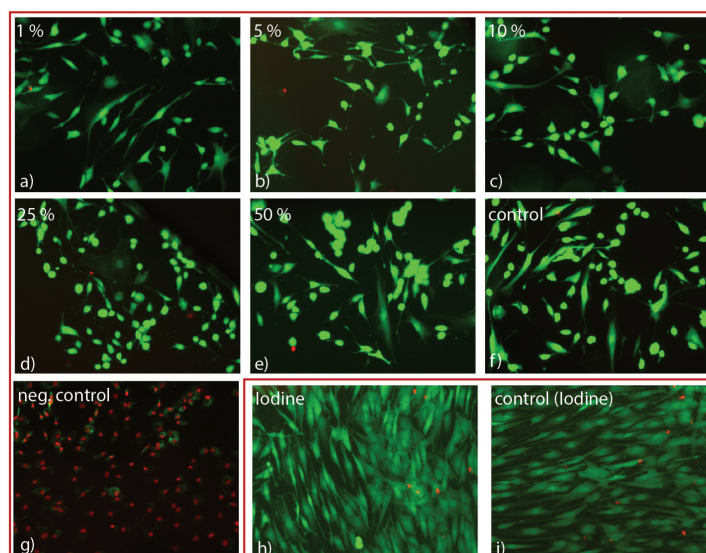


Figure 4.6: Live/Dead assay using human nucleus pulposus cells. Red box (a - g) liquid un-polymerized precursor on cells. h) and i) solid polymerized hydrogel on cells.

## Chapter 4. A photopolymerized composite hydrogel and surgical implanting tool for a nucleus pulposus replacement

---

No significant difference was observed between the composite hydrogel and the native NP tissue at each level of deformation ( $0.20 < p < 0.84$ ). The equilibrium swelling pressure of the NP and the composite hydrogel were  $78 (\pm 8)$  and  $83 (\pm 6)$  kPa respectively (fig. 4.5b). No significant difference was found ( $p = 0.69$ ). The extrusion data illustrates that the native NP tissue is more resistant to extrusion compared to the composite hydrogel. The native NP tissue was extruded through a 0.5 mm hole at a pressure of  $16.6 (\pm 8.7)$  MPa, whereas the composite hydrogel was extruded at a pressure of  $5.3 (\pm 0.1)$  MPa. The NP tissue was always stronger:  $p = 0.087$  (hole: 0.5 mm),  $p = 0.035$  (0.7 mm),  $p = 0.0000015$  (1 mm),  $p = 0.11$  (1.5 mm) and  $p = 0.23$  (2 mm). However, the difference between the extrusion pressure is less pronounced at bigger hole sizes, e.g. a hole of 2 mm hole, where the NP and the composite hydrogel are extruded at  $3.2 (\pm 2.4)$  and  $1.2 (\pm 0.05)$  MPa respectively.

### 4.4.3 Cytotoxicity

Polyethylene glycol was shown to have a low cytotoxicity [230]. However, the methacrylate groups have a high toxicity [231] and so do photoinitiators [232]. Therefore liquid precursor and solid hydrogels were evaluated. Figure 4.6a) to g) shows the results of Live/Dead assay of liquid precursor at different concentrations. Figure 4.6h) shows the solid hydrogel and i) the solid hydrogel where the water within the PBS was replaced by Iopamiro® 370 Iodine marker. Based on the Live/Dead assay no significant negative impact of the photoinitiator or the Iodine marker was found.

### 4.4.4 Implantation

The extracted samples originated all from the same tail, had a diameter between 14.7 and 16.7 mm, an initial height between 9.6 and 11.2 mm and weighted initially between 2.5 and 4.2 g. The dose of papain injected was between 90 and 150  $\mu$ l. The composite hydrogel was injected (fig. 4.7a) at the same position as the papain previously. Between 0.75 to 0.95 ml of hydrogel could be injected per specimen. It was possible to inject the liquid hydrogel precursor through the interspace between the needle (cannula) and the optical fiber (fig. 4.7b). During illumination (fig. 4.7d), the photopolymerization state of the injected sample was evaluated (fig. 4.7c) by recording the reflected illumination spectra at different time points and by tracking the signal intensity over time.

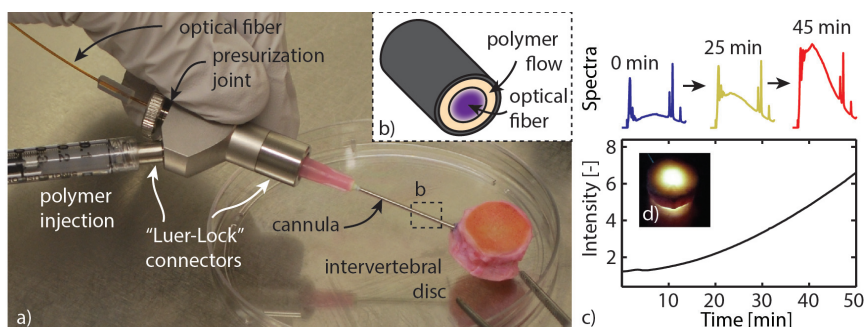


Figure 4.7: a) Customized minimally invasive surgical probe used for the hydrogel implantation. Liquid hydrogel precursor injection and illumination are combined within one single needle (cannula). Different joints ensure high pressurization during the injection. An optical fiber permits the light delivery for photopolymerization. b) At the distal tip of the instrument, the hydrogel precursor flows between cannula wall and optical fiber into the intervertebral disc. c) By recording the reflected illumination spectra a signal intensity is calculated. The intensity of the signal correlates with the amount of photopolymerized material and therefore provides valuable information about the reaction state of the implant in real time. d) Intervertebral disc during photopolymerization.

In figure 4.8, the results of the IVD loading in the bioreactor are presented. The conditioning cycles (12 h free swelling, 2 h cyclic compression, c.f. red boxes in fig. 2) resulted always, as expected, in a disc height increase during the free swelling phase and a decrease during the compression phase (not shown in fig. 4.8). During papain degeneration, the disc height decreased ( $p = 0.00022$ ) to  $65.6 (\pm 0.9) \%$  of the initial, healthy disc height (fig. 4.8a).

After the hydrogel injection (again including 12 h swelling and 2 h cyclic compression), the normalized disc height increased ( $p = 0.0020$ ) to  $99.0 (\pm 1.9) \%$ . There was no significant ( $p = 0.73$ ) difference between the initial healthy disc and the repaired state. After one week of loading (0.5 million cycles), the disc height decreased to  $91.1 (\pm 6.1) \%$  of healthy initial height, i.e the disc height suffered less than 10% height change after 0.5 million loading cycles. Compared to the degenerated state, the increase in disc height remained significant ( $p = 0.021$ ) and compared to the initial healthy state, no significant ( $p = 0.11$ ) difference was found. Figure 4.8b and c illustrate graphically the increase of disc height after the surgery.

#### 4.4.5 Histology

In figure d the macroscopic integration of the composite hydrogel after loading is illustrated, surrounded by annulus fibrosus tissue and the endplates. In figure 4.8e and f, the implanted hydrogel was compared to native NP tissue (both after mechanical loading). The healthy integrity of the nuclei of the NP cells can be seen (fig. 4.8e), while in figure 6f the fibrous structure of hydrogel can be observed. Figure 4.8g depicts the tissue integration of the hydrogel. The interface between native tissue and implanted hydrogel remained undisturbed after 0.5 million loading cycles. This suggested that the *in situ* photopolymerized composite



## Chapter 4. A photopolymerized composite hydrogel and surgical implanting tool for a nucleus pulposus replacement

hydrogel was able to integrate well into existing tissue and that the created interface was able to resist the extensive loading regime.

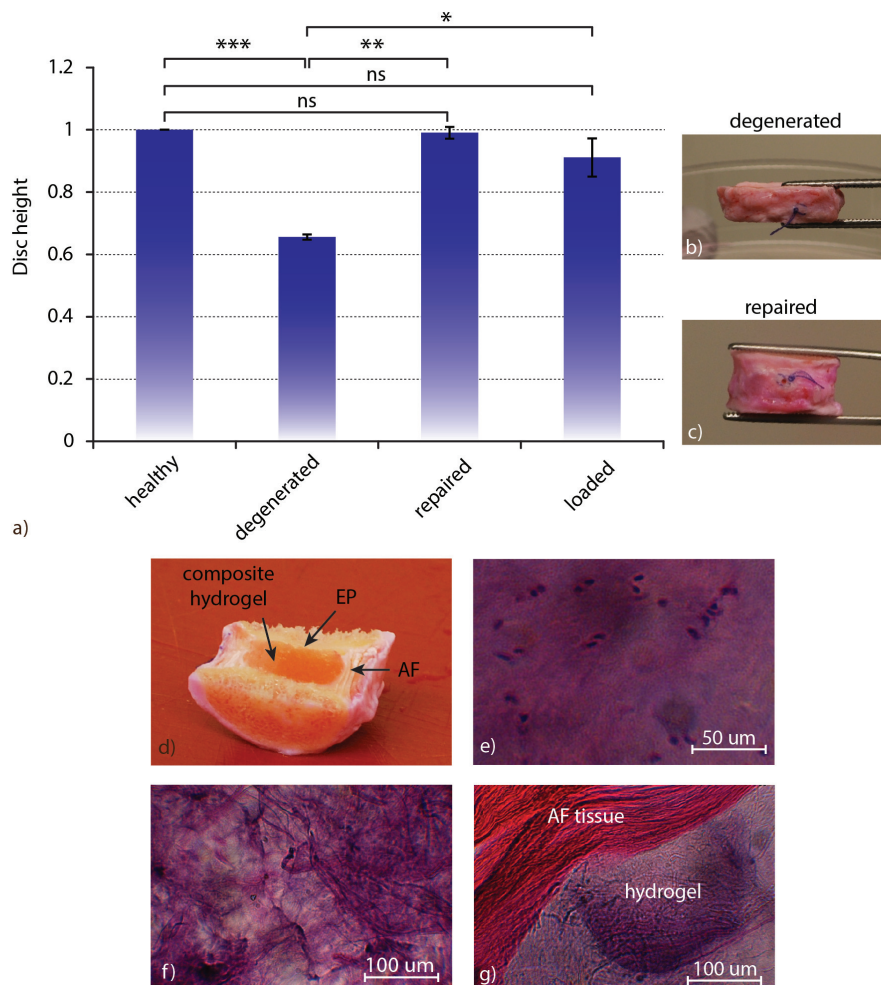


Figure 4.8: a) Disc height of bovine tail IVD ( $n = 3$ ) before surgery (degenerated state), after surgery (repaired state) and after 0.5 million cycles of *ex vivo* compressive loading (loaded state) are compared to the initial disc height (healthy disc). The disc height significantly increased after implantation of the PEGDMA-NFC composite hydrogel. The increase in disc height remained significant after loading. b) Bovine tail IVD before surgery and c) after surgery. d) IVD cut in half showing the hydrogel, annulus fibrosus (AF) and the endplate (EP). Histological sections of the bovine IVD samples (H&E-staining): annulus fibrosus tissue (purple) and nucleus pulposus tissue (violet). e) Native nucleus pulposus, f) nucleus pulposus replaced with implanted hydrogel and g) interface between native tissue and implanted tissue.

## 4.5 Discussion

To our knowledge, this is the first study which presents the design, implantation and testing of an *in situ* photopolymerized, functional orthopedic implant. A novel tuned material for NP

repair was designed specifically to comply with mechanical and bio-optical requirements. A device was developed to initiate and control the photo-chemical reaction *in situ*. The surgical procedure, medical device and implant were able to significantly restore IVD height after 0.5 million loading cycles within an ex vivo organ culture model. The hydrogel implant also showed an excellent tissue integration during histology analysis. The results not only demonstrate the feasibility of photopolymerized, mechanically loaded implants, but also opens a new pathway for the minimally invasive and controlled implantation of material within the human or animal body. Often novel materials, implantation methods and surgery devices are developed separately. In the proposed approach, the parallel development and testing significantly contributed to the obtained promising results: To reach the goal of a working implant it was necessary to 1) tune the bio-optical and mechanical properties of the composite hydrogel, 2) design a device which allowed for *in situ* injection, photopolymerization and reaction monitoring and 3) evaluate the material, the device and the implantation procedure all together. The discussion will then successively focus on these three aspects.

### 4.5.1 Material design

#### 4.5.1.1 Mechanical properties

Using pre-formed polymers, such as poly(ethylene glycol) instead of monomer/cross-linker systems is advantageous since the more homogeneously formed network is stronger and shows less brittleness [210]. The composite hydrogel made of the highly deformable PEGDMA matrix reinforced with NFC has a similar modulus and water content as the healthy NP tissue. An increase of the PEGDMA's molecular weight, decreases the cross-linker density and thus improves the deformability of the hydrogel. The reinforcement effect provided by the NFC addition is induced by hydrogen bonds interactions between the cellulose fibrils and by the entanglement between the cellulose and the polymer networks [233]. This interactions still allow the deformation of the networks and do not add any brittleness to the resulting composite hydrogel. The obtained composite hydrogel has a high water content owing to the hydrophilic nature of the polymer matrix and the NFCs. The material properties were tuned in order to mimic elastic modulus and water content of native tissue while keeping the high deformability. Similar properties for the implant and the tissue result in a smooth gradient of shear stresses at the tissue/implant interface, further enhance the integration of the implant into the tissue and thus, reduce the risk of extrusion or expulsion. In order to evaluate the possible failure modes of the implant, different testing methods were designed. The PEGDMA-NFC composite hydrogel was tested in a confined and unconfined compression mode. The similar behavior of the composite hydrogel and the native tissue in confined compression demonstrated that the material interaction with water is similar to that of the NP tissue for the range of applied stresses and testing rates. The comparable swelling pressures of the composite hydrogel and of the native NP indicate that the implant might restore the healthy IVD height by swelling. Furthermore, the swelling also leads to a continuous tissue/implant interface and ensures an homogenous load distribution. The extrusion test

## Chapter 4. A photopolymerized composite hydrogel and surgical implanting tool for a nucleus pulposus replacement

---

evaluates the hydrogel performance in the harshest condition where the material is squeezed until it ruptures completely. It cannot bulge or adhere to surrounding tissue as it would do in reality. The composite hydrogel ruptures to pieces at high pressures whereas the native tissue is irreversibly deformed, but without rupturing. This different behavior might be due to a lack of available energy dissipation within the composite hydrogel system compared to the native NP tissue. This indicates that by adding energy dissipation routes in the hydrogel, e.g. via ionic interactions, an increased resistance to extrusion of the hydrogel could be expected.

### 4.5.1.2 Bio-optical properties

Photopolymerization allows for controlled curing and also increases the implant's adherence to native tissue. The photopolymerizable curing system is highly advantageous compared to other *in situ* cured systems (e.g. heat reactive or chemical curing) because it provides the surgeon with an extra degree of freedom by decoupling the material insertion and curing. Additionally, the photopolymerization of an injected, low-viscosity liquid enables the precursor to flow into tissue interstices and leads to an optimal contact between implanted material and tissue. During illumination, the penetration of liquid precursor into the microroughness of the surrounding tissue results in the formation of mechanical interlocking which improves the tissue/implant interface [215]. The illumination from an optical fiber results in a cone of light. We have previously developed a Monte Carlo model to simulate the curing light distribution in the hydrogel [234]. It was shown that the addition of light scattering elements such as intralipid particles change the conic polymerization shape to a homogenous spherical shape. However lipid addition drastically weakened the mechanical properties of the hydrogel. Experimental data illustrated that the NFC fibers and the network they form, also act as light scattering element resulting in accelerated curing [195] and more homogeneously cured volumes [234].

### 4.5.2 Surgical device design

Injection, photopolymerization or monitoring of a photopolymer using a probe have been achieved previously, but the combination of the three functions in one probe is novel. We have shown that the probe can monitor the whole curing volume [229]. The extrusion results indicate that the hydrogel insertion site diameter should be less than 0.5 mm in order to avoid extrusion up to maximal pressures of 2.5 MPa measured in humans [81]. To achieve this, a smaller optical fiber and needle would be required to do the surgery. In the current study a LED light was used for illumination. The LED can easily be replaced with laser illumination and be delivered within a small diameter fiber with an external diameter of 125  $\mu\text{m}$ . This would allow performing the surgery through a needle as small as 25 or 26 Gauges (0.51 and 0.46 mm respectively) which is a relevant factor for the delivery of hydrogels as has been shown from clinics and experimentally in animal studies [235, 121, 236].



### 4.5.3 Evaluation of minimally invasive implantation procedure

Usually the biomechanical evaluation of tissue is associated with high inter-sample variance and strong creep within the first two hours of loading [237]. The conditioning method (free swelling and cyclic loading – c.f. red boxes in figure 2) counters this effect and allowed reaching standard deviations between 0.9 and 6.1 % over 15 days which is low in the field [238, 239, 240]. Between day 2 and 8 the disc height decreased by 1.0 % and between day 9 and 15 another 7.9 %. Although these changes were not significant, one could argue that ideally there should not be any decrease in disc height. However, the natural degradation of the IVD in *ex vivo* condition is important and usually much higher height decreases were observed over such a time frame for healthy disc [241]. Thus it can be concluded that the obtained 7.9 % are negligible. In order to evaluate the procedure and the implant, two options are available: *in vivo* or *in vitro* animal model. Due to their size and metabolism, bovine, canine and ovine IVD models show high resemblance to human IVDs [124]. Yet, degraded *in vivo* IVD models come along with high ethical issues and limited options to control loading. The *ex vivo* model in the bioreactors is an attractive solution to evaluate IVD replacements. The used bovine NP tissue has similar mechanical properties compared to human NP [23, 84]. Additionally, bovine NP tissue can be easily obtained while human non-degenerated tissue is difficult to obtain. The results are not only a proof-of-concept, but also demonstrate the potential of clinical translation. In the 4.9, the water in the hydrogel was replaced with a water-based Iodine marker. Figure 4.9a illustrated how the injected material can be imaged in a clinical situation using X-ray tomography to inject the material and visualize its position after injection. Figure 4.9b illustrates how the T2 signal during magnetic resonance imaging can be used to differentiate between an empty and a filled cavity.

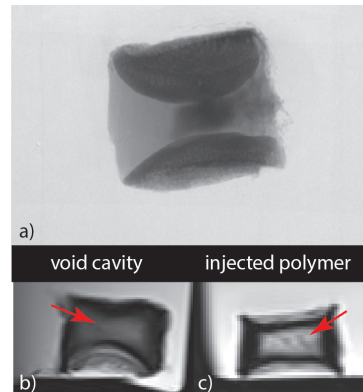


Figure 4.9: a) Micro CT and b-c) MRI scans of an IVD. Red arrows: control with an empty cavity (grey) and cavity filled with composite hydrogel (whitish). The injected volume can be monitored by CT scans by replacing the water in the hydrogel with a water-based, biocompatible Iodine marker (Iopamiro® 370, Bracco Suisse SA, Manno, Switzerland). A similar effect can be achieved by exploiting the T2 signal of MRI without using a marker [64]

A remaining challenge is to decrease the total illumination curing time, which, for this study, was chosen to be excessively long (45 min) to assure optimal tissue integration. However, we

## Chapter 4. A photopolymerized composite hydrogel and surgical implanting tool for a nucleus pulposus replacement

---

demonstrated previously that volumes of more than 2 ml (i.e. enough for a human NP) can be photopolymerized in less than 10 min using the same optical device [234]. It is also possible to choose different photoinitiators such as Eosin Y with higher photopolymerization rates in the range between 10 s and 3 min [136]. Moreover, the curing power in the experiment was limited to 4 mW in the fiber and can easily be increased by more than one order of magnitude using a laser light source. In summary, the procedure could easily be translated into clinics and seems to have a high potential to be successful.

### 4.6 Conclusion

A composite hydrogel having similar functional properties as a native NP was developed. Using a specifically designed probe for *in situ* photopolymerization, the composite hydrogel was implanted into an IVD model and was able to withstand loading without signs of damage. The composite hydrogel showed promising performance during implantation and significantly reestablished IVD disc height from 65.6 to 99.0 % and maintained it on a significantly higher level over 0.5 million loading cycles during an *ex vivo* study. After 15 days of loading, a continuous, undisturbed tissue/implant interface was observed during histology.

## 5 General discussion and conclusions

The present research project consists of two PhD theses covering the development of a functional NP replacement. The first thesis contains the design of a nano-fibrillated cellulose hydrogel. The present thesis is related to the development of a photopolymerization method and an implantation device. The global outcome of the project as presented in chapter 4 is **a functional NP replacement which was able to withstand 0.5 million fatigue cycles without a significant decrease in disc height**. These results were enabled by the present work through 1) the development of a *in situ* photopolymerization method based on scattering lipid additives, 2) the design of an optical fluorescence monitoring device to initiate and track the photopolymerization and 3) the development of a set of test setups to evaluate material candidates and compare them to native NP tissue.

### 5.1 Monte Carlo model of photopolymerization

The developed Monte Carlo model in chapter 2 is the first model which takes simultaneously into account **photopolymerization, light scattering, polymer/tissue interfaces and liquid/solid polymer-interfaces**. Based on these simulations it was possible to predict photopolymerization within tissue cavities and later design the bio-optical properties of the implanted material. The developed model enables simulating light transport in materials which dynamically change their shape and their optical properties and therefore can also be of interest to other domains of research such as additive manufacturing.

Yet, although the current model is functional in 3D (except for the automatic calculation of the evolving surface between liquid and solid polymer), it was only used in 2D. Calculations in three dimensions are too time consuming, but could be enabled if the code was implemented in C++ instead of Matlab.

The measurement of the absorption and scattering coefficients for the simulations could be improved. Here, four types of gel (two scattering and two absorption coefficients) were evaluated and certain effects were neglected. For instance it is not clear what percentage of absorbed photons is converted into radicals or results in heat dissipation. Thus, to further improve the accuracy of the model, more testing and validation on different known materials

would be required.

Finally, combining the simulations with an in-depth study of the photochemistry of photopolymerization might help to better understand the effects occurring on the micro and nano scale. Although the algorithm was able to predict photopolymerized shapes for most volumes, the polymer growth at larger scales (several cm) was not computed very accurately the Monte Carlo model (c.f. fig. 2.6). Therefore, studying nucleation processes and diffusion of molecules might lead to a better understanding of photopolymerization of large volumes.

### 5.2 Monitoring device

In chapter 3, a probe was developed to **inject, illuminate, photopolymerize** a liquid precursor and **monitor** the photopolymerization reaction *in situ* and in real-time. The method and device can be used for any type of surgical intervention transforming a liquid to a solid. Therefore, they hold considerable potential for different applications such as in dentistry, oncology and drug delivery.

A major weakness of the probe might be that currently it is not able to distinguish between different illuminated areas. The specificity could be improved by additional illumination or collection channels. Moreover, nano-structuring of the probe tip would allow directing light more precisely to a given location. This would permit to selectively control and monitor a reaction in space, and not only in time.

The dimensions of the device are still big ( $\phi \sim 1$  mm). Using smaller fibers and injection channels, the impact of the device on the tissue could be reduced.

### 5.3 *Ex vivo* evaluation

In chapter 4, a composite hydrogel was implanted and was able to resist 0.5 million fatigue-loading cycles within a bioreactor. To our knowledge this is the first **orthopedic implant** which was implanted in a **minimally invasive manner** (incision of  $\sim 1$  mm) using **photopolymerization**. In particular, the material was able to withstand cyclic loads of 0.2 MPa *ex vivo* and up to 3 MPa when implanted in a non-sterile environment (Appendix C) and therefore presents good extrusion properties. An explanation for this resistance to extrusion might be the tissue integration and adhesion of the implant induced through the photopolymerization procedure. However, this has not been investigated sufficiently. For instance it is unclear whether tissue and composite hydrogel are able to bond covalently.

Moreover, further mechanical tests would be required to assure a complete functionality of the implant. Especially, the neutral zone and range of motion were not measured. The implant was only evaluated under compressive loading. Flexion, bending and torsion need to be considered. Also, more surgeries are required to better understand the extrusion behavior of the implant (e.g. to study the impact of non-sterile, previously frozen tissue on extrusion). Finally, further fatigue and degradation testing is necessary to conclude about the efficiency of the proposed NP replacement.

### 5.4 Impact and potential of photopolymerized implants

The global approach covering **device & implant development**, **functional testing** and **implantation** allowed to tackle tissue replacements in the IVD in an iterative manner. Several sets of hydrogel and device generations were tested. Based on each result the requirements were redefined and the next generation was adapted accordingly. This is valuable because it allowed to correct errors at every step and adapt the implant and the device constantly.

The main impact of this work might be the proposition of a strategy to improve **tissue integration of biomaterials in a minimally invasive manner**. Both, tissue integration and invasiveness are crucial in clinics to reduce re-operation rates and treatment costs [27].

A crucial aspect for a translation into clinics is the **photopolymerization time**. On one hand, because it is correlated directly with safety (shorter illumination times and lower photoinitiator concentrations, have a direct impact on the cytotoxicity of the procedure) and on the other hand, because a fast photopolymerization (30 s to 3 min) is an essential requirement in a clinical setting. Such fast and efficient photopolymerizations could be achieved by using visible-light-absorbing photoinitiators for instance based on Lithium or Phosphorus [137, 242].

As a method, the proposed surgery technique and device also hold considerable potential for other applications such as light induced photopolymerization of materials injected into the vascular tree. We could envision injecting and solidifying an agent in a controlled manner for instance to treat aneurysms (filling aneurysm cavities), cancers (occlusion of the nourishing vascular branches) or strokes (injection of a biomaterial into heart tissue for regeneration [243]).

### 5.5 Requirement for a NP replacement

**Adhesion** and **ultimate tensile strength** of NP tissue replacements might have been underestimated in the past, especially when considering implants for Pfirrmann grades between 3 and 5. Many authors consider that mimicking native tissue properties is essential [243, 244, 245, 246, 247]. Although the importance of the interface between native and implanted material has been highlighted by others [204], especially adhesion as a key property still goes against the current understanding of what needs to be repaired when replacing IVD tissue. Thus, interactions between tissue and implant might be more important than characterization with elaborated models of the tissue or implant. It might not make sense to separate AF and NP replacement strictly. During the insertion of an NP replacement usually a lesion in the AF is introduced. Moreover, fissures in the AF will appear during a later stage of IVD degeneration. Thus, any NP replacement should have properties which will avoid later extrusion.

### 5.6 Outlook

In this study rather simple concepts were selected to identify suitable materials. For instance, it could be argued that an aggregate modulus is more relevant than a linear elastic modulus. The simpler models are sufficient to cover a physiological loading range. However, when compressed, tissues deform in a non-linear manner, which is due to their fiber-based composite (sometimes also multi-filament) structure. Synthetic materials can be designed homogeneously and therefore may deform in more linear way (e.g. fig. 4.4). Yet, the non-linear behavior of tissues might play a role when materials are close to failure, an aspect which might not have been sufficiently investigated in this work and thus deserves further attention.

Another issue which is related to the strength of the material and merits further investigation is the extrusion of the hydrogel and the NP. During extrusion of the hydrogel the samples rupture directly in the center (the first rupture occurs in the middle of the volume, as if the volume would implode), while the NP tissue is extruded in a viscous manner (similar to tooth past). It would be interesting to identify the rupture mechanisms and the role of fatigue. In general, IVD herniation seems to be poorly understood at the microlevel. A better understanding might lead to improved implant and treatment design for patients with disc herniation.

Finally, it is difficult to predict whether the current hydrogel would withstand loads when implanted into a human being. An *in vivo* study in a large animal model would be necessary to ultimately corroborate whether an implant is adapted for functional tissue repair [248].

In summary, numerous studies have shown that it is possible to build sufficiently strong materials (in terms of elastic modulus and ultimate strength) for NP tissue replacements, but it is not yet clear whether the interface between tissue and material can be designed to resist the loads present [204]. In the future, the following directions might be of interest:

- Currently, it might not be realistic to expect that the holy grail of bioactive scaffolds will lead to viable solutions first. A more realistic approach might be to design materials and methods fulfilling the biomechanical requirements first and then modify these materials into scaffolds. Thus, current implant and bioactive scaffold design might converge in terms of properties over time.
- Most IVD replacement research is based on the hypothesis that reestablishing joint motion is the ideal solution to treat DDD and associated diseases. However, although this seems logic, it has not been proven so far that disc arthroplasty is superior to fusion. It could be argued that arthroplasty is not mature yet, however, it should also be considered that natural degeneration and stiffening of the motion segment (including osteophytes and spongylophytes) could be optimal. This is why research on semi-rigid devices might be a path to follow. There are some promising solutions such as hybrid total IVD replacements [249].
- Finally, requirements need to be defined carefully for NP replacements. Mimicking tissue properties might not be sufficient. Requirements beyond this gold standard could be necessary.

# A Appendix - Monte Carlo

## A.1 Probability distribution of a point source

For a point source the vector of an initial photon path was calculated using two different angles  $\phi$  and  $\theta$  with the following distributions:

$$p_{\phi}(\phi) = \begin{cases} \frac{1}{2\pi} & \text{if } \phi = [0, 2\pi] \\ 0 & \text{otherwise} \end{cases} \quad (\text{A.1})$$

$$p_{\theta}(\theta) = \begin{cases} \frac{\sin(\theta)}{2} & \text{if } \theta = [-\frac{\pi}{2}, \frac{\pi}{2}] \\ 0 & \text{otherwise} \end{cases} \quad (\text{A.2})$$

Using equation 2.1  $\chi = f^{-1}(\xi)$  results in:

$$\phi = f_{\phi}^{-1}(\xi) = 2\pi \cdot \xi \quad (\text{A.3})$$

$$\theta = f_{\theta}^{-1}(\xi) = \cos^{-1}(1 - 2\xi) \quad (\text{A.4})$$

$\xi$  being a random variable between 0 and 1 which is calculated for every probabilistic event separately.

## A.2 Refraction and reflection at interfaces

Based on the assumption that half the photons have a linear or an the other half a circular polarization, the probability of reflection is calculated as following:

$$p(R) = 0.5 \cdot \left( \frac{\sin(\alpha_i - \alpha_t)^2}{\sin(\alpha_i + \alpha_t)^2} + \frac{\tan(\alpha_i - \alpha_t)^2}{\tan(\alpha_i + \alpha_t)^2} \right) \quad (A.5)$$

Where  $\alpha_t = \sin^{-1}(n_1/n_2 \cdot \sin(\alpha_i))$ ,  $\alpha_i$  and  $\alpha_t$  are the angles between the vector orthogonal to the interface and the incident or transmitted beam, and  $n_1$  and  $n_2$  the indexes of refraction of the medium on the incident or transmitted side of the interface. A photon is reflected if:

$$\xi < p(R) \quad (A.6)$$

or refracted otherwise. In both cases a new vector based on  $\alpha_i$  or  $\alpha_t$  is computed.

## A.3 Absorption

After every absorption event inducing photopolymerization (equ. 2.6) the weight of a photon-package (initially equal 1) is ajusted:

$$W \leftarrow W \cdot (1 - a); \quad (A.7)$$

Where  $a = \mu_a / (\mu_s + \mu_a)$  is the albedo.

## A.4 Scattering

Applying equation 2.1 to the Henyey-Greenstein function (1.5) results in:

$$\theta = \cos^{-1} \left( \frac{1}{2 \cdot g} \left[ 1 + g^2 - \left( \frac{1 - g^2}{1 - g + 2 \cdot g \cdot \xi} \right)^2 \right] \right) \quad (A.8)$$

And using equation A.3 the angular coordinates  $\theta$  and  $\phi$  of the scattering vector  $\vec{r}$  is computed.

## A.5 Propagation

One propagation step is calculated as following:

$$t = \frac{-\log(\xi)}{\mu_a + \mu_s} \quad (A.9)$$



And:

$$\vec{x} = \vec{x}_0 + t \cdot \vec{v} \tag{A.10}$$



## **B Appendix - Loading up to 3 MPa**

If bovine IVDs are loaded cyclically above  $\sim 0.8$  MPa, loading results in apoptosis [123]. However, to evaluate an implanted material it is necessary to load IVDs up to  $\sim 3$  MPa. Hydrogels were implanted into IVDs using a 19 Gauge needle and then loaded cyclically. After each 300 cycles the average load was increased by 0.3 MPa (fig. B.1a).

After 3000 cycles disc heights were reduced significantly by approximately 40 %, but no significant difference was found between healthy IVDs (with NP tissue inside) and replaced IVDs (degenerated by Papain as described in section 4.3.4.2 and replaced with hydrogels). Usually, the NP tissue should extrude at such loads although the amount of cycles until extrusion might be higher [250]. No extrusion patterns were observed. The NP partially extruded, but not for all samples. The gels did not exude, although water or liquid hydrogel was observed at the hole created by the 19 Gauge needle for most samples. It is possible that the amount of cycles was too low to induce extrusion. More extensive testing would be required to understand the extrusion mechanisms.

## Appendix B. Appendix - Loading up to 3 MPa

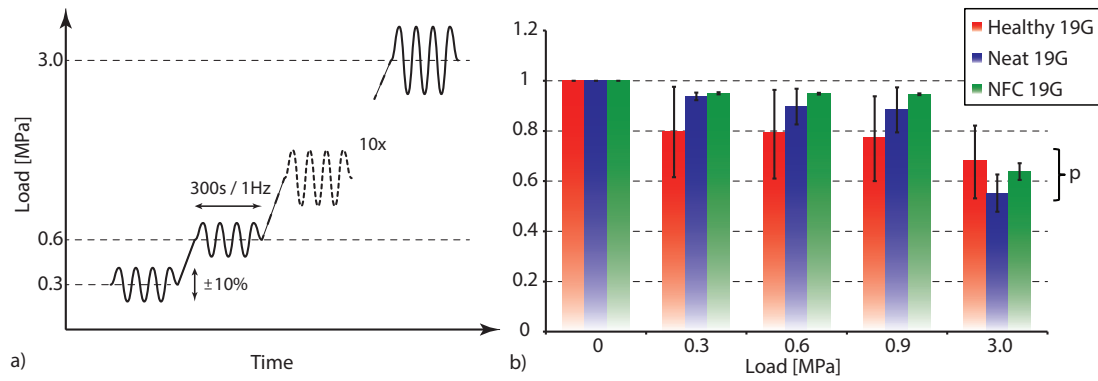


Figure B.1: High compressive loading of IVDs up to 3 MPa. a) Protocol: First, a cyclic load of  $0.3 \pm 0.015$  MPa was applied over 300 cycles. Then the load was increased stepwise by 0.3 MPa with a loading amplitude of 10 % of the nominative load (each time 300 cycles) until reaching a load of  $3 \text{ MPa} \pm 0.15$  MPa. b) The disc height was measured after each 300 loading cycles. The disc height decreased faster for healthy IVDs, than for IVDs with hydrogel and no NFC fibers or hydrogel with NFC fibers. However, the final disc height was not significantly different  $p = 0.68$  (healthy vs. no NFC)  $p = 0.26$  (healthy vs. NFC).

# Bibliography

- [1] Samantha C W Chan, Alexander Bürki, Harald M Bonél, Lorin M Benneker, and Benjamin Gantenbein-Ritter. Papain-induced in vitro disc degeneration model for the study of injectable nucleus pulposus therapy. *The spine journal : official journal of the North American Spine Society*, 13(3):273–83, March 2013.
- [2] ASTM. F2423 - Standard Guide for Functional, Kinematic, and Wear Assessment of Total Disc Prostheses. In *Annual Book of ASTM Standards*. ASTM International, 2011.
- [3] David Borenstein. Mechanical low back pain—a rheumatologist’s view. *Nature reviews. Rheumatology*, 9(11):643–53, November 2013.
- [4] Andersson GBJ. The epidemiology of spinal disorders. In Frymoyer JW, editor, *The adult spine: principles and practice*, pages 107–46. New York: Raven Press, Ltd., 1991.
- [5] G B Andersson. Epidemiological features of chronic low-back pain. *Lancet*, 354(9178):581–5, August 1999.
- [6] George E Ehrlich. Low back pain. *Bulletin of the World Health Organization*, 81(9):671–6, January 2003.
- [7] B Vällfors. Acute, subacute and chronic low back pain: clinical symptoms, absenteeism and working environment. *Scandinavian journal of rehabilitation medicine. Supplement*, 11:1–98, January 1985.
- [8] Simon Dagenais, Jaime Caro, and Scott Haldeman. A systematic review of low back pain cost of illness studies in the United States and internationally. *The spine journal : official journal of the North American Spine Society*, 8(1):8–20, January 2008.
- [9] Jeffrey N Katz. Lumbar disc disorders and low-back pain: socioeconomic factors and consequences. *The Journal of bone and joint surgery. American volume*, 88 Suppl 2(suppl 2):21–4, April 2006.
- [10] Damian Hoy, Christopher Bain, Gail Williams, Lyn March, Peter Brooks, Fiona Blyth, Anthony Woolf, Theo Vos, and Rachelle Buchbinder. A systematic review of the global prevalence of low back pain. *Arthritis and rheumatism*, 64(6):2028–37, June 2012.

## Bibliography

---

- [11] J B Wahlig, M R McLaughlin, B R Subach, R W Haid, and G E Rodts. Management of low back pain. *Neurologist*, 6(6):326–337, January 2000.
- [12] Bart Morlion. Chronic low back pain: pharmacological, interventional and surgical strategies. *Nature reviews. Neurology*, 9(8):462–73, August 2013.
- [13] Rahman Shiri, Jaro Karppinen, Paivi Leino-Arjas, Svetlana Solovieva, and Eira Viikari-Juntura. The association between obesity and low back pain: a meta-analysis. *American journal of epidemiology*, 171(2):135–54, January 2010.
- [14] J W Frymoyer, M H Pope, J H Clements, D G Wilder, B MacPherson, and T Ashikaga. Risk factors in low-back pain. An epidemiological survey. *The Journal of bone and joint surgery. American volume*, 65(2):213–8, February 1983.
- [15] F Balagui, B. Troussier, and J. J. Salminen. Non-specific low back pain in children and adolescents: risk factors. *European Spine Journal*, 8(6):429–438, December 1999.
- [16] Frank Heuer, Herbert Schmitt, Hendrik Schmidt, Lutz Claes, and Hans-Joachim Wilke. Creep associated changes in intervertebral disc bulging obtained with a laser scanning device. *Clinical Biomechanics*, 22(7):737–744, August 2007.
- [17] Stephen J. Ferguson, Keita Ito, and Lutz-P. Nolte. Fluid flow and convective transport of solutes within the intervertebral disc. *Journal of Biomechanics*, 37(2):213–221, February 2004.
- [18] J.B. Martinez, V.O.a. Oloyede, and N.D. Broom. Biomechanics of load-bearing of the intervertebral disc: an experimental and finite element model. *Medical Engineering and Physics*, 19(2):145–156, March 1997.
- [19] M Argoubi and A Shirazi-Adl. Poroelastic creep response analysis of a lumbar motion segment in compression. *Journal of biomechanics*, 29(96):1331–1339, 1996.
- [20] Neil Roberts, David Hogg, Graham H. Whitehouse, and Peter Dangerfield. Quantitative analysis of diurnal variation in volume and water content of lumbar intervertebral discs. *Clinical Anatomy*, 11(1):1–8, 1998.
- [21] C Nguyen-minh, V M Haughton, R a Papke, H An, and S C Censky. Measuring diffusion of solutes into intervertebral disks with MR imaging and paramagnetic contrast medium. *AJNR. American journal of neuroradiology*, 19(9):1781–4, October 1998.
- [22] Rosemary E Thompson, Mark J Pearcy, and Timothy M Barker. The mechanical effects of intervertebral disc lesions. *Clinical biomechanics (Bristol, Avon)*, 19(5):448–55, June 2004.
- [23] Wade Johannessen and Dawn M Elliott. Effects of Degeneration on the Biphasic Material Properties of Human Nucleus Pulposus in Confined Compression. *Spine*, 30(24), 2005.

- [24] T W Stadnik, R R Lee, H L Coen, E C Neirynck, T S Buisseret, and M J Osteaux. Annular tears and disk herniation: prevalence and contrast enhancement on MR images in the absence of low back pain or sciatica. *Radiology*, 206(1):49–55, January 1998.
- [25] CWA Pfirrmann, A Metzdorf, and M Zanetti. Magnetic resonance classification of lumbar intervertebral disc degeneration. *Spine*, 2001.
- [26] J P Thompson, R H Pearce, M T Schechter, M E Adams, I K Tsang, and P B Bishop. Preliminary evaluation of a scheme for grading the gross morphology of the human intervertebral disc. *Spine*, 15(5):411–415, 1990.
- [27] Jan Van Zundert and Maarten Van Kleef. Low Back Pain : From Algorithm to Cost-Effectiveness? *Pain Practice*, 5(3):179–189, 2005.
- [28] Shira Schechter Weiner and M Nordin. Prevention and management of chronic back pain. *Best practice and research. Clinical rheumatology*, 24(2):267–79, April 2010.
- [29] Eija Roine, Risto P Roine, Pirjo Räsänen, Ilkka Vuori, Harri Sintonen, and Tiina Saarto. Cost-effectiveness of interventions based on physical exercise in the treatment of various diseases: a systematic literature review. *International journal of technology assessment in health care*, 25(4):427–54, October 2009.
- [30] Andrea S Wallace, Janet K Freburger, Jane D Darter, Anne M Jackman, and Timothy S Carey. Comfortably numb? Exploring satisfaction with chronic back pain visits. *The spine journal : official journal of the North American Spine Society*, 9(9):721–8, September 2009.
- [31] Bridget A Martell, Patrick G O'Connor, Robert D Kerns, William C Becker, Knashawn H Morales, Thomas R Kosten, and David A Fiellin. Systematic review: opioid treatment for chronic back pain: prevalence, efficacy, and association with addiction. *Annals of internal medicine*, 146(2):116–27, January 2007.
- [32] Janna Friedly, Christopher Standaert, and Leighton Chan. Epidemiology of spine care: the back pain dilemma. *Physical medicine and rehabilitation clinics of North America*, 21(4):659–77, December 2010.
- [33] J W Frymoyer and W L Cats-Baril. An overview of the incidences and costs of low back pain. *The Orthopedic clinics of North America*, 22(2):263–271, April 1991.
- [34] K Zarghooni, J Siewe, and P Eysel. State of the art of lumbar intervertebral disc replacement. *Der Orthopäde*, 40(2):141–7, February 2011.
- [35] Sylvia I. Watkins-Castillo and Gunnar B J Andersson. Economic Burden | BMUS: The Burden of Musculoskeletal Diseases in the United States, 2008.
- [36] Richard A Deyo, Sohail K Mirza, Brook I Martin, William Kreuter, David C Goodman, and Jeffrey G Jarvik. Trends, major medical complications, and charges associated with surgery for lumbar spinal stenosis in older adults. *JAMA*, 303(13):1259–65, April 2010.

## Bibliography

---

- [37] Jens Ivar Brox, Roger Sørensen, Astrid Friis, Øystein Nygaard, Aage Indahl, Anne Keller, Tor Ingebrigtsen, Hege R Eriksen, Inger Holm, Anne Kathrine Koller, Rolf Riise, and Olav Reikerås. Randomized clinical trial of lumbar instrumented fusion and cognitive intervention and exercises in patients with chronic low back pain and disc degeneration. *Spine*, 28(17):1913–21, September 2003.
- [38] P Fritzell, O Hägg, P Wessberg, and A Nordwall. 2001 Volvo Award Winner in Clinical Studies: Lumbar fusion versus nonsurgical treatment for chronic low back pain: a multicenter randomized controlled trial from the Swedish Lumbar Spine Study Group. *Spine*, 26(23):2521–32; discussion 2532–4, December 2001.
- [39] Peter Fritzell, Olle Hägg, Per Wessberg, and Anders Nordwall. Chronic low back pain and fusion: a comparison of three surgical techniques: a prospective multicenter randomized study from the Swedish lumbar spine study group. *Spine*, 27(11):1131–41, June 2002.
- [40] Lucio Palma, Biagio Carangelo, Vitaliano F Muzii, Aldo Mariottini, Alessandro Zalaffi, and Serena Capitani. Microsurgery for recurrent lumbar disk herniation at the same level and side: do patients fare worse? Experience with 95 consecutive cases. *Surgical Neurology*, 70(6):619–621, December 2008.
- [41] M H Pelletier, W R Walsh, and New South. *Nucleus Replacement*. Elsevier Ltd., 2011.
- [42] C Schizas, G Kulik, and V Kosmopoulos. Disc degeneration: current surgical options. *European cells and materials*, 20:306–15, January 2010.
- [43] Ingrid Zechmeister, Roman Winkler, and Philipp Mad. Artificial total disc replacement versus fusion for the cervical spine: a systematic review. *European spine journal : official publication of the European Spine Society, the European Spinal Deformity Society, and the European Section of the Cervical Spine Research Society*, 20(2):177–84, March 2011.
- [44] H G Edeland. Some additional suggestions for an intervertebral disc prosthesis. *Journal of biomedical engineering*, 7(1):57–62, January 1985.
- [45] R W Hu, S Jaglal, T Axcell, and G Anderson. A population-based study of reoperations after back surgery. *Spine*, 22(19):2265–2270; discussion 2271, 1997.
- [46] Hassan Serhan, Devdatt Mhatre, Henri Defossez, and Christopher M. Bono. Motion-preserving technologies for degenerative lumbar spine: The past, present, and future horizons. *SAS Journal*, 5(3):75–89, September 2011.
- [47] ASTM. F2267 - Standard Test Method for Measuring Load Induced Subsidence of Intervertebral Body Fusion Device Under Static Axial Compression. In *Annual Book of ASTM Standards*, volume 04. ASTM International, 2012.



- [48] J C Iatridis, L a Setton, M Weidenbaum, and V C Mow. Alterations in the mechanical behavior of the human lumbar nucleus pulposus with degeneration and aging. *Journal of orthopaedic research : official publication of the Orthopaedic Research Society*, 15(2):318–22, March 1997.
- [49] Jordan M Cloyd, Neil R Malhotra, Lihui Weng, Weiliam Chen, Robert L Mauck, and Dawn M Elliott. Material properties in unconfined compression of human nucleus pulposus, injectable hyaluronic acid-based hydrogels and tissue engineering scaffolds. *European spine journal : official publication of the European Spine Society, the European Spinal Deformity Society, and the European Section of the Cervical Spine Research Society*, 16(11):1892–8, November 2007.
- [50] John J Costi, Brian J C Freeman, and Dawn M Elliott. Intervertebral disc properties: challenges for biodevices. *Expert review of medical devices*, 8(3):357–76, 2011.
- [51] Maurice L Goins, David W Wimberley, Philip S Yuan, Laurence N Fitzhenry, and Alexander R Vaccaro. Nucleus pulposus replacement: an emerging technology. *The spine journal : official journal of the North American Spine Society*, 5(6 Suppl):317S–324S, 2005.
- [52] Emily M Lindley, Sami Jaafar, Andriy Noshchenko, Todd Baldini, Devatha P Nair, Robin Shandas, Evalina L Burger, and Vikas V Patel. A Case Report and Biomechanical Study. *Spine*, 35(22):1241–1247, 2010.
- [53] Luiz Pimenta, Luis Marchi, Etevaldo Coutinho, and Leonardo Oliveira. Lessons Learned After 9 Years’ Clinical Experience with 3 Different Nucleus Replacement Devices. *Seminars in Spine Surgery*, 24(1):1–5, March 2012.
- [54] Henry Halm Hansen Yuan, Michael Ahrens and Jean Charles LeHuec Peter Donkersloot, Ulf Liljenqvist, Anthony Tsantrizos, John Sherman. Two-Year Follow-Up Results of Nucleus Replacement With the DASCOR Device: A Prospective European Multicenter Clinical Study. *Proceedings of the NASS 21st Annual Meeting / The Spine Journal*, 6(5):79–80, September 2006.
- [55] a Tsantrizos. Mechanical and Biomechanical Characterization of a Polyurethane Nucleus Replacement Device Injected and Cured In Situ Within a Balloon. *SAS Journal*, 2(1):28–39, March 2008.
- [56] Ulrich Berlemann and Othmar Schwarzenbach. An injectable nucleus replacement as an adjunct to microdiscectomy: 2 year follow-up in a pilot clinical study. *European spine journal : official publication of the European Spine Society, the European Spinal Deformity Society, and the European Section of the Cervical Spine Research Society*, 18(11):1706–12, November 2009.
- [57] Allen Carl, Eric Ledet, Hansen Yuan, and Alok Sharan. New developments in nucleus pulposus replacement technology. *The spine journal : official journal of the North American Spine Society*, 4(6 Suppl):325S–329S, 2004.

## Bibliography

---

- [58] RA Bader. *Development and characterization of novel hydrogels for nucleus pulposus replacement*. PhD thesis, Oregon State University, 2007.
- [59] Inc Replication Medical and Therapeutic Options. GelStix™ - Scientific and Clinical Rationale, 2011.
- [60] Jingen Hu, Bin Chen, Fang Guo, Jingyu Du, Pengcheng Gu, Xiangjin Lin, Weiping Yang, Hailong Zhang, Min Lu, Yiping Huang, and Gewen Xu. Injectable silk fibroin/polyurethane composite hydrogel for nucleus pulposus replacement. *Journal of Materials Science: Materials in Medicine*, 23(3):711–722, January 2012.
- [61] Jennifer Vernengo. *Injectable Bioadhesive Hydrogels for Nucleus Pulposus Replacement and Repair of the Damaged Intervertebral Disc*. PhD thesis, Drexel University, 2007.
- [62] J Vernengo, G W Fussell, N G Smith, and a M Lowman. Synthesis and characterization of injectable bioadhesive hydrogels for nucleus pulposus replacement and repair of the damaged intervertebral disc. *Journal of biomedical materials research. Part B, Applied biomaterials*, 93(2):309–17, May 2010.
- [63] Anna T Reza and Steven B Nicoll. Characterization of novel photocrosslinked carboxymethylcellulose hydrogels for encapsulation of nucleus pulposus cells. *Acta biomaterialia*, 6(1):179–86, January 2010.
- [64] Matthew J. Allen, Joanne E. Schoonmaker, Thomas W. Bauer, Philip F. Williams, Paul A. Higham, and Hansen A. Yuan. Preclinical Evaluation of a Poly (Vinyl Alcohol) Hydrogel Implant as a Replacement for the Nucleus Pulposus. *Spine*, 29(5):515–523, 2004.
- [65] Laura Calderon, Estelle Collin, Diego Velasco-Bayon, Mary Murphy, Damien O’Halloran, and Abhay Pandit. Type II collagen-hyaluronan hydrogel—a step towards a scaffold for intervertebral disc tissue engineering. *European cells and materials*, 20:134–48, January 2010.
- [66] Wen-Yu Su, Yu-Chun Chen, and Feng-Huei Lin. Injectable oxidized hyaluronic acid/adipic acid dihydrazide hydrogel for nucleus pulposus regeneration. *Acta biomaterialia*, 6(8):3044–55, August 2010.
- [67] Daniel G T Strange and Michelle L. Oyen. Composite hydrogels for nucleus pulposus tissue engineering. *Journal of the Mechanical Behavior of Biomedical Materials*, 11:16–26, October 2012.
- [68] a.C. Borges, P-E. Bourban, D.P. Pioletti, and J.-a.E. Månson. Curing kinetics and mechanical properties of a composite hydrogel for the replacement of the nucleus pulposus. *Composites Science and Technology*, 70(13):1847–1853, November 2010.
- [69] Lawrence M Boyd and Andrew J Carter. Injectable biomaterials and vertebral endplate treatment for repair and regeneration of the intervertebral disc. *European spine journal : official publication of the European Spine Society, the European Spinal Deformity Society*,

- and the European Section of the Cervical Spine Research Society*, 15 Suppl 3:S414–21, August 2006.
- [70] Nadine Wismer, Sibylle Grad, Giuseppino Fortunato, Stephen J Ferguson, Mauro Alini, and David Eglin. Biodegradable electrospun scaffolds for annulus fibrosus tissue engineering: effect of scaffold structure and composition on annulus fibrosus cells in vitro. *Tissue engineering. Part A*, 20(3-4):672–82, February 2014.
  - [71] J L Bron, G H Koenderink, V Everts, and T H Smit. Rheological characterization of the nucleus pulposus and dense collagen scaffolds intended for functional replacement. *Journal of orthopaedic research : official publication of the Orthopaedic Research Society*, 27(5):620–6, May 2009.
  - [72] R M Schek, A J Michalek, and J C Iatridis. Genipin-crosslinked fibrin hydrogels as a potential adhesive to augment intervertebral disc annulus repair. *European cells and materials*, 21:373–83, January 2011.
  - [73] Clare C Guterl, Olivia M Torre, Devina Purmessur, Khyati Dave, Morakot Likhitpanichkul, Andrew C Hecht, Steven B Nicoll, and James C Iatridis. Characterization of mechanics and cytocompatibility of fibrin-genipin annulus fibrosus sealant with the addition of cell adhesion molecules. *Tissue engineering. Part A*, 20(17-18):2536–45, September 2014.
  - [74] P Grunert, BH Borde, and KD Hudson. Annular repair using high-density collagen gel: a rat-tail in vivo model. *Spine*, 2014.
  - [75] Daisuke Sakai and Gunnar B J Andersson. Stem cell therapy for intervertebral disc regeneration: obstacles and solutions. *Nature reviews. Rheumatology*, 11(4):243–56, April 2015.
  - [76] James Melrose, Susan M Smith, Christopher B Little, Robert J Moore, Barrie Vernon-Roberts, and Robert D Fraser. Recent advances in annular pathobiology provide insights into rim-lesion mediated intervertebral disc degeneration and potential new approaches to annular repair strategies. *European spine journal : official publication of the European Spine Society, the European Spinal Deformity Society, and the European Section of the Cervical Spine Research Society*, 17(9):1131–48, September 2008.
  - [77] PJ Flory. Thermodynamics of high polymer solutions. *The Journal of chemical physics*, 1942.
  - [78] D. N. Sun, W. Y. Gu, X. E. Guo, W. M. Lai, and V. C. Mow. A mixed finite element formulation of triphasic mechano-electrochemical theory for charged, hydrated biological soft tissues. *International Journal for Numerical Methods in Engineering*, 45(10):1375–1402, August 1999.
  - [79] Diane R Wagner and Jeffrey C Lotz. Theoretical model and experimental results for the nonlinear elastic behavior of human annulus fibrosus. *Journal of orthopaedic research : official publication of the Orthopaedic Research Society*, 22(4):901–9, July 2004.

## Bibliography

---

- [80] V C Mow, S C Kuei, W M Lai, and C G Armstrong. Biphasic creep and stress relaxation of articular cartilage in compression? Theory and experiments. *Journal of biomechanical engineering*, 102(1):73–84, 1980.
- [81] H J Wilke, P Neef, M Caimi, T Hoogland, and L E Claes. New in vivo measurements of pressures in the intervertebral disc in daily life. *Spine*, 24(8):755–62, April 1999.
- [82] J P Urban and J F McMullin. Swelling pressure of the lumbar intervertebral discs: influence of age, spinal level, composition, and degeneration. *Spine*, 13(2):179–187, February 1988.
- [83] Arin M Ellingson and David J Nuckley. Intervertebral disc viscoelastic parameters and residual mechanics spatially quantified using a hybrid confined/in situ indentation method. *Journal of biomechanics*, 45(3):491–6, February 2012.
- [84] Delphine Périé, David Korda, and James C Iatridis. Confined compression experiments on bovine nucleus pulposus and annulus fibrosus: sensitivity of the experiment in the determination of compressive modulus and hydraulic permeability. *Journal of biomechanics*, 38(11):2164–71, November 2005.
- [85] Anthony Tsantrizos, Keita Ito, Max Aebi, and Thomas Steffen. Internal strains in healthy and degenerated lumbar intervertebral discs. *Spine*, 30(19):2129–37, October 2005.
- [86] Paul Heneghan and Philip E Riches. The strain-dependent osmotic pressure and stiffness of the bovine nucleus pulposus apportioned into ionic and non-ionic contributors. *Journal of biomechanics*, 41(11):2411–6, August 2008.
- [87] D Greg Anderson and Chadi Tannoury. Molecular pathogenic factors in symptomatic disc degeneration. *The spine journal : official journal of the North American Spine Society*, 5(6 Suppl):260S–266S, 2005.
- [88] J C Iatridis, M Weidenbaum, L A Setton, and V C Mow. Is the nucleus pulposus a solid or a fluid? Mechanical behaviors of the nucleus pulposus of the human intervertebral disc. *Spine*, 21(10):1174–1184, 1996.
- [89] Nandan L Nerurkar, Dawn M Elliott, and Robert L Mauck. Mechanical design criteria for intervertebral disc tissue engineering. *Journal of biomechanics*, 43(6):1017–30, April 2010.
- [90] T. P. Green, M. A. Adams, and P. Dolan. Tensile properties of the annulus fibrosus. *European Spine Journal*, 2(4):209–214, December 1993.
- [91] J C Iatridis, S Kumar, R J Foster, M Weidenbaum, and V C Mow. Shear mechanical properties of human lumbar annulus fibrosus. *Journal of orthopaedic research : official publication of the Orthopaedic Research Society*, 17(5):732–7, September 1999.

- [92] Robert Eberlein, Gerhard a. Holzapfel, and Christian a. J. Schulze-Bauer. An Anisotropic Model for Annulus Tissue and Enhanced Finite Element Analyses of Intact Lumbar Disc Bodies. *Computer Methods in Biomechanics and Biomedical Engineering*, 4(March 2015):209–229, 2001.
- [93] JJ Cassidy, A Hiltner, and E Baer. Hierarchical structure of the intervertebral disc. *Connective tissue research*, 1989.
- [94] J O Galante. Tensile properties of the human lumbar annulus fibrosus. *Acta orthopaedica Scandinavica*, 38(100):Suppl 100:1–91, 1967.
- [95] F Marchand and a M Ahmed. Investigation of the laminate structure of lumbar disc anulus fibrosus., 1990.
- [96] Peter J Fazey, Swithin Song, Shild Mø nsås, Linda Johansson, Tone Haukalid, Roger I Price, and Kevin P Singer. An MRI investigation of intervertebral disc deformation in response to torsion. *Clinical biomechanics (Bristol, Avon)*, 21(5):538–42, June 2006.
- [97] S Holm, A Maroudas, J P Urban, G Selstam, and A Nachemson. Nutrition of the intervertebral disc: solute transport and metabolism. *Connect Tissue Res*, 8(2):101–119, 1981.
- [98] Nandan L Nerurkar, Brendon M Baker, Sounok Sen, Emily E Wible, Dawn M Elliott, and Robert L Mauck. Nanofibrous biologic laminates replicate the form and function of the annulus fibrosus. *Nature materials*, 8(12):986–92, December 2009.
- [99] MV Risbud, MW Izzo, and CS Adams. An organ culture system for the study of the nucleus pulposus: description of the system and evaluation of the cells. *Spine*, 2003.
- [100] Rodolfo Cappello, Joseph L E Bird, Dirk Pfeiffer, Michael T Bayliss, and Jayesh Dudhia. Notochordal cell produce and assemble extracellular matrix in a distinct manner, which may be responsible for the maintenance of healthy nucleus pulposus. *Spine*, 31(8):873–82; discussion 883, 2006.
- [101] Samantha C W Chan and Benjamin Gantenbein-Ritter. Intervertebral disc regeneration or repair with biomaterials and stem cell therapy–feasible or fiction? *Swiss medical weekly*, 142:w13598, January 2012.
- [102] M D Humzah and R W Soames. Human intervertebral disc: structure and function. *The Anatomical record*, 220(4):337–56, 1988.
- [103] H. a L Guerin and Dawn M. Elliott. Degeneration affects the fiber reorientation of human annulus fibrosus under tensile load. *Journal of Biomechanics*, 39(8):1410–1418, 2006.
- [104] N Bogduk. *Clinical and Radiological Anatomy of the Lumbar Spine*. Elsevier Health Sciences, 2005.

## Bibliography

---

- [105] Giacomo Marini and Stephen J Ferguson. Modelling the influence of heterogeneous annulus material property distribution on intervertebral disk mechanics. *Annals of biomedical engineering*, 42(8):1760–72, August 2014.
- [106] ASTM. F2789 - Standard Guide for Mechanical and Functional Characterization of Nucleus Devices. In *Annual Book of ASTM Standards*. ASTM International, 2012.
- [107] Frank Heuer, Hendrik Schmidt, and Hans-Joachim Wilke. The relation between intervertebral disc bulging and annular fiber associated strains for simple and complex loading. *Journal of biomechanics*, 41(5):1086–94, January 2008.
- [108] Rudolf Bertagnoli, Christopher T. Sabatino, Jean T. Edwards, Gerald a. Gontarz, Ann Prewett, and J. Russell Parsons. Mechanical testing of a novel hydrogel nucleus replacement implant. *The Spine Journal*, 5(6):672–681, November 2005.
- [109] Michelle L. Oyen, Tamaryn a.V. Shean, Daniel G.T. Strange, and Matteo Galli. Size effects in indentation of hydrated biological tissues. *Journal of Materials Research*, 27(01):245–255, October 2011.
- [110] Jayanth K Katta, Michele Marcolongo, Anthony Lowman, and Kevin A Mansmann. Friction and wear behavior of poly ( vinyl alcohol )/ poly ( vinyl pyrrolidone ) hydrogels for articular cartilage replacement. *Journal of Biomedical Materials Research Part A*, 2007.
- [111] Achim Göpferich. Mechanisms of polymer degradation and erosion. *Biomaterials*, 17(2):103–114, January 1996.
- [112] GN Greaves, AL Greer, RS Lakes, and T. Rouxel. Poisson’s ratio and modern materials. *Nature Materials*, 10(11):823–837, 2011.
- [113] Jeong-Yun Sun, Xuanhe Zhao, Widusha R K Illeperuma, Ovijit Chaudhuri, Kyu Hwan Oh, David J Mooney, Joost J Vlassak, and Zhigang Suo. Highly stretchable and tough hydrogels. *Nature*, 489(7414):133–6, September 2012.
- [114] Arne Vogel and Dominique P Pioletti. Damping properties of the nucleus pulposus. *Clinical biomechanics (Bristol, Avon)*, 27(9):861–5, November 2012.
- [115] ASTM. E8 / E8M-04 - Standard Test Methods for Tension Testing of Metallic Materials. In *Annual Book of ASTM Standards*. ASTM International, 2015.
- [116] ASTM. D1876 - Standard Test Method for Peel Resistance of Adhesives (T-Peel Test). In *Annual Book of ASTM Standards*. ASTM International, 2015.
- [117] ASTM. D 3359 - Standard Test Methods for Measuring Adhesion by Tape Test. In *Annual Book of ASTM Standards*. ASTM International, 2007.
- [118] ASTM. D2197 - Standard Test Method for Adhesion of Organic Coatings by Scrape Adhesion. In *Annual Book of ASTM Standards*. ASTM International, 2013.



- [119] ASTM. D4562 - Standard Test Method for Shear Strength of Adhesives Using Pin-and-Collar Specimen. In *Annual Book of ASTM Standards*. ASTM International, 2013.
- [120] ASTM. Standard Test Method for Lap Shear Adhesion for Fiber Reinforced Plastic (FRP) Bonding. In *Annual Book of ASTM Standards*. ASTM International, 2014.
- [121] Dong-An Wang, Shyni Varghese, Blanka Sharma, Iossif Strehin, Sara Fermanian, Justin Gorham, D Howard Fairbrother, Brett Cascio, and Jennifer H Elisseeff. Multifunctional chondroitin sulphate for cartilage tissue-biomaterial integration. *Nature materials*, 6(5):385–92, May 2007.
- [122] International Standard 10993 Biological evaluation of medical devices, 2009.
- [123] Samantha C W Chan, Stephen J Ferguson, and Benjamin Gantenbein-Ritter. The effects of dynamic loading on the intervertebral disc. *European spine journal : official publication of the European Spine Society, the European Spinal Deformity Society, and the European Section of the Cervical Spine Research Society*, pages 1796–1812, May 2011.
- [124] Mauro Alini, Stephen M Eisenstein, Keita Ito, Christopher Little, a Annette Kettler, Koichi Masuda, James Melrose, Jim Ralphs, Ian Stokes, and Hans Joachim Wilke. Are animal models useful for studying human disc disorders/degeneration? *European spine journal : official publication of the European Spine Society, the European Spinal Deformity Society, and the European Section of the Cervical Spine Research Society*, 17(1):2–19, January 2008.
- [125] Neil R Malhotra, Woojin M Han, Jesse Beckstein, Jordan Cloyd, Weiliam Chen, and Dawn M Elliott. An injectable nucleus pulposus implant restores compressive range of motion in the ovine disc. *Spine*, 37(18):E1099–105, August 2012.
- [126] Nü-zhao Yao, Zhong-min Zhang, and Da-di Jin. [In vivo experimental study of lumbar nucleus replacement with pectin/polyvinyl alcohol composite hydrogel]. *Zhonghua wai ke za zhi [Chinese journal of surgery]*, 48(10):784–7, May 2010.
- [127] Johannes L Bron, Albert J van der Veen, Marco N Helder, Barend J van Royen, and Theodoor H Smit. Biomechanical and in vivo evaluation of experimental closure devices of the annulus fibrosus designed for a goat nucleus replacement model. *European spine journal : official publication of the European Spine Society, the European Spinal Deformity Society, and the European Section of the Cervical Spine Research Society*, 19(8):1347–55, August 2010.
- [128] Stephanie J Bryant, Kristi S Anseth, David a Lee, and Dan L Bader. Crosslinking density influences the morphology of chondrocytes photoencapsulated in PEG hydrogels during the application of compressive strain. *Journal of orthopaedic research : official publication of the Orthopaedic Research Society*, 22(5):1143–9, October 2004.
- [129] K S Anseth, C N Bowman, and L Brannon-Peppas. Mechanical properties of hydrogels and their experimental determination. *Biomaterials*, 17(17):1647–57, September 1996.

## Bibliography

---

- [130] Helen M Simms, Christopher M Brotherton, Brian T Good, Robert H Davis, Kristi S Anseth, and Christopher N Bowman. In situ fabrication of macroporous polymer networks within microfluidic devices by living radical photopolymerization and leaching. *Lab on a chip*, 5(2):151–7, February 2005.
- [131] a I Chou, S O Akintoye, and S B Nicoll. Photo-crosslinked alginate hydrogels support enhanced matrix accumulation by nucleus pulposus cells in vivo. *Osteoarthritis and cartilage / OARS, Osteoarthritis Research Society*, 17(10):1377–84, October 2009.
- [132] Blanka Sharma, Sara Fermanian, Matthew Gibson, Shimon Unterman, Daniel A Herzka, Brett Cascio, Jeannine Coburn, Alexander Y Hui, Norman Marcus, Garry E Gold, and Jennifer H Elisseeff. Human cartilage repair with a photoreactive adhesive-hydrogel composite. *Science translational medicine*, 5(167):167ra6, January 2013.
- [133] T Matsuda, M J Moghaddam, H Miwa, K Sakurai, and F Iida. Photoinduced prevention of tissue adhesion. *ASAIO journal (American Society for Artificial Internal Organs : 1992)*, 38(3):M154–7, 1992.
- [134] Kytai Truong Nguyen and Jennifer L West. Photopolymerizable hydrogels for tissue engineering applications. *Biomaterials*, 23(22):4307–4314, November 2002.
- [135] NA. Safety of laser products. Equipment classification and requirements. Technical report, British Standard Institution, 2014.
- [136] Yanjun An and Jeffrey a Hubbell. Intraarterial protein delivery via intimately-adherent bilayer hydrogels. *Journal of Controlled Release*, 64(1-3):205–215, February 2000.
- [137] Benjamin D Fairbanks, Michael P Schwartz, Christopher N Bowman, and Kristi S Anseth. Photoinitiated polymerization of PEG-diacrylate with lithium phenyl-2,4,6-trimethylbenzoylphosphinate: polymerization rate and cytocompatibility. *Biomaterials*, 30(35):6702–7, December 2009.
- [138] Stephanie J Bryant, Garret D Nicodemus, and Idalis Villanueva. Designing 3D photopolymer hydrogels to regulate biomechanical cues and tissue growth for cartilage tissue engineering. *Pharmaceutical research*, 25(10):2379–86, October 2008.
- [139] CK Rhodes. Review of ultraviolet laser physics. *Quantum Electronics, IEEE Journal of*, 1974.
- [140] H Liu, DJ Spence, DW Coutts, H Sato, and T Fukuda. Broadly tunable ultraviolet miniature cerium-doped LiLuF lasers. *Optics express*, 2008.
- [141] J W Schultz and R P Chartoff. Photopolymerization of nematic liquid crystal monomers for structural applications: molecular order and orientation dynamics. *Polymer*, 39(2):319–325, 1998.



- 
- [142] N Desilles, L Lecamp, P Lebaudy, and C Bunel. Gradient structure materials from homogeneous system induced by UV photopolymerization. *POLYMER*, 44(20):6159–6167, 2003.
- [143] MF Perry and GW Young. A mathematical model for photopolymerization from a stationary laser light source. *Macromolecular theory and simulations*, 2005.
- [144] Roland Bays. Oral communication. *Medlight SA*, 2012.
- [145] T. Durduran, A. G. Yodh, B. Chance, D. A. Boas, L. WANG, S. L. Jacques, and L. Zheng. MCML - Monte Carlo modeling of light transport in multi-layered tissues. *Computer methods and programs in biomedicine*, 47(2):3358, December 1995.
- [146] L. C. Henyey and J. L. Greenstein. Diffuse radiation in the Galaxy. *The Astrophysical Journal*, 93:70, January 1941.
- [147] Steven L Jacques. Optical properties of biological tissues: a review. *Physics in medicine and biology*, 58(11):R37–61, June 2013.
- [148] Yves Brulle, Alain Bouchy, Bénédicte Valance, and Jean Claude André. Industrial photochemistry XXI. Chemical, transport and refractive index effects in space-resolved laser photopolymerization. *Journal of Photochemistry and Photobiology A: Chemistry*, 83(1):29–37, September 1994.
- [149] W.F. Cheong, S.A. Prahl, and A.J. Welch. A review of the optical properties of biological tissues. *IEEE Journal of Quantum Electronics*, 26(12):2166–2185, 1990.
- [150] John W. Pickering, Scott A. Prahl, Niek van Wieringen, Johan F. Beek, Henricus J. C. M. Sterenborg, and Martin J. C. van Gemert. Double-integrating-sphere system for measuring the optical properties of tissue. *Applied optics*, 32(4):399–410, February 1993.
- [151] J F Beek, P Blokland, P Posthumus, M Aalders, J W Pickering, H J Sterenborg, and M J van Gemert. In vitro double-integrating-sphere optical properties of tissues between 630 and 1064 nm. *Physics in medicine and biology*, 42(11):2255–61, November 1997.
- [152] Andre Roggan, Moritz Friebel, K Doerschel, Andreas Hahn, and G Mueller. Optical properties of circulating human blood in the wavelength range 400–2500 nm. *Journal of Biomedical Optics*, 4(1):36, 1999.
- [153] Paola Di Ninni, Yves Bérubé-Lauzière, Luca Mercatelli, Elisa Sani, and Fabrizio Martelli. Fat emulsions as diffusive reference standards for tissue simulating phantoms? *Applied optics*, 51(30):7176–82, October 2012.
- [154] Hanna Karlsson, Ingemar Fredriksson, Marcus Larsson, and Tomas Strömberg. Inverse Monte Carlo for estimation of scattering and absorption in liquid optical phantoms, 2012.

## Bibliography

---

- [155] H Günhan Akarçay, Stefan Preisser, Martin Frenz, and Jaro Rička. Determining the optical properties of a gelatin TiO(2) phantom at 780 nm. *Biomedical optics express*, 3(3):418–34, March 2012.
- [156] Dean C S Tai, Darren a Hooks, John D Harvey, Bruce H Smaill, and Christian Soeller. Illumination and fluorescence collection volumes for fiber optic probes in tissue. *Journal of biomedical optics*, 12(3):034033, 2012.
- [157] Philippe Thuelier. *Optical Spectral Probing for Epithelial Tissue Characterisation*. PhD thesis, École Polytechnique Fédérale De Lausanne, 2000.
- [158] MG Shim, BC Wilson, Eric Marple, and M Wach. Study of fiber-optic probes for in vivo medical Raman spectroscopy. *Applied Spectroscopy*, 53(6):619–627, 1999.
- [159] D.D. Goller, R.T. Phillips, and I.G. Sayce. Structural relaxation of SiO<sub>2</sub> at elevated temperatures monitored by in situ Raman scattering. *Journal of Non-Crystalline Solids*, 355(34-36):1747–1754, September 2009.
- [160] a Part and Sm Sensing. *Topics in Fluorescence Spectroscopy*, volume 5. Springer, 2002.
- [161] Xianmin Zhang, Jian Xu, Kaori Okawa, Yoshinori Katsuyama, Jianping Gong, Kangsheng Chen, Yoshihito Osada, and Kangsheng Chen. In Situ Monitoring of Hydrogel Polymerization Using Speckle Interferometry. *The Journal of Physical Chemistry B*, 103(15):2888–2891, April 1999.
- [162] Timothy R. McCaffery and Yvon G. Durant. Application of low-resolution Raman spectroscopy to online monitoring of miniemulsion polymerization. *Journal of Applied Polymer Science*, 86(7):1507–1515, November 2002.
- [163] S Kara and Ö Pekcan. In situ photon transmission technique for monitoring formation of hydrogels in real-time at various water contents. *Polymer*, 41(16):6335–6339, 2000.
- [164] Francis W Wang, Robert E Lowry, and Warren H Grant. Novel excimer fluorescence method for monitoring polymerization: 1. Polymerization of methyl methacrylate. *Polymer*, 25(5):690–692, May 1984.
- [165] Joanna Ortyl, Mariusz Galek, Piotr Milart, and Roman Popielarz. Aminophthalimide probes for monitoring of cationic photopolymerization by fluorescence probe technology and their effect on the polymerization kinetics. *Polymer Testing*, 31(3):466–473, May 2012.
- [166] E. Frauendorfer, A. Wolf, and W.-D. Hergeth. Polymerization Online Monitoring. *Chemical Engineering and Technology*, 33(11):1767–1778, November 2010.
- [167] E Leiss-Holzinger, U. D. Cakmak, B. Heise, J. L. Bouchot, E. P. Klement, M. Leitner, D. Stifter, and Z. Major. Evaluation of structural change and local strain distribution in polymers comparatively imaged by FFSA and OCT techniques. *Express Polymer Letters*, 6(3):249–256, January 2012.

- 
- [168] WF Jager, AA Volkers, and DC Neckers. Solvatochromic fluorescent probes for monitoring the photopolymerization of dimethacrylates. *Macromolecules*, pages 8153–8158, 1995.
- [169] C Eyholzer, a Borges de Couraça, F Duc, P E Bourban, P Tingaut, T Zimmermann, J a E Må nson, and K Oksman. Biocomposite hydrogels with carboxymethylated, nanofibrillated cellulose powder for replacement of the nucleus pulposus. *Biomacromolecules*, 12(5):1419–27, May 2011.
- [170] Andreas Schmocker, Azadeh Khoushabi, Constantin Schizas, Pierre-Etienne Bourban, Dominique P Pioletti, and Christophe Moser. Photopolymerizable hydrogels for implants: Monte-Carlo modeling and experimental in vitro validation. *Journal of biomedical optics*, 19(3):35004, March 2014.
- [171] James S. Owens. Patent US2344785 - Photopolymerization methode, 1944.
- [172] Gerald Oster. Dye-Sensitized Photopolymerization. *Nature*, 173(4398):300–301, February 1954.
- [173] George Odian. Radical chain polymerization. *Principles of Polymerization*, 58(6):198–349, 2004.
- [174] Marco Sangermano, Federica Sordo, Alessandro Chiolerio, and Yusuf Yagci. One-pot photoinduced synthesis of conductive polythiophene-epoxy network films. *Polymer*, 54(8):2077–2080, April 2013.
- [175] K. S. Anseth, C. M. Wang, and C. N. Bowman. Kinetic evidence of reaction diffusion during the polymerization of multi(meth)acrylate monomers. *Macromolecules*, 27(3):650–655, May 1994.
- [176] Haiying Zhang, Rongrong Qi, Mingkan Tong, Yaozhen Su, and Mark Huang. In situ solvothermal synthesis and characterization of transparent epoxy/TiO<sub>2</sub> nanocomposites. *Journal of Applied Polymer Science*, 125(2):1152–1160, July 2012.
- [177] Kunio Ikemura, Kensuke Ichizawa, Mariko Yoshida, So Ito, and Takeshi Endo. UV-VIS spectra and photoinitiation behaviors of acylphosphine oxide and bisacylphosphine oxide derivatives in unfilled, light-cured dental resins. *Dental Materials Journal*, 27(6):765–774, November 2008.
- [178] M P Lutolf and J a Hubbell. Synthetic biomaterials as instructive extracellular microenvironments for morphogenesis in tissue engineering. *Nature biotechnology*, 23(1):47–55, January 2005.
- [179] Katsumi Yamaguchi and Takeshi Nakamoto. Micro fabrication by UV laser photopolymerization. *Memoirs of the School of Engineering, Nagoya University*, 50(1/2):33–82, 1998.

## Bibliography

---

- [180] Lihong Wang and SL Jacques. *Monte Carlo modeling of light transport in multi-layered tissues in standard C*. PhD thesis, University of Texas, 1992.
- [181] Alexander C Thompson, Scott A Wade, William G A Brown, and Paul R Stoddart. Modeling of light absorption in tissue during infrared neural stimulation. *Journal of biomedical optics*, 17(7):075002, July 2012.
- [182] Xueding Wang, Gang Yao, and Lihong V. Wang. Monte Carlo Model and Single-Scattering Approximation of the Propagation of Polarized Light in Turbid Media Containing Glucose. *Applied Optics*, 41(4):792, February 2002.
- [183] Kyle Steenland and Sander Greenland. Monte Carlo sensitivity analysis and Bayesian analysis of smoking as an unmeasured confounder in a study of silica and lung cancer. *American journal of epidemiology*, 160(4):384–92, August 2004.
- [184] M Heuberger, T Drobek, and N D Spencer. Interaction forces and morphology of a protein-resistant poly(ethylene glycol) layer. *Biophysical journal*, 88(1):495–504, January 2005.
- [185] Sheng Lin-Gibson, Sidi Bencherif, James A Cooper, Stephanie J Wetzel, Joseph M Antonucci, Brandon M Vogel, Ferenc Horkay, and Newell R Washburn. Synthesis and characterization of PEG dimethacrylates and their hydrogels. *Biomacromolecules*, 5(4):1280–7, January 2004.
- [186] Yusuke Hiraku, Kimiko Ito, Kazutaka Hirakawa, and Shosuke Kawanishi. Photosensitized DNA damage and its protection via a novel mechanism. *Photochemistry and photobiology*, 83(1):205–12, 2007.
- [187] Consultant. Report on Carcinogens Background Document for Broad-Spectrum Ultraviolet ( UV ) Radiation and UVA, and UVD, and UVC. Technical report, U.S. Department of Health and Human Services, 2000.
- [188] Andreas Schmocker, Azadeh Khoushabi, Salma Farahi, Dominique Pioletti, Pierre-Etienne Bourban, Jan A. Manson, and Christophe Moser. Multi-scale modeling of photopolymerization for medical hydrogel-implant design. In Adam P. Wax and Vadim Backman, editors, *SPIE BiOS*, pages 85921D–85921D–8. International Society for Optics and Photonics, February 2013.
- [189] Hamid J. Naghash, Oguz Okay, and Yusuf Yagci. Gel formation by chain-crosslinking photopolymerization of methyl methacrylate and ethylene glycol dimethacrylate. *Polymer*, 38(5):1187–1196, March 1997.
- [190] V.V. Krongauz and R.M. Yohannan. Photopolymerization kinetics and monomer diffusion in polymer matrix. *Polymer*, 31(6):1130–1136, June 1990.
- [191] Andreas Schmocker, Azadeh Khoushabi, Constantin Schizas, Pierre-Etienne Bourban, Dominique P Pioletti, and Christophe Moser. Miniature probe for the delivery and

- monitoring of a photopolymerizable material. *Journal of biomedical optics*, Accepted o, 2015.
- [192] Jamie L Ifkovits and Jason A Burdick. Review: photopolymerizable and degradable biomaterials for tissue engineering applications. *Tissue engineering*, 13(10):2369–85, October 2007.
- [193] Aurélie Botella, Jérôme Dupuy, Alain-André Roche, Henry Sautereau, and Vincent Verney. Photo-Rheometry/NIR Spectrometry: An in situ Technique for Monitoring Conversion and Viscoelastic Properties during Photopolymerization. *Macromolecular Rapid Communications*, 25(12):1155–1158, June 2004.
- [194] R.L Oréfice, J.A.C Discacciati, A.D Neves, H.S Mansur, and W.C Jansen. In situ evaluation of the polymerization kinetics and corresponding evolution of the mechanical properties of dental composites. *Polymer Testing*, 22(1):77–81, February 2003.
- [195] Azadeh Khoushabi, Andreas Schmocker, D.P. Pioletti, Christophe Moser, Constantin Schizas, J.A. Månson, and P.E. Bourban. Photo-polymerization, swelling and mechanical properties of cellulose fibre reinforced poly(ethylene glycol) hydrogels. *Composites Science and Technology*, 119:93–99, 2015.
- [196] M W van Tulder, B W Koes, and L M Bouter. Conservative treatment of acute and chronic nonspecific low back pain. A systematic review of randomized controlled trials of the most common interventions. *Spine*, 22(18):2128–56, September 1997.
- [197] G Waddell. 1987 Volvo award in clinical sciences. A new clinical model for the treatment of low-back pain. *Spine*, 12(7):632–44, September 1987.
- [198] Alison H McGregor and Sean P F Hughes. The evaluation of the surgical management of nerve root compression in patients with low back pain: Part 2: patient expectations and satisfaction. *Spine*, 27(13):1471–6; discussion 1476–7, July 2002.
- [199] Christopher M Bono and Casey K Lee. Critical analysis of trends in fusion for degenerative disc disease over the past 20 years: influence of technique on fusion rate and clinical outcome. *Spine*, 29(4):455–63; discussion Z5, February 2004.
- [200] N Miyakoshi, E Abe, Y Shimada, K Okuyama, T Suzuki, and K Sato. Outcome of one-level posterior lumbar interbody fusion for spondylolisthesis and postoperative intervertebral disc degeneration adjacent to the fusion. *Spine*, 25(14):1837–42, July 2000.
- [201] Manohar M. Panjabi. Clinical spinal instability and low back pain. *Journal of Electromyography and Kinesiology*, 13(4):371–379, August 2003.
- [202] Domagoj Coric and Praveen V Mummaneni. Nucleus replacement technologies. *Journal of neurosurgery. Spine*, 8(2):115–20, February 2008.

## Bibliography

---

- [203] James C Iatridis, Steven B Nicoll, Arthur J Michalek, Benjamin A Walter, and Michelle S Gupta. Role of biomechanics in intervertebral disc degeneration and regenerative therapies: what needs repairing in the disc and what are promising biomaterials for its repair? *The spine journal : official journal of the North American Spine Society*, 13(3):243–62, March 2013.
- [204] Sandra Reitmaier, Uwe Wolfram, Anita Ignatius, Hans-Joachim Wilke, Antonio Gloria, José M Martín-Martínez, Joana Silva-Correia, Joaquim Miguel Oliveira, Rui Luís Reis, and Hendrik Schmidt. Hydrogels for nucleus replacement—facing the biomechanical challenge. *Journal of the mechanical behavior of biomedical materials*, 14:67–77, October 2012.
- [205] Gladius Lewis. Nucleus pulposus replacement and regeneration/repair technologies: present status and future prospects. *Journal of biomedical materials research. Part B, Applied biomaterials*, 100(6):1702–20, August 2012.
- [206] M Buonocore. Adhesive sealing of pits and fissures for caries prevention, with use of ultraviolet light. *Journal of the American Dental Association (1939)*, 80(2):324–30, February 1970.
- [207] J A Burdick, A J Peterson, and K S Anseth. Conversion and temperature profiles during the photoinitiated polymerization of thick orthopaedic biomaterials. *Biomaterials*, 22(13):1779–86, July 2001.
- [208] J L Hill-West, S M Chowdhury, M J Slepian, and J A Hubbell. Inhibition of thrombosis and intimal thickening by in situ photopolymerization of thin hydrogel barriers. *Proceedings of the National Academy of Sciences of the United States of America*, 91(13):5967–71, June 1994.
- [209] Mark W Grinstaff. Designing hydrogel adhesives for corneal wound repair. *Biomaterials*, 28(35):5205–14, December 2007.
- [210] Sina Naficy, Hugh R. Brown, Joselito M. Razal, Geoffrey M. Spinks, and Philip G. Whitten. Progress Toward Robust Polymer Hydrogels. *Australian Journal of Chemistry*, 64(8):1007, August 2011.
- [211] G. J. Lake and A. G. Thomas. The Strength of Highly Elastic Materials. *Proceedings of the Royal Society A: Mathematical, Physical and Engineering Sciences*, 300(1460):108–119, August 1967.
- [212] Charles W. Peak, Jonathan J. Wilker, and Gudrun Schmidt. A review on tough and sticky hydrogels. *Colloid and Polymer Science*, 291(9):2031–2047, July 2013.
- [213] Y. Okumura and K. Ito. The Polyrotaxane Gel: A Topological Gel by Figure-of-Eight Cross-links. *Advanced Materials*, 13(7):485–487, April 2001.



- 
- [214] J.P. Gong, Y. Katsuyama, T. Kurokawa, and Y. Osada. Double-Network Hydrogels with Extremely High Mechanical Strength. *Advanced Materials*, 15(14):1155–1158, July 2003.
- [215] J. Elisseeff, K. Anseth, D. Sims, W. McIntosh, M. Randolph, and R. Langer. Transdermal photopolymerization for minimally invasive implantation. *Proceedings of the National Academy of Sciences*, 96(6):3104–3107, March 1999.
- [216] Jeffrey A. Hubbell. In Situ Material Transformations in Tissue Engineering. *MRS Bulletin*, 21(11):33–35, November 1996.
- [217] Stephanie J Bryant and Kristi S Anseth. Hydrogel properties influence ECM production by chondrocytes photoencapsulated in poly(ethylene glycol) hydrogels. *Journal of biomedical materials research*, 59(1):63–72, January 2002.
- [218] Stephanie J Bryant and Kristi S Anseth. Controlling the spatial distribution of ECM components in degradable PEG hydrogels for tissue engineering cartilage. *Journal of biomedical materials research. Part A*, 64(1):70–9, January 2003.
- [219] Nobuhiro Nagai, Hirokazu Kaji, Hideyuki Onami, Yumi Ishikawa, Matsuhiko Nishizawa, Noriko Osumi, Toru Nakazawa, and Toshiaki Abe. A polymeric device for controlled transscleral multi-drug delivery to the posterior segment of the eye. *Acta biomaterialia*, 10(2):680–7, February 2014.
- [220] István Siró and David Plackett. Microfibrillated cellulose and new nanocomposite materials: a review. *Cellulose*, 17(3):459–494, February 2010.
- [221] T. Zimmermann, E. Pöhler, and T. Geiger. Cellulose Fibrils for Polymer Reinforcement. *Advanced Engineering Materials*, 6(9):754–761, September 2004.
- [222] Ana C. Borges, Christian Eyholzer, Fabien Duc, Pierre-Etienne Bourban, Philippe Tingaut, Tanja Zimmermann, Dominique P. Pioletti, and Jan-Anders E. Manson. Nanofibrillated cellulose composite hydrogel for the replacement of the nucleus pulposus. *Acta Biomaterialia*, 7(9):3412–3421, September 2011.
- [223] Benjamin Gantenbein, Svenja Illien-Jünger, Samantha C W Chan, Jochen Walser, Lisbet Haglund, Stephen J Ferguson, James C Iatridis, and Sibylle Grad. Organ culture bioreactors—platforms to study human intervertebral disc degeneration and regenerative therapy. *Current stem cell research and therapy*, 10(4):339–52, January 2015.
- [224] Jesse C Beckstein, Sounok Sen, Thomas P Schaer, Edward J Vresilovic, and Dawn M Elliott. Comparison of animal discs used in disc research to human lumbar disc: axial compression mechanics and glycosaminoglycan content. *Spine*, 33(6):E166–73, March 2008.
- [225] Caroline N Demers, John Antoniou, and Fackson Mwale. Value and limitations of using the bovine tail as a model for the human lumbar spine. *Spine*, 29(24):2793–9, December 2004.

## Bibliography

---

- [226] Casey L Korecki, John J Costi, and James C Iatridis. Needle puncture injury affects intervertebral disc mechanics and biology in an organ culture model. *Spine*, 33(3):235–41, February 2008.
- [227] Sandra Reitmaier, Ludwika Kreja, Katharina Gruchenberg, Britta Kanter, Joana Silva-Correia, Joaquim Miguel Oliveira, Rui Luís Reis, Valeria Perugini, Matteo Santin, Anita Ignatius, and Hans-Joachim Wilke. In vivo biofunctional evaluation of hydrogels for disc regeneration. *European spine journal : official publication of the European Spine Society, the European Spinal Deformity Society, and the European Section of the Cervical Spine Research Society*, 23(1):19–26, January 2014.
- [228] Samantha C.W. Chan and Benjamin Gantenbein-Ritter. Preparation of Intact Bovine Tail Intervertebral Discs for Organ Culture. *Journal of Visualized Experiments*, 2(60)(February):1–7, January 2012.
- [229] Andreas Schmocker, Azadeh Khoushabi, Constantin Schizas, Pierre-Etienne Bourban, Dominique P Pioletti, and Christophe Moser. In-situ photopolymerization and monitoring device for controlled shaping of tissue fillers, replacements or implants. *SPIE BiOS*, "in press", 2015.
- [230] O. Biondi. Low molecular weight polyethylene glycol induces chromosome aberrations in Chinese hamster cells cultured in vitro. *Mutagenesis*, 17(3):261–264, May 2002.
- [231] S Fujisawa, T Atsumi, and Y Kadoma. Cytotoxicity of methyl methacrylate (MMA) and related compounds and their interaction with dipalmitoylphosphatidylcholine (DPPC) liposomes as a model for biomembranes. *Oral diseases*, 6(4):215–21, July 2000.
- [232] Christopher G. Williams, Athar N. Malik, Tae Kyun Kim, Paul N. Manson, and Jennifer H. Elisseeff. Variable cytocompatibility of six cell lines with photoinitiators used for polymerizing hydrogels and cell encapsulation. *Biomaterials*, 26(11):1211–1218, 2005.
- [233] M.-P Lowys, J Desbrières, and M Rinaudo. Rheological characterization of cellulosic microfibril suspensions. Role of polymeric additives. *Food Hydrocolloids*, 15(1):25–32, January 2001.
- [234] Andreas M. Schmocker, Azadeh Khoushabi, Benjamin Gantenbein-Ritter, Samantha Chan, Harald Marcel Bonél, Pierre-Etienne Bourban, Jan Anders Månson, Constantin Schizas, Dominique Pioletti, and Christophe Moser. Minimally invasive photopolymerization in intervertebral disc tissue cavities. In Adam Wax and Vadim Backman, editors, *SPIE BiOS*, page 895206. International Society for Optics and Photonics, March 2014.
- [235] Dawn M. Elliott, Chandra S. Yerramalli, Jesse C. Beckstein, John I. Boxberger, Wade Johannessen, and Edward J. Vresilovic. The Effect of Relative Needle Diameter in Puncture and Sham Injection Animal Models of Degeneration. *Spine*, 33(6):588–596, March 2008.
- [236] Eugene J Carragee, Angus S Don, Eric L Hurwitz, Jason M Cuellar, John a Carrino, and Richard Herzog. 2009 ISSLS Prize Winner: Does discography cause accelerated



- progression of degeneration changes in the lumbar disc: a ten-year matched cohort study. *Spine*, 34(21):2338–2345, 2009.
- [237] M A Adams, D W McMillan, T P Green, and P Dolan. Sustained loading generates stress concentrations in lumbar intervertebral discs. *Spine*, 21(4):434–8, February 1996.
- [238] R. D. Bowles, H. H. Gebhard, R. Hartl, and L. J. Bonassar. Tissue-engineered intervertebral discs produce new matrix, maintain disc height, and restore biomechanical function to the rodent spine. *Proceedings of the National Academy of Sciences*, 108(32), August 2011.
- [239] Niklas Bergknut, Lucas a Smolders, Leo H Koole, George Voorhout, Ragnvi E Hagman, Anne-Sofie Lagerstedt, Keti Saralidze, Herman a W Hazewinkel, Albert J van der Veen, and Björn P Meij. The performance of a hydrogel nucleus pulposus prosthesis in an ex vivo canine model. *Biomaterials*, 31(26):6782–8, September 2010.
- [240] Karin Wuertz, Karolyn Godburn, Jeffrey J MacLean, Ana Barbir, Justin Stinnett Donnelly, Peter J Roughley, Mauro Alini, and James C Iatridis. In vivo remodeling of intervertebral discs in response to short- and long-term dynamic compression. *Journal of orthopaedic research : official publication of the Orthopaedic Research Society*, 27(9):1235–42, September 2009.
- [241] Casey L Korecki, Jeffrey J MacLean, and James C Iatridis. Characterization of an in vitro intervertebral disc organ culture system. *European spine journal : official publication of the European Spine Society, the European Spinal Deformity Society, and the European Section of the Cervical Spine Research Society*, 16(7):1029–37, July 2007.
- [242] Alex Huber, Andreas Kuschel, Timo Ott, Gustavo Santiso-Quinones, Daniel Stein, Judith Bräuer, Reinhard Kissner, Frank Krumeich, Hartmut Schönberg, Joëlle Levalois-Grützmaker, and Hansjörg Grützmaker. Phosphorous-Functionalized Bis(acyl)phosphane Oxides for Surface Modification. *Angewandte Chemie*, 124(19):4726–4730, May 2012.
- [243] Estelle C Collin, Sibylle Grad, Dimitrios I Zeugolis, Claire S Vinatier, Johann R Clouet, Jérôme J Guicheux, Pierre Weiss, Mauro Alini, and Abhay S Pandit. An injectable vehicle for nucleus pulposus cell-based therapy. *Biomaterials*, 32(11):2862–70, April 2011.
- [244] Katherine D Hudson, Marjan Alimi, Peter Grunert, Roger Härtl, and Lawrence J Bonassar. Recent advances in biological therapies for disc degeneration: tissue engineering of the annulus fibrosus, nucleus pulposus and whole intervertebral discs. *Current opinion in biotechnology*, 24(5):872–9, October 2013.
- [245] Antonio Gloria, Filippo Causa, Roberto De Santis, Paolo Antonio Netti, and Luigi Ambrosio. Dynamic-mechanical properties of a novel composite intervertebral disc prosthesis. *Journal of materials science. Materials in medicine*, 18(11):2159–65, November 2007.

## Bibliography

---

- [246] Benjamin R Whatley, Jonathan Kuo, Cijun Shuai, Brooke J Damon, and Xuejun Wen. Fabrication of a biomimetic elastic intervertebral disk scaffold using additive manufacturing. *Biofabrication*, 3(1):015004, March 2011.
- [247] F Causa, L Manto, a Borzacchiello, R De Santis, P a Netti, L Ambrosio, and L Nicolais. Spatial and structural dependence of mechanical properties of porcine intervertebral disc. *Journal of materials science. Materials in medicine*, 13(12):1277–80, December 2002.
- [248] C C Guterl, E Y See, S B G Blanquer, A Pandit, S J Ferguson, L M Benneker, D W Grijpma, D Sakai, D Eglin, M Alini, J C Iatridis, and S Grad. Challenges and strategies in the repair of ruptured annulus fibrosus. *European cells and materials*, 25:1–21, January 2013.
- [249] Axiomed Inc. Freedom® Lumbar Disc - Clinical Outcomes Benchmarked Against All TDRs in the SWISSpine Registry.
- [250] Jack P Callaghan and Stuart M McGill. Intervertebral disc herniation: studies on a porcine model exposed to highly repetitive flexion/extension motion with compressive force. *Clinical Biomechanics*, 16(1):28–37, January 2001.



Andreas Schmocker  
 Av. de Cour 87  
 1007 Lausanne, Switzerland  
 +41 76 679 18 19  
 andreas.schmocker@gmx.ch

Swiss  
 Born on the 7<sup>th</sup> of February 1985  
 Single

## Education and qualification

10/2010	<b>Master of Science in Biomechanics, Minor in Management of Technology</b> Federal Institute of Technology in Lausanne (EPFL), Switzerland
09/2009 - 03/2010	> Master's thesis, Institute for Bioengineering of Catalonia, Barcelona, Spain Topic: Optimization of collagen fibre orientation in the annulus fibrosus
2007 – 2008	> Exchange year, Polytechnic University Tomsk (TPU), Siberia, Russia
07/2007	<b>Bachelor in Mechanical Engineering, EPFL</b> > Bachelor's thesis: Characterization of Swiss Cube satellite sun-sensors
06/2004	<b>Swiss Matura in mathematics and applied physics</b> , Gymnasium Burgdorf
01/2003	<b>Argentinean high school-degree</b> , Escuela La Consolata, Sampacho, Argentina

## Work experience

01/2012 –	PhD, <b>EPFL</b> , Lausanne, Switzerland > Topic: c.f. above
08/2010 – 07/2011	Civil service, <b>Buissonnets Foundation</b> , Fribourg, Switzerland > Supervise, motivate and support handicapped children during their learning process
03 – 08/2009 <i>Part-time</i>	Intern, <b>Swiss Climate Credit Ltd. (now World Climate Credit)</b> , Lausanne > Market and competitor analysis including writing these business plan sections > Investor presentation: McKinsey award > Setting-up and executing of customer surveys in Switzerland and Germany
08/2008 – 08/2009	Founder, <b>Cominteg</b> - IT-support-venture, Lausanne, Bern and Zürich > Customer attendance and supervision of employed students > Advertising, IT-support, invoicing
11/2008 – 06/2009 <i>Part-time</i>	Research assistant, <b>Lab. of Hemodynamics and Cardiovascular Tech.</b> , EPFL > Construction of a 3D eye model with Rhino and Matlab > Supervision of a student project
12/2007 – 06/2008 <i>One day a week</i>	Intern, <b>INTEGRAL research center</b> , Tomsk, Russia > Modelling of blood-flows, construction of Finite Element Models
03 – 07/2007 <i>Part-time</i>	Research assistant, <b>Lab. of Hydraulic Machines</b> , EPFL > Data treatment of Kaplan turbine using Matlab: Data sets were integrated in simulation software
07 – 08/2006	Intern, <b>Ypsomed AG</b> , Burgdorf, Switzerland > Mechanical and thermodynamically optimization of a Stirling engine
1998 – 2010	Student jobs, different companies > Repairing mobile phones (Siemens, Motorola) > Sales in French language > Construction- and metalwork, teaching and others

## Extracurricular activities

Since 2010	<b>Vice president, Choir of EPFL/university of Lausanne</b> <ul style="list-style-type: none"><li>&gt; Overall organization of concerts (~ 2000 guests per year)</li><li>&gt; Organization of exchanges and choir trips for ~100 choir members to/from Budapest, Hungary and Vilnius, Lithuania</li></ul>
2003 – 09	<b>American Field Service</b> <ul style="list-style-type: none"><li>&gt; Organizing and leading camps for international exchange-students</li><li>&gt; Home interviews with departing students or host families</li></ul>
2007	<b>Educational journey</b> for 3 <sup>rd</sup> year students to Greece <ul style="list-style-type: none"><li>&gt; Planning, fundraising, execution</li></ul>
2003/06	<b>Camp leader</b> , Foundation Feriengestaltung Kinder Schweiz

## Peer reviewed publications

A. Schmocker, A. Khoushabi, C. Schizas, D. A. Frauchiger, B. Gantenbein-Ritter, P.E. Bourban, J.A. Manson, C. Moser, D. Pioletti, "A photopolymerized composite hydrogel and surgical implanting tool for a nucleus pulposus replacement", *Biomaterials*, *under review*.

A. Schmocker, A. Khoushabi, C. Schizas, P.E. Bourban, J.A. Manson, D.P. Pioletti, C. Moser, "Miniature probe for the delivery and monitoring of a photopolymerizable material", *Journal of Biomedical Optics*, November 2015.

A. Khoushabi, A. Schmocker, D.P. Pioletti, C. Moser, C. Schizas, J.A. Manson, P.E. Bourban, "The combined roles of NFC fibres and PEGDM molecular weight on photo-polymerization and hydromechanics of composite hydrogels", *Composite Materials*, July 2015.

A. Schmocker, A. Khoushabi, C. Schizas, P.E. Bourban, D.P. Pioletti, C. Moser, "Photopolymerizable hydrogels for implants: Monte-Carlo modeling and experimental in-vitro validation", *Journal of Biomedical Optics*, January 2014.

## Awards

09/2015	<b>Academy-Industry training award</b> , Rio de Janeiro, Brazil
06/2015	<b>Gold award</b> , IFMBE Student Competition on Medical Device Design, IUMPESM World Congress on Medical Physics and Biomedical Engineering, Toronto, Canada
05/2009	<b>McKinsey-Award</b> , Start-up Rodeo at EPFL, investor presentation of Swiss Climate Credit Ltd.

## Diverse

### Languages

German	Native language
English	Fluent (effective operational proficiency), C1-level of European Framework of Reference for Languages
Spanish	Fluent, C1 (Argentinian high school-degree, daily use in private life)
French	Fluent, C1 (Bachelor studies)
Russian	Intermediate, B1 (exchange year in Russia)

### Computer skills

High level	Microsoft Office, Matlab, Latex, Illustrator
Intermediate level	Labview, C++, Fortran, Solid works, Fluent

### Other activities

singing, climbing, language studies

